To the Graduate Council:

I am submitting herewith a thesis written by Suzanne Parete-Koon entitled "Reaction Rate of $^{17}F(p,\gamma)^{18}Ne$ and Its Implications for Nova Nucleosynthesis." I have examined the final electronic copy of this thesis for form and content and recommend that it be accepted in partial fulfillment of the requirements for the degree of Masters of Science, with a major in Physics.

Mike Guidry
Mike Guidry, Major Professor

We have read this thesis
and recommend its acceptance:

Marianne Breinig

W. Rapheal Hix

Michael S. Smith

Kermit Duckett

Accepted for the Council:

Anne Mayhew
Vice Provost and Dean of Graduate Studies

(Original Signatures are on file in the Graduate Student Services Office)

Reaction Rate of $^{17}F(p,\gamma)^{18}Ne$ and Its Implications for Nova Nucleosynthesis

A Thesis

Presented for the

Masters of Science

Degree

The University of Tennessee, Knoxville

Suzanne T. Parete-Koon

December, 2001

ACKNOWLEDGMENTS

I would like to thank my advisors Dr. Mike Guidry, Dr Michael Smith and Dr. Raphael Hix for the knowledge of astrophysics I acquired under their guidance and for their support and encouragement. In addition I would like to thank the other members of my committee: Dr. Kermit Duckett and Dr. Marianne Breining also for their help and guidance with the development of my thesis.

Thanks also to members of my group: Erin McMahon, Eric Lingerfelt, Luc Dessieux, Wayne Kincaid, John Meyer, and Viktor Chupryna for their help with editing my thesis and practicing my defense.

Thanks to Paul Lewis, James Sternberg, Dr. William Blass, and Dr. G. Mahan for giving me the confidence and courage to continue graduate school after a very rough start.

Special thanks to my husband Tim Koon and my parents Jo and Jesse Parete for supporting me in the pursuit of this degree.

I would also like to Thank Dr. Lee Riedinger and Dr. Soren Sorensen, the former and present head of the physics department, for the award of a teaching assistantship while I pursued this degree and also Dr. Mike Guidry and Dr. Michael Smith for the award of a research assistantship.

ABSTRACT

The rate of the $^{17}F(p,\gamma)^{18}Ne$ reaction has a profound effect on the abundances of several isotopes produced during a nova outburst. In 1999 a new rate for $^{17}F(p,\gamma)^{18}Ne$ was determined from a measurement of the excitation function for the $^{1}H(^{17}F,p)^{17}F$ reaction at Oak Ridge National Laboratory's (hereafter ORNL) Holifield Radioactive Ion Beam Facility[1]. This experiment yielded the first definite evidence of a $J^{\pi} = 3^{+}$ state in ^{18}Ne. This state provided a new resonance in the ^{17}F +p capture, which could, depending on its properties, dominate the rate of $^{17}F(p,\gamma)^{18}Ne$ at stellar explosive temperatures. The new rate for $^{17}F(p,\gamma)$ ^{18}Ne was determined from these parameters and several other resonance parameters that had been previously determined [2].

A nuclear reaction network was used to calculate abundances produced during a nova outburst. The network required the input of an initial abundance profile, a reaction rate library and a set of hydrodynamic trajectories for each nova. The reaction network was run with the new $^{17}F(p,\gamma)^{18}Ne$ rate placed in the reaction rate library and also with three previous determination of the rate by Wiescher *et al.*, Sherr *et al.* and Garcia *et al.* [3][4][5]. Abundances for 169 isotopes from hydrogen to chromium were calculated. The final abundances produced by each earlier rate were compared to the final abundances produced by the new ORNL rate. This was done for simulations of novae occurring on a 1.35 $M_{\odot}$ ONeMg white dwarf, a 1.25 $M_{\odot}$ ONeMg white dwarf, and a 1.00 $M_{\odot}$ CO white dwarf.

The hotter 1.35 $M_\odot$ white dwarf nova simulation showed the greatest variation in the abundance patterns produced by the four rates. In this simulation, the new ORNL rate changed the abundances of some nuclei, such as ^{17}O, that are synthesized in the hottest zones of the nova by up to 15,000 times, when compared to the network results with the Wiescher rate and up to 4 times, when compared to the network results with the Wiescher rate when all zones of the nova were considered. Similar results were achieved for the ORNL to Wiescher rate comparisons for the 1.25 $M_\odot$ WD nova nucleosynthesis calculations, with differences of up to 600 times for the hottest zones and up to 2 times when all zones of the nova were considered.

For both the 1.35 $M_\odot$ and 1.25 $M_\odot$ white dwarf nova nucleosynthesis calculations the abundance patterns produced by the networks with the Sherr and Garcia rates were similar to those of the network with the new ORNL rate, with the exception of small differences for a few key isotopes such as ^{17}O and ^{15}N. The 1.00 $M_\odot$ WD nova calculations showed that there was little variation in the abundance patterns produced by the networks with the four rates, even in the hottest zones.

TABLE OF CONTENTS

CHAPTER **PAGE**

List of Figures

FIGURE PAGE

CHAPTER 1

Introduction

A classical nova outburst is caused by a thermonuclear runaway occurring on the surface of a white dwarf that has been accreting hydrogen-rich matter from a close binary companion star. The thermonuclear runaway is triggered under degenerate conditions by the reactions of the proton-proton chain. The main sources of energy during the thermonuclear runaway (hereafter TNR) are the reactions of the hot CNO cycle [6]. While novae are only thought to have processed 0.3 % of the matter in our galaxy, observation and theoretical calculations suggest novae may be important sources of the nuclides ^{13}C, ^{15}N, ^{15}O, and ^{17}O [7]. The rate of the $^{17}F(p,\gamma)^{18}Ne$ reaction, may have a large effect on the amount of ^{15}N, ^{15}O, ^{17}O,^{18}O and ^{18}F produced by novae. The following sections give a brief overview of the nova process and the importance of the $^{17}F(p,\gamma)^{18}Ne$ rate in nova nucleosynthesis.

1.1 Pre-Nova Accretion

Binary systems have a gravitational potential energy contour that intersects itself at a point, called the inner Lagrange point, between the two members of the system. The lobe-shaped part of this potential energy contour that surrounds each member is called a Roche lobe. The gravity of each member dominates within its own Roche lobe. In the case of a nova system, the companion star has evolved to become a late main sequence star or red giant so that its outer layers swell to fill its Roche lobe. This causes some of the outer hydrogen-rich envelope to flow through the inner Lagrange point into the region dominated by the gravity of the white dwarf. See figure 1.1. This matter has a high specific angular momentum due to the orbital motion of the companion star and the white dwarf about their common center of mass. Because of this high angular momentum, matter spirals into an accretion disk around the white dwarf. This matter eventually falls to the surface of the white dwarf. The exact mechanism for this is yet unknown, but it is believed that viscous forces within the disk cause its angular momentum to be transferred outward so that the matter's orbit decays until it spirals down onto the surface of the white dwarf.

1.2 White Dwarf Composition

White dwarfs are the cores of stars that have ceased nuclear burning prior to oxygen burning. The matter in a white dwarf is thought to be almost completely electron degenerate. There are two general classes of white dwarfs considered in this study of novae. These are oxygen-neon-magnesium white dwarfs (hereafter ONeMg) and the carbon-oxygen white dwarfs (hereafter CO). The ONeMg white dwarfs result from the evolution of stars with an initial main sequence mass of 8-10 solar masses [8]. Stars of this size are able to fuse carbon into oxygen, neon and heavier elements during core burning late in their evolution, before degeneracy prevents further processing. A white dwarf of mass 1.2-1.35 solar mass units is produced, which is rich in these heavier elements. CO white dwarfs are thought to result from the evolution of stars having initial masses of 1-8 solar masses [8]. They create white dwarfs with masses less than 1.2 solar masses, which are rich in carbon and oxygen but lack the heavier elements found in ONeMg white dwarfs.

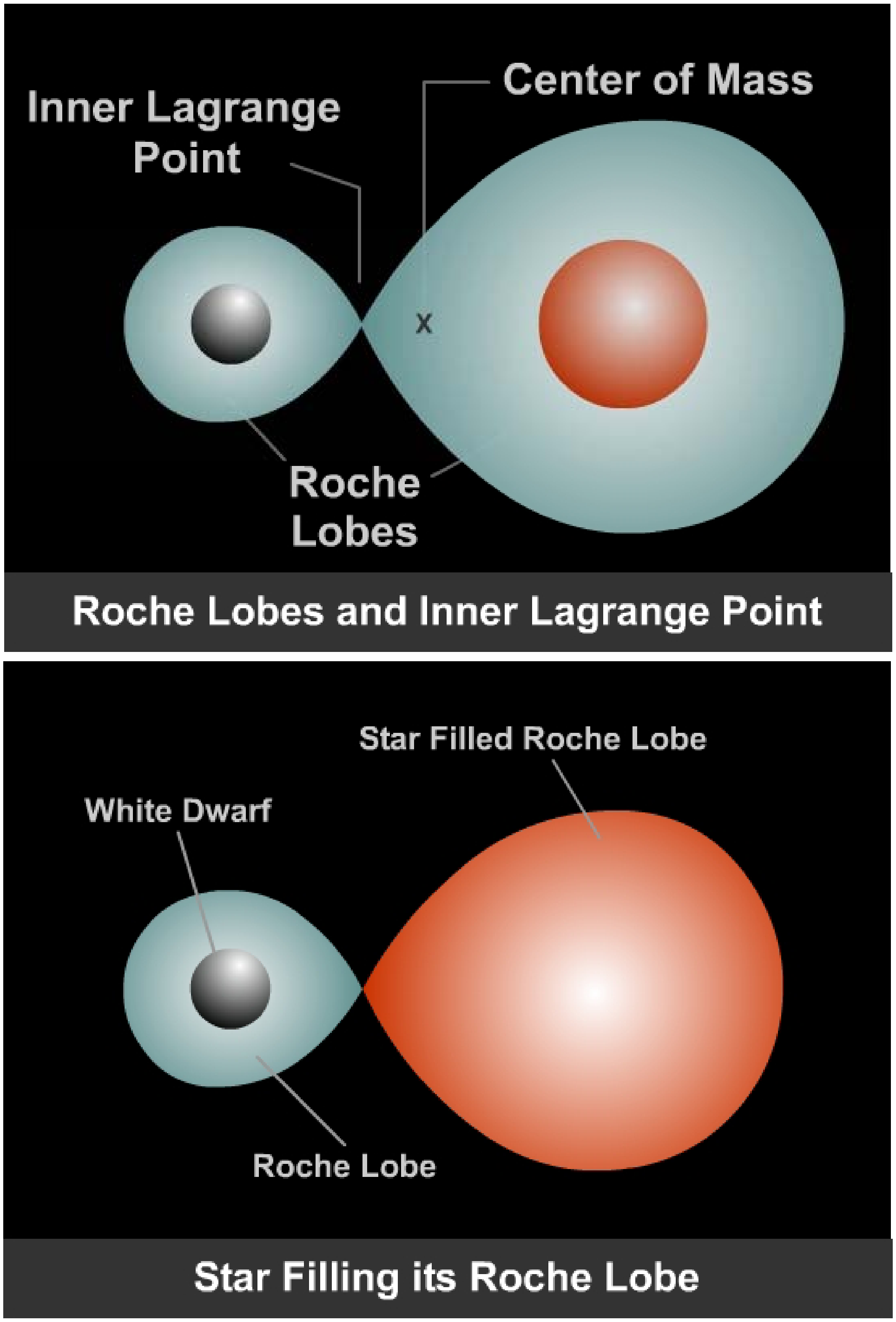

Source: http://www.onlineastronomy.com (2001)

Figure 1.1 The Roche Lobes of a binary system .

Spectroscopic studies of nova systems have determined that the secondary star is of roughly solar composition. Therefore the accreted matter from the companion star is assumed to be of roughly solar composition. However, spectroscopic data from several well-studied novae show that their ejecta are substantially enhanced relative to solar composition in helium, carbon, nitrogen, oxygen, neon, sodium, magnesium and aluminum [8] (See Table (1.1)). It is not expected that a nova starting with only the low abundance of heavy elements characteristic of pure solar composition could synthesize significant abundances of the heavier elements during the explosion.

For the temperatures generated in a nova, nucleosynthesis occurs mainly though the hot CNO cycles shown figure 1.2. In these cycles a series of proton captures on intermediate mass isotopes like carbon, nitrogen and fluorine and beta decay reactions catalyzes the fusion of four protons into helium. One of the primary factors that limits how much energy the hot CNO cycles generate is the abundance of the hot CNO cycles' isotopes, shown in figure 1.2, present in the nova envelope. Models of nova nucleosynthesis do not reproduce the gross features of a typical *fast* nova outburst unless the envelope of accreted matter is enhanced in CNO isotopes significantly above solar abundance [9]. Observationally, a fast nova is defined as one that reaches its maximum brightness in only a few hours after the outburst and fades by two orders of magnitude within 25 days [10]. This requires a fast and energetic TNR.

The fast energy generation of CNO cycle reactions is what drives the TNR. If the envelope is enhanced significantly over solar abundance in CNO isotopes, processing by the CNO cycles is accelerated and the TNR gets started sooner and runs faster than in an envelope (of similar temperature) with sparse CNO abundances [10].

Table 1.1 Heavy-Element Abundances in Novae

	Mass Fraction										
Object	H	He	C	N	O	Ne	Na	Mg	Al	Si	S
RR Pic	0.53	0.43	0.0039	0.022	0.0058	0.011	…	…	…	…	…
HR Del	0.45	0.48	…	0.027	0.047	0.0030	…	…	…	…	…
T Aur	0.47	0.40	…	0.079	0.051	…	…	…	…	…	…
V1500 Cyg	0.49	0.21	0.070	0.075	0.13	0.023	…	…	…	…	…
V1668Cyg	0.45	0.23	0.047	0.14	0.13	0.0068	…	…	…	…	…
V693Cr A	0.29	0.32	0.0046	0.080	0.12	0.17	0.0016	0.0076	0.0043	0.0022	…
DQ Her	0.34	0.095	0.045	0.23	0.29	…	…	…	…	…	…
V1370 Aql	0.053	0.085	0.031	0.095	0.061	0.47	….	0.0092	…	0.0012	0.19

Source: J.W Turan & M. Livio, Ap.J., **308**: 721-727 (1986)

The mass fraction of a particular element is the fraction of nucleons in the sample, which in this case is the nova envelope, which are of that species of element. The mass fraction of an element is related to the abundance of that element by the element's atomic mass such that mass fraction equals abundance multiplied by the atomic mass.

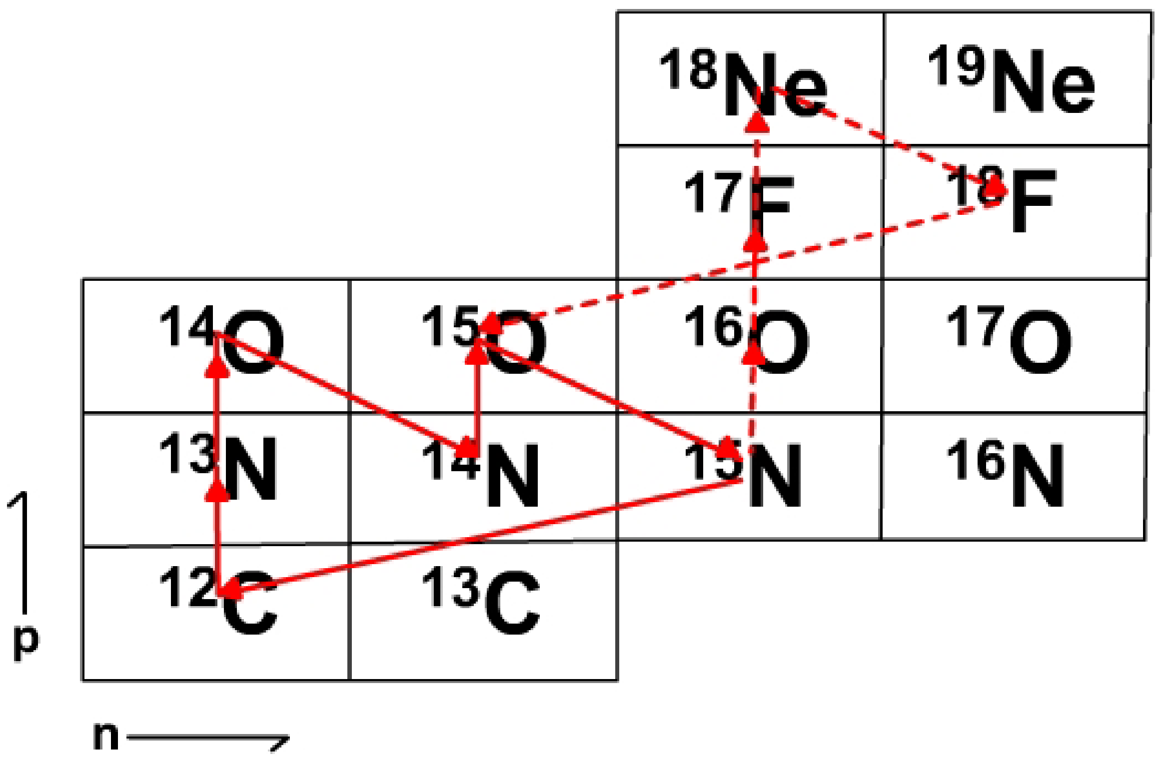

Source: M. Wiescher, J. Gorres and H. Schatz , J. Phys. G: Nucl. Part. Phys.,**25,** R133 (1999)

Figure 1.2 The hot CNO cycles are a series of proton captures on intermediate mass isotopes like carbon, nitrogen, and fluorine that coupled with beta decay reactions lead to the fusion of four protons into helium. The First cycle shown by the red solid line is $^{12}C(p,\gamma)^{13}N(p,\gamma)^{14}O(\beta^{+}\nu)^{14}N(p,\gamma)^{15}O(\beta^{+}\nu)^{15}N(p,\alpha)^{12}C$. The second cycle shown by the red dotted line is $^{16}O(p,\gamma)^{17}F(p,\gamma)^{18}Ne(\beta^{+}\nu)^{18}F(p,\alpha)^{15}O(\beta^{+}\nu)^{15}N(p,\gamma)^{16}O$ [6]. Here (p,γ) means "captures a proton and releases a gamma ray", (p,α) means "captures a proton and releases ^{4}He" and $(\beta^{+}\nu)$ denotes at beta decay.

It is generally accepted that the envelope must be enriched in heavier isotopes prior to, or in the early phases, of the nova outburst. There have been many scenarios proposed for how this enrichment takes place, but the theory that the enrichment comes from matter dredged off of the white dwarf is the only one that can explain the enrichment of heavy isotopes like sodium, magnesium and aluminum [8]. Two theories are that the mixing takes place by shear-induced turbulence [11] or by diffusion-induced convection [12]. The exact mechanism for how the matter is dredged up is not yet known.

1.3 Mass Accretion Rate and White Dwarf Luminosity

The pre-nova luminosity of the white dwarf and its accreted envelope is an indication of the mass accretion rate and temperature [10]. The accreting matter releases energy as it collides with the white dwarf and the previously accreted matter in the disk. These collisions increase the average kinetic energy of the gas and excite nuclei, increasing the luminosity of the gas. The larger the mass accretion rate, the hotter and more luminous the white dwarf and its accreted envelope become.

The pre-nova temperature of the white dwarf can have a large effect on the amount of time before the TNR is initiated and the degree of degeneracy present when TNR is initiated. Many of the key thermonuclear reactions are charged-particle interactions. Most of these reactions involve the capture of a proton on a heavier and more positively charged nucleus. For nuclei of like charges to interact, the repulsive Coulomb barrier between them must be overcome. The larger the kinetic energy of the particles, the greater the probability that they can overcome the Coulomb barrier. The kinetic energy of the particles is directly related to the temperature by $E = k\ T$, where $k = 8.617\times10^{-8}$ keV/Kelvin is the Boltzman constant and T is the temperature in Kelvin [13].

Heavier nuclei have more protons that give them a higher Coulomb barrier than light nuclei that have fewer protons. Therefore higher temperatures are required for heavier nuclei to interact.

In the preoutburst phase of a nova there are two possible sources for thermonuclear energy generation. They are the proton-proton chain (hereafter pp-chain), which generates energy by direct fusion of hydrogen into helium, and the CNO cycle in which energy is generated by a cycle of proton capture reactions and beta decays on carbon, oxygen and nitrogen that result in the release of an atom of helium.

The reaction rates and energy production of the pp-chain and the CNO cycle have very different temperature dependencies. For temperatures up to about 18 MK (where MK means millions of Kelvin) the rates of the controlling reactions in the pp-chain dominate over the rates of the controlling reaction for the CNO cycle [14]. The rate of nuclear energy generation for the pp-chain is proportional to the temperature raised to the fourth power [10]. At temperatures above 18 MK the CNO cycle becomes dominant [14]. The rate of energy release by the CNO cycle at these temperatures is proportional to the temperature raised to the 16^{th} to 18^{th} power, which is orders of magnitude greater than the rate of energy release of the pp-chain at the temperatures where it is dominant [10]. If the luminosity of the white dwarf is high enough to make CNO reactions the dominant form of energy generation, then the time to initiate TNR is much shorter than for a less luminous white dwarf of similar size and chemical composition.

For novae occurring on white dwarfs of similar mass and composition, a slower accreting, less luminous white dwarf allows much more matter to accrete before TNR is initiated than a faster accreting, more luminous white dwarf. The larger amount of accreted material allows for a thicker layer of degenerate material to form around the core of the white dwarf. When TNR is finally ignited in this layer, much more energy is available to break the degeneracy because there is more fuel present. This gives the nova outburst a greater violence and a greater luminosity [15].

There is an upper limit on the accretion rate for a nova. If the rate is above this limit, the material become hot enough during accretion to burn hydrogen to helium at a steady rate. The white dwarf becomes surrounded by a layer of helium-rich material. This type of accretion may produce a Type 1a supernova, which has a thermonuclear runaway that is so violent that it disrupts the white dwarf core. (This is just one possible mechanism for Type 1a supernovae; for more detail refer to [15].)

1.4 Thermonuclear Runaway

When enough heat energy has been released from gravitational compression and pp-chain reactions for the thermonuclear reactions of the hot CNO cycle to become important sources of energy, the rates of the reactions may increase quickly by orders of magnitude and then run out of control. This is the thermonuclear runaway. After TNR has produced enough energy to generate temperatures on the order of 10^8 Kelvin, the nova reaches a maximum luminosity. The TNR releases enough energy to eject most of the accreted material.

Another source of outward pressure on the nova envelope is the escaping photons, which provide the luminosity. If enough photons are generated that their outward force on the envelope is greater than the inward force of the white dwarf's gravity, a rapid expansion occurs that can be powerful enough to eject the envelope of the nova. The luminosity limit above which this occurs is called the Eddington limit. The maximum luminosity for most novae approaches the Eddington limit and in the case of *fast* novae exceeds it [7].

The ejected shells of material burn hydrogen, keeping the system at a nearly constant luminosity, but over a period of time the ejected material expands and cools to the point that thermonuclear reactions cease. As this happens the luminosity fades to it's preoutburst magnitude [10].

The basic requirement for the ignition of a thermonuclear runaway is that a critical pressure must be reached at the interface between the accreted mass envelope and the white dwarf. The pressure at the white dwarf's surface is given by:

$$P = \frac{GM_1}{R^2} \times \frac{M_e}{4\pi R^2}$$

where M_e is the mass accretion rate of the envelope, M_1 is the mass of the white dwarf and R_1 is the radius of the white dwarf. To produce a *fast* nova, MacDonald *et al* have estimated that a pressure on the order of 10^{20} dyn cm $^{-2}$ must be reached at the interface [17].

The mass of the white dwarf dictates how fast the nova will be and how often a nova will recur. More massive white dwarfs can reach the critical pressure for TNR faster and with less accreted material than less massive white dwarfs [8][18]. This means they can recur more frequently than the lower-mass white dwarf novae. The more massive white dwarfs also produce more violent nova outbursts. This is because a more massive white dwarf permits stronger degeneracy [18]. More massive white dwarfs also produce greater luminosity just after the peak of the nova [7]. About 1/3 of all novae that we observe occur on white dwarfs with masses between 1.2 and 1.35 solar masses.[7].

1.5 Degeneracy

Electron degeneracy is one of the key conditions for TNR. In the matter surrounding the white dwarf, the atoms are squeezed so close together by the gravity of the white dwarf that the average separation between atoms is smaller than the ionic radius of the atom. The effective volume of each atom becomes too small to contain the electrons and as a result, all the atoms become completely ionized creating an electron gas. This is called pressure ionization. Temperature in the accreted matter of the nova envelope is high enough that temperature ionization also occurs, but pressure ionization is important because it leads to ionization even at temperatures which are low relative to the Fermi temperature, a temperature set by the density of the gas that will be defined in the following discussion.

Since the electrons are unbound, the most convenient way of expressing the quantum energy state of an electron is in phase space where the position and momentum of the electron are given by six components x, y, z, p_x, p_y, p_z. Electrons belong to a class of particles, having half integer spins, which are known as Fermions. Spin is the quantum number that specifies the intrinsic angular momentum of the electron. Electrons can have a spin projection of 1/2 or -1/2.

Heisenberg's uncertainty principle states that we can not know both the position and the momentum of an electron with certainty at the same time. There is an uncertainty δx in any position coordinate and δp in any momentum coordinate such that

$$\delta x \delta p \geq \hbar / 2$$

This is means that in a two-dimensional phase space each quantum state would be represented by an area $\hbar/2$ for each spin projection quantum number of the electron. This generalizes to 6 dimensional phase space by saying that each quantum state is represented by a volume proportional to $\hbar^3$ for each spin projection quantum number of the electron.

The Pauli exclusion principle states that no two Fermions can occupy identical quantum states. This means that each volume of phase space, $\hbar^3$, can contain two electrons, provided that the electrons do not have the same spin projection quantum numbers [19].

A completely degenerate gas is one in which all the lowest available momentum states are full. One situation in which this happens is when the temperature of the gas is at absolute zero. This can also happen when the density of the gas is high relative even if the temperature is not zero. The matter in the white dwarf is one such case. The gravity of the white dwarf compresses the electrons in position space so that several electrons have almost the same position. To avoid violating the Pauli exclusion principle, the electrons must occupy significantly different momentum states. All the lowest available momentum states fill. The highest momentum state occupied by electrons is called the Fermi momentum [20].

The Fermi momentum increases as the density of the gas increases. The momentum and energy are directly related. Thus the Fermi energy is the energy state that corresponds to the Fermi momentum. The Fermi temperature is the temperature that corresponds to the Fermi energy such that $T_{Fermi} = E_{Fermi}/k$. It is important to note that this is not the temperature of the gas. The Fermi temperature sets a temperature scale for the gas. A cold degenerate gas is one in which the thermal temperature of the gas is below the Fermi temperature of the gas.

In a normal gas the electrons supply most of the pressure. When the temperature increases in a normal electron gas the electrons to absorb energy and move faster, increasing the pressure. The result is an expansion of the gas. In the case of a cold degenerate electron gas, the quantum restrictions on the allowed energy states of the electron gas make it difficult for the electrons to absorb energy as the temperature increases. Most of the kinetic energy absorbed would result in electrons occupying higher energy states because all the lowest energy states are full. As a result, there is little increase in pressure inside the volume of the degenerate gas and therefore no expansion as temperature rises. The energy instead excites the heavy (relative to the electrons) positive ions of the gas which are not degenerate and do not contribute much to the pressure of the gas [13].

Therefore, when thermonuclear burning begins in degenerate material, the thermonuclear reactants are kept close together in an environment that is rapidly heating. The hotter the matter gets, the more kinetic energy reactant ions have to overcome the repulsive Coulomb barrier between them. This increases their reaction rate. There is no expansion to separate the fuel and the temperature is increasing rapidly from the energy liberated by the reactions. The rates of the thermonuclear reactions increase by orders of magnitude and thermonuclear runaway begins. Eventually enough energy is generated by the TNR that the degenerate electrons become excited above the Fermi energy and the degeneracy is broken. This is followed by a rapid expansion that ejects most of the accreted matter off the white dwarf into space. The stronger the degeneracy, the more energy TNR must produce before the degeneracy can be lifted. Thus, stronger degeneracy produces a more violent explosion and leads to greater nova luminosity [18]. Also, with stronger degeneracy, higher temperatures are achieved in the envelope before it expands. This allows for the nucleosynthesis of heavier elements.

The mass and pre-nova luminosity of the white dwarf, and the rate of mass accretion, are all factors that ultimately determine how much degenerate material will be present at the time of TNR.

1.6 The Importance of the ^{17}F(p,γ)^{18}Ne reaction rate.

The two hot CNO cycles that provide a large part of the energy driving the nova explosion are ^{12}C(p,γ)^{13}N(p,γ)^{14}O($\beta^+\nu$)^{14}N(p,γ)^{15}O($\beta^+\nu$)^{15}N(p,α)^{12}C and ^{16}O(p,γ)^{17}F(p,γ)^{18}Ne($\beta^+\nu$)^{18}F(p,α)^{15}O [2]. Refer to Figure 1.2. The ^{17}F(p,γ)^{18}Ne reaction, which is an integral part of the second chain of reactions, competes with the beta decay reaction ^{17}F($\beta^+\nu$)^{17}O, which has a half-life of 64.49s [21]. The fate of ^{17}F may determine the final mass fractions of ^{15}O, ^{15}N, ^{17}O, ^{18}F and ^{18}O present in the nova ejecta. If the beta decay is faster than the proton capture rate, as is typical in novae where the peak temperatures are generally no higher than 0.4 GK (1GK = 10^9 K), the reaction sequence ^{17}F($\beta^+\nu$)^{17}O(p,α)^{14}N(p,γ)^{15}O closes the second cycle. The beta decay product of ^{15}O is ^{15}N. The observation of a large overabundance of ^{15}N in nova ejecta may support the proposition that this reaction sequence is the dominant fate for ^{17}F in novae [22].

However, if the ^{17}F(p,γ)^{18}Ne rate approaches that of the beta decay there will be significant flux through ^{17}F(p,γ)^{18}Ne($\beta^+\nu$)^{18}F(p,α). It has been suggested that convection within the envelope of the nova could bring a significant fraction of ^{18}F to cooler surface regions of the nova where it would survive to beta decay to ^{18}O rather than proton capture to ^{15}O. If this were the case, the mass fraction ratios of ^{18}F/^{17}F and ^{18}O/^{17}O would be increased in nova ejecta. It is believed that satellite-based observatories could detect the 511-keV gamma rays produced through e+ e- annihilation after the beta decay of ^{18}F to ^{18}O.

Until, recently there were large uncertainties in the rate of the ^{17}F(p,γ)^{18}Ne due to the possibility of an unmeasured excited quantum state in ^{18}Ne that could dominate the ^{17}F(p,γ)^{18}Ne reaction rate. Experiments at Oak Ridge National Laboratory have found this excited state and precisely determined its properties. This new physical information has changed the ^{17}F(p,γ)^{18}Ne rate by up to a factor of 30 from the most widely used previous estimate [1]. This thesis uses computer models of novae to compare the nucleosynthesis implied by this rate with the nucleosynthesis resulting from three previous, widely-used estimates of this rate.

Chapter 2

Reaction Rates and Cross Sections

2.1 The Cross Section

The interactions of an atom's nucleus are governed by the laws of quantum mechanics. An incident particle can be captured into a quantum energy state of the compound nucleus and then lose energy through emission of gamma rays and other particles from that nucleus. Because the system is quantum mechanical, only certain captures are allowed, those that conserve the energy, angular momentum, and parity of the nucleus and incident particle. We provide here a brief summary of the calculation and measurement of reaction rates. For more detail we refer the reader to references [14],[23],and [24].

The most basic piece of information that can be determined about a nuclear reaction is its nuclear cross section. The cross section is defined as:

$$\sigma = (\text{\# of reactions per target nuclei per second})/(\text{Incident nuclei per cm}^2)$$

The cross section is a measure of the probability per particle pair that a nuclear reaction will occur between the particles. It is used to calculate reaction rates and it can be determined in laboratory experiments where beams of particles bombard a target made of reactants to produce the desired reaction.

To see how the reaction rate follows from the cross section, consider a gas made up of particles of two reactant nuclei j and k. Assume for simplicity that the relative velocity, ν, between all particles of j and k is constant. Arbitrarily j denotes the target nuclei and k the projectiles. Thus, all particles of j are considered to be at rest and all particles k are considered to have velocity ν. The projectiles see an effective reaction area which is the product of the cross section for one target nucleus, j, multiplied by the number density n_j of the species j. The number of reactions occurring in the reaction area is proportional to the incident flux of projectiles, which is the product of the number density of k, n_k, and the velocity, ν. The rate, r, of the reaction is simply the product of the reaction area and the incident flux [23].

$$r = n_j n_k \, \sigma(\nu) \, \nu \tag{2.1}$$

In a gas the relative velocity between particles varies over a wide range and the rate must be averaged over the velocity distribution. In the case of astrophysical envionments at sufficiently low densities, we may often assume that this velocity distribution is a Maxwell-Boltzmann distribution [13][14]. The rate then becomes

$$R = n_j n_k < \sigma\nu >_{j,k} = n_j n_k (\frac{8}{\mu\pi})^{\frac{1}{2}} (k_B T)^{\frac{-3}{2}} \int_0^{\infty} E\sigma(E)\exp(-E/(k_B T))dE \tag{2.2}$$

where μ is the reduced mass of the target and projectile, E is the center of mass energy, T is the temperature and k_B is Boltzmann's constant.

2.2 The Astrophysical S-factor

The cross section for charged-particle-induced reactions can be expressed as the product of three factors: the astrophysical S-factor, the DeBrogile wavelength factor and the Coulomb penetration factor [13][14].

The Coulomb penetration factor is an expression of the probability that two charged particles of charge Z_1 and Z_2, travelling toward one another with velocity ν, will penetrate the electrostatic Coulomb barrier between them.

$$P \sim \exp(-(2\pi Z_1 Z_2 e^2)/(\hbar\nu)) \tag{2.3}$$

This factor was first shown by Gamow [14]. Since Coulomb barrier penetration is a requirement for charged nuclei to interact, it makes sense that the cross section is proportional to this factor.

The DeBroglie wavelength λ is a measure of the quantum size of a particle. Classically particles are represented as a point with finite width. Quantum mechanically particles can be represented as wave packets. The deBroglie wavelength is a measure of how localized the wave packet is. The quantum interactions between two particles are proportional to $\pi\lambda^2$, where λ is the DeBroglie wavelength. The deBroglie wavelength is proportional to the momentum of the particle, p, such that $\lambda = 2\pi\hbar/p$. The energy, E, of a particle is related to its momentum by $E=p^2/2m$, where m is the mass of the particle (for non-relativistic particles). Thus, the square of the deBroglie wavelength is inversely proportional to the energy of the particle. Thus, $\pi\lambda^2 \cong 1/E$, where E is energy.

The astrophysical S-factor, S(E), contains all other energy dependent factors of the cross section. This factor represents all the intrinsically nuclear parts of the probability for the occurrence of a nuclear reaction [14]. Thus the equation for the cross section is expressed as

$$\sigma(E) = S(E)\,(1/E)\,\exp(-(2\pi Z_1 Z_2)/\hbar\nu) \tag{2.4}$$

For the interaction of two particles the astrophysical factor is a slowly varying function of energy compared to the cross section, $\sigma(E)$, unless the interaction energy of the two particles nearly coincides with an energy that will cause the two particles to resonate in a quasistationary state of the two particles [14]. This quasistationary state, which is also called a resonance, has a definite lifetime to decay by emission of a gamma ray or a particle to the lowest energy configuration (the 'ground' state) of the nucleus.

In the case of the $^{17}F(p,\gamma)^{18}Ne$ rate, the direct capture cross section was calculated by A. Garcia *et al* in 1991 [5]. However this cross section by itself is insufficient to calculate the rate of the reaction at stellar explosive temperatures because there are resonances in the $^{17}F(p,\gamma)^{18}Ne$ reaction which occur at energies corresponding to stellar explosive temperatures. If the reaction occurs at an energy that creates a quasistable state (a resonance), the state's stability greatly increases the cross section.

2.3 The Breit-Wigner Resonant Cross Section

A resonant cross section is often expressed in the Breit-Wigner form where the cross section is defined in terms of the energy and quantum energy widths, but before this can be discussed it will be useful to define the energy width of a quantum state.

The nucleons of an atom are arranged in bound states which are characterized by a discrete energy and quantized angular momentum. If transitions can occur between the states, the states are not completely stationary. The transitions cause each state to have an energy width, Γ, such that $\Gamma = \hbar/\tau$, where τ is the mean lifetime for the state to decay. Thus, a finite energy width also describes a quasistable state. In the case of a bound state the lifetime of the state is long so that Γ is small compared to the energy distance between states and the bound state is a good approximation of a stationary state. However in the case of a quasistable state the lifetime of the state is sufficiently small to give that state a significant energy width.

The entrance channel of a reaction is the quantum state that the nuclei have when entering into the reaction. The exit channel is the quantum state that the nuclei have at the end of the reaction. Entrance and exit channel widths are the energy widths of the quantum states that the nuclei and other particles enter and exit the reaction with.

The Breit-Wigner cross section is given by

$$\sigma_{ab} = g\,\pi\lambda^2\,\Gamma_a\Gamma_b/((E-E_r)^2+(\Gamma/2)^2) \qquad (2.6)$$

where Γ_a and Γ_b are the energy width of the entrance and exit channels of the reaction, respectively, $\Gamma = \Sigma\Gamma_i$ is the total width of the reaction and E_r is the resonance energy. The statistical factor, g, contains information about the spins of the projectile target and compound nucleus. The energy widths are dependent on E_r, the energy of the resonance.

Several quasistable states can occur for one reaction. The total cross section takes into account all the possible resonances that can occur in the range of energies that the incident particles could have coming in to the reaction.

2.4 Reaction Rate Determination for $^{17}F(p,\gamma)^{18}Ne$

Several resonance energies in ^{18}Ne that influence the $^{17}F(p,\gamma)^{18}Ne$ reaction were previously measured with beams of stable nuclei, but until 1999 a proposed $J^{\pi} = 3^{+}$ quantum excited state of ^{18}Ne had never been observed (J is the total spin angular momentum of the state and π is the parity). In 1989, Wiescher, Gorres, and Thielemann proposed that the $J^{\pi} = 3^{+}$ state existed due to the existence of a similar state in ^{18}O. Based on shell model calculations, they estimated the excitation energy of the $J^{\pi} = 3^{+}$ ^{18}Ne excited state to be 4.328 MeV, with a width of 5.34 keV [3]. Later calculations by Sherr and Fortune predicted the excitation energy to be 4.642 MeV, with a width of 42 keV [4].

Garcia *et al*, in 1991 conducted an experiment with the $^{16}O(^{3}He,n)^{18}Ne$ reaction and found a signal which showed an energy peak which they believed corresponded to the $J^{\pi} = 3^{+}$ $^{18}Ne^{*}$ state. But the result could not be reproduced in further studies with other reactions. Based on this measurement Garcia *et al* calculated the excitation energy for the state to be 4.561 MeV ± 0.009 MeV [5].

In 1999 the Nuclear Astrophysics group at Oak Ridge National Laboratory unambiguously found the $J^{\pi} = 3^{+}$ excited state for ^{18}Ne with an experiment that measured the excitation function for the $^{1}H(^{17}F,p)^{17}F$ reaction. This reaction was ideally suited to create the $J^{\pi} = 3^{+}$ state because the ground state of the ^{17}F nucleus has a total spin angular momentum of $J = 5/2^{+}$ and a proton has a spin of $J=1/2^{+}$. The resulting spin angular momentum of the ^{17}F + p state could only be $J=2^{+}$ or $J=3^{+}$. The reason this reaction had never been used before was the difficulty of generating a sufficiently intense beam of radioactive ^{17}F for the experiment. ORNL's Holifield Radioactive Beam Facility was the first to produce a suitable low energy beam of 10-13 MeV radioactive ^{17}F for the experiment. The beam bombarded a thin CH_2 target to produce the $^{1}H(^{17}F, p)^{17}F$ reaction. Protons elastically scattered from the reaction were detected by an array of silicon detectors called SIDAR, while ^{17}F ions were measured in coincidence using a gas ionization detector [2]. Analysis of the data from the detectors yielded the excitation function of the reaction and allowed a precise determination of the excitation energy and width of the $J^{\pi} = 3^{+}$ state of $^{18}Ne^{*}$ [25]. The excitation energy was measured to be 4.5237 MeV ± 2.9 keV with a width of 18±2 keV [2].

This excitation energy, energy width, and the previously determined excitation energies from the other resonances, were used along with the nonresonant cross section to determine a more complete cross section for the $^{17}F(p,\gamma)^{18}Ne$ reaction. From this cross section the rate of the reaction was determined. Rates were also determined from cross sections using the three previous calculations by Wiescher, Sherr and Garcia of the $J^{\pi} = 3^{+}$ $^{18}Ne^{*}$ excitation energy.

Figure 2.1 shows the rates plotted as function of temperature for the range of temperatures that occur in novae. The Wiescher rate, which is the most widely used in astrophysical reaction rate libraries, differs by up to a factor of 30 from the ORNL rate at nova temperatures. The Sherr and Garcia rates differ only slightly from the ORNL rate [25].

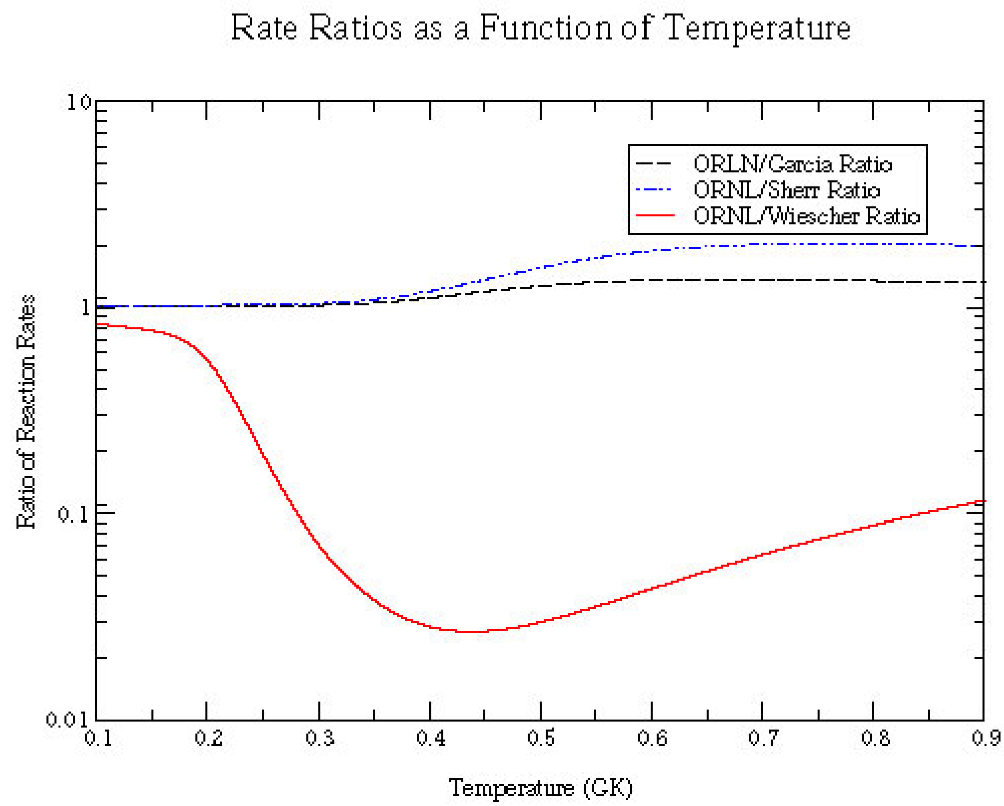

Figure 2.1 The Wiescher rate, which is the most widely used in astrophysical reaction rate libraries, differs by up to a factor of 30 from the ORNL rate at nova temperatures. The Sherr and Garcia rates differ only slightly from the ORNL rate.

CHAPTER 3

Nuclear Reaction Networks

The final abundance, *Y*, of any one species is dependent on the sum of reactions that create or destroy it during the nova outburst. Many of the rates of these reactions are dependent on the temperature and density of their surrounding which are in turn greatly affected by the energy released or absorbed by the reactions themselves. The set of coupled differential equations that link the physics of all these interdependent interactions for individual species of nuclei to an abundance pattern for all the nuclei involved is called a nuclear reaction network [26].

A specific differential equation can be written for each species that describes how its abundance changes during the outburst. In principle, the solution for each abundance is as simple as:

$$Y(t) = \int_0^t \dot{Y}(t')dt' \tag{3.1}$$

However, the nuclear reaction equations for the network often contain rate terms that are second order or higher in *Y*, meaning that their rates have a very broad range of reaction time scales. The rate reaction of each species is dependent on several species. Equation systems that behave in this manner are called stiff. A set of stiff differential equations calls for a special scheme of approximations and numerical methods to obtain solutions.

The nuclear network used to solve for the abundances in this project is a computer program written by W.R. Hix and F-K. Thielemann.

The number density of a species is defined as the number of particles of that species per unit volume. To obtain a differential equation for each species, the rate of change in its number density is written as a sum of contributions from the three groups of reactions. These are, (1), reactions involving one reactant nucleus such as decays, electron and position captures, and neutrino induced reactions, (2), reactions involving two reactant nuclei like proton and alpha particle captures, and (3), reactions involving three reactant nuclei such as the triple alpha process [24].

$$\left.\frac{\partial n_i}{\partial t}\right|_{\rho=const} = \sum_{j} N^{i}_{j} r_j + \sum_{j,k} N^{i}_{j,k} r_{j,k} + \sum_{j,k,l} N^{i}_{j,k,l}\, r_{j,k,l} \qquad (3.2)$$

Here the r's represent the rates of the reactions and the N's represent the number of nuclei created or destroyed by each reaction. The sign of N is positive if it represents the number for species that create i and negative if it represents a number for species that destroy i. For 1-nuclus reactions $N_i = N_i$, the number of particles of a reactant. For 2- and 3-nuclei reactions $N_i = N_i/\Pi\ |N!|$ and $N_i = N_i/\Pi\ |N!|$ The denominators in these cases are only greater than 1 when identical particles are involved in the reaction. For example, in the case of $^{12}C + ^{12}C = ^{24}Mg$, there are two identical reactants giving a denominator of 2, which is necessary to avoid double counting.

Number density changes in proportion to the density as an expansion or contraction of the reacting medium occurs. To split the hydrodynamic changes from the nuclear changes, we rewrite this equation in terms of abundance, *Y*, which is not affected by changes in density alone and has units of mol/g.

$$Y_i = \frac{n_i}{\rho \cdot N_a} \tag{3.3}$$

Where ρ is density and N_a is Avagadro's number.

Reaction rates are given in the following forms

$r_j = \lambda\,(T,\, n_e)\;\; n_j$ for one body interactions. (3.4)

$r_{ij} = n_i\, n_j < \sigma,\, \nu >_{j,k}$ for multiple body interactions. (3.5)

Given equations 3.3, 3.4 and 3.5, equation 3.2 becomes

$$\frac{\partial Y_i}{\partial t} = \sum_i N^i_j\; Y_j \lambda + \sum_{j,k} N^i_{j,k}\, \rho\, Na < \sigma, \nu >_{j,k} Y_j Y_k + \sum_{j,k} N^i_{j,k,l}\, \rho\, Na < \sigma, \nu >_{j,k,l} Y_j Y_k Y_l \tag{3.6}$$

Here λ is the rate of one particle interactions and $<\sigma, \nu>$ is the reaction rate for multiple body interactions, which is expressed as the product of the cross section and the relative velocity in the center of mass system, averaged over the appropriate distribution function. See the previous section for reaction rate derivations.

To find the overall change in each abundance, Y_i, for the outburst, the sum of the changes in Y_i over small increments of time is calculated. For the full set of nuclear abundances $\vec{Y}$, the derivative is written as a finite change in $\vec{Y}$.

$$\dot{\vec{Y}}(t + \Delta t) = \frac{\vec{Y}(t + \Delta t) - \vec{Y}(t)}{\Delta t} \tag{3.7}$$

The solution to this fully implicit equation can be found by finding the zeros of the following equation,

$$\vec{Z}(t+\Delta t) \equiv \frac{\vec{Y}(t+\Delta t)-\vec{Y}(t)}{\Delta t} - \dot{\vec{Y}}(t+\Delta t) = 0 \quad (3.8)$$

using the Newton-Raphson method .

A Taylor expansion of $\vec{Z}$ yields:

$$\vec{Z}(t+\Delta t) + \frac{\partial \vec{Z}(t+\Delta t)}{\partial \vec{Y}(t+\Delta t)} \Delta \vec{Y} + \text{Second order terms.} \quad (3.9)$$

The 2nd and higher order terms are neglected, thus,

$$\vec{Z}(t+\Delta t) = \frac{\partial \vec{Z}(t+\Delta t)}{\partial \vec{Y}(t+\Delta t)} \Delta \vec{Y} \quad (3.10)$$

and solving for $\Delta \vec{Y}$,

$$\Delta \vec{Y} = \left[\frac{\partial \vec{Z}(t+\Delta t)}{\partial \vec{Y}(t+\Delta t)} \right]^{-1} \vec{Z}(t+\Delta t) \quad (3.11)$$

where $\frac{\partial \vec{Z}}{\partial \vec{Y}}$ is the Jacobian of $\vec{Z}$.

The network program chooses the time step, Δt, for each iteration so that it is significantly smaller than the burning time scale for the most abundant species. Since burning time scales are proportional to abundance, this is done by setting the time increment equal to the burning time scale of one of the lesser abundant species. The network program iterates this equation until *Y(t+dt)* converges.

In principle, every isotope in the network is coupled through reactions to every other isotope in the network. This leads to a very dense Jacobian matrix $\partial Z/\partial Y$ that is computationally expensive to solve. However, there are several physical factors that limit the interrelation of the reactions considered by the network. For example, heavier isotopes must overcome a much greater Coulomb potential to bind with each other than do lighter isotopes. Therefore, at the temperatures present in novae and most astrophysical circumstances, capture reactions of free neutrons and light isotopes of hydrogen and helium dominate. In most cases, there are no more than twelve reactions for each isotope that relate it strongly to other isotopes. These reactions are captures of protons, neutrons, alpha particles or other nuclei, the emission of each of these different particles and beta decay reactions. Given this, the Jacobian matrix becomes not only very sparse, but also takes the form of a doubly bordered, band diagonal matrix [24]. The nuclear reaction network used for my project solved coupled equations for 169 isotopes involving 882 reactions.

Many nucleosynthesis calculations for novae have been done where the nuclear reactions were evolved under conditions of constant temperature and density. While this is an acceptable approximation to a point, in a real nova the temperature and density of the envelope are directly coupled to the nuclear reactions. The nuclear reactions generate the energy that drives the outburst and ejects the nova envelope into space, allowing it to cool and diffuse. At the same time, the rate of reaction between any two nuclei depends linearly on the density and exponentially on the temperature of the envelope [25].

A more physically accurate simulation would couple a full nuclear reaction network with multidimensional calculations of the temperature and density within the nova envelope. This kind of calculations is difficult and beyond the scope of the present investigation. To approximate this coupling, Starrfield and collaborators generated sets of 1-dimensional spherically symmetric hydrodynamic trajectories (temperature and density as a function of time) for several zones at different radii within the nova envelope [27]. Each zone represented a shell within the exploding envelope of the nova. Then separate nucleosynthesis calculations were done using the trajectory for each zone with a full nuclear reaction network to study the details of the nucleosynthesis [25].

CHAPTER 4

Procedure

The motivation for my project was to determine the influence of the new ORNL rate for the $^{17}F(p,\gamma)^{18}Ne$ reaction on nova nucleosynthesis. I carried out nucleosynthesis calculations with four different $^{17}F(p,\gamma)^{18}Ne$ rates to make a detailed determination of the difference produced in the nucleosynthesis by the four rates. To do this I ran calculations for all spatial zones that would be ejected by the outburst. I ran the nucleosynthesis calculations for a 1.35 $M_\odot$ WD nova, a 1.25 $M_\odot$ WD nova and a 1.00 $M_\odot$ WD nova. In the process I made modifications to the nuclear network code that did the nucleosynthesis calculations and wrote a suite of FORTRAN programs that analyzed the output of the network code.

I have already described the nuclear reaction network used for these calculations in previous sections but I have not described specifically my use of it. I will begin by describing the three main parts of the network I had to manipulate to generate data.

4.1 Reaction rate Library

The rate parameters for each of the four reaction rates were obtained from references [2],[3],[4] and [5]. A reaction rate library that contained all the rate parameters needed for the 882 reactions in the network was obtained from Thielemann and collaborators [28]. For the four $^{17}F(p,\gamma)^{18}Ne$ rates, we generated forward reaction rate parameters in the Theilemann et al reaction rate library format. Then a program called param.f was used to generate the reverse reaction rate parameters. Both forward and reverse reaction rate parameters are need for the nucleosynthesis calculations. The reaction rate library was copied to a separate directory for each of the four $^{17}F(p,\gamma)$ ^{18}Ne rates. The parameters for each of the four $^{17}F(p,\gamma)^{18}Ne$ rates were substituted into the proper place in the library in each directory. No other reactions were changed in the four reaction rate libraries.

From here on I will call the network with the ORNL rate for the $^{17}F(p,\gamma)^{18}Ne$ reaction in the reaction rate library the "ORNL case". Likewise, the networks with the Wiescher, Sherr and Garcia $^{17}F(p,\gamma)^{18}Ne$ reaction rates will be called the "Wiescher case", the "Sherr case" and the "Garcia case".

4.2 Hydrodynamic Trajectories

As stated in Chapter 3, the hydrodynamic trajectories give the temperature and density within each zone of the nova as a function of time. The interval between time steps is based on the size of the changes in abundance in the previous step of species with a total abundance less than 10^{-7} g/mol. The time between steps becomes smaller as the nova progresses toward the peak intensity of its outburst. Further discussion of this criterion for time step size selection will be discussed in section 4.7.

We chose to stop the calculation at 3600s or 1 hour after the peak intensity (highest temperature) of the simulated nova occurred. This is the earliest practical time that a real nova could be observed. Each of the trajectories gave temperatures and densities for many seconds beyond where we chose to stop the calculation. Discussion of how we picked the stop time will come later in this section.

Starrfield and collaborators generated trajectories for all zones in the nova. We only did calculations for the trajectories of the zones that would be ejected in the outburst. A representative sampling was done of the outer zones to limit the computations. This is a reasonable approximation because the outer zones are very similar to one another in temperature and density. This sampling consisted of all of the 10 innermost zones of the ejecta, then every other zone for the next 10 zones, and then every fourth zone for the last 8 zones. The sampling was denser for the inner zones because they differ more from one another in temperature and density than the outer zones.

Figures 4.1-4.3 show plots of the hydrodynamic trajectories for the 1.00 $M_{\odot}$ WD nova, 1.25 $M_{\odot}$ WD nova and the 1.35 $M_{\odot}$ WD nova. The highest temperatures and densities are reached in the 1.35 $M_{\odot}$ WD nova, followed by the 1.25 $M_{\odot}$ nova. However the 1.35 $M_{\odot}$WD nova also cools faster than the 1.25 or the 1.00 cases because it produces a faster, more violent explosion. This rapid cooling will play a large role in the difference between the nucleosynthesis done in the 1.35 case and the 1.25 case.

4.3 Initial Abundances

The network must begin the calculation with a set of initial abundances. The initial abundances for the 1.25 $M_{\odot}$ WD nova and 1.35 $M_{\odot}$ WD nova were adopted from Politano *et al.* 1995 [18]. They assumed a solar composition that was enhanced 50% by mass in oxygen, neon and magnesium. This enhancement was representative of the envelope material mixing with the oxygen, neon and magnesium rich matter from the underlying white dwarf. A 50% enhancement was chosen because it gave them the typical outburst energetics and final abundance patterns produced by ONeMg novae [18]. The initial abundances for the 1.00 $M_{\odot}$ WD nova was 50% solar and 50% enhanced by an equal mix of ^{12}C and ^{16}O with a trace of ^{22}Ne [29].

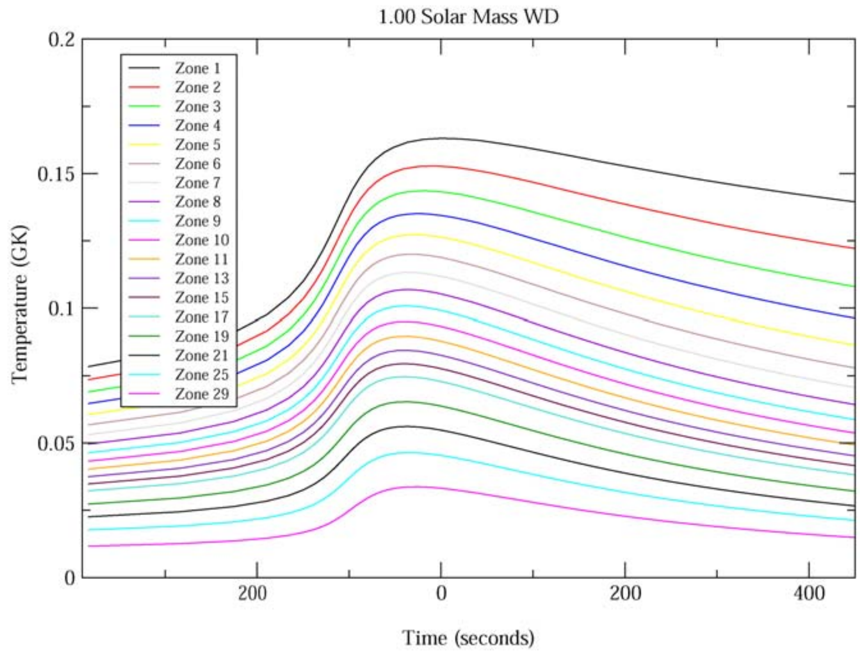

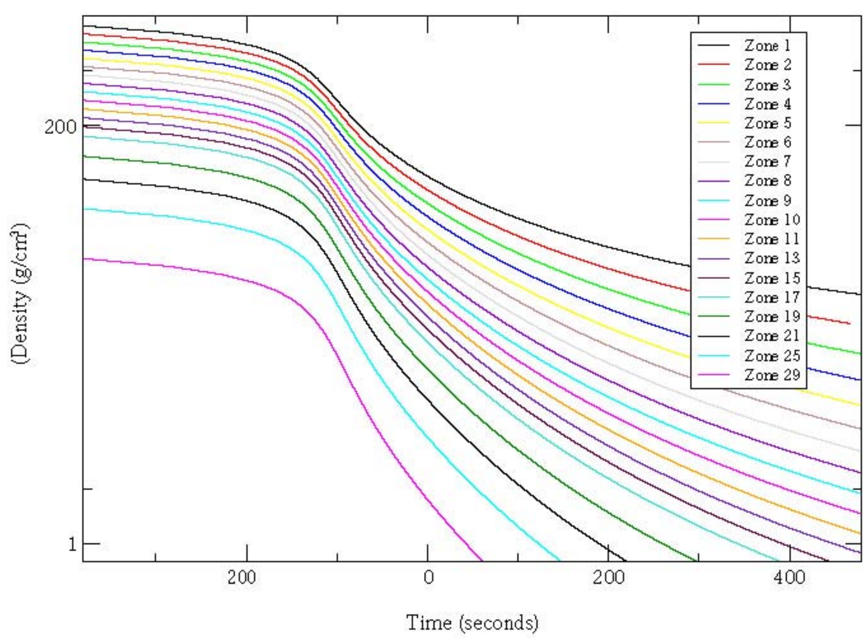

Figure 4.1 Thermodynamic Trajectory for 1.00 $M_\odot$ WD nova.

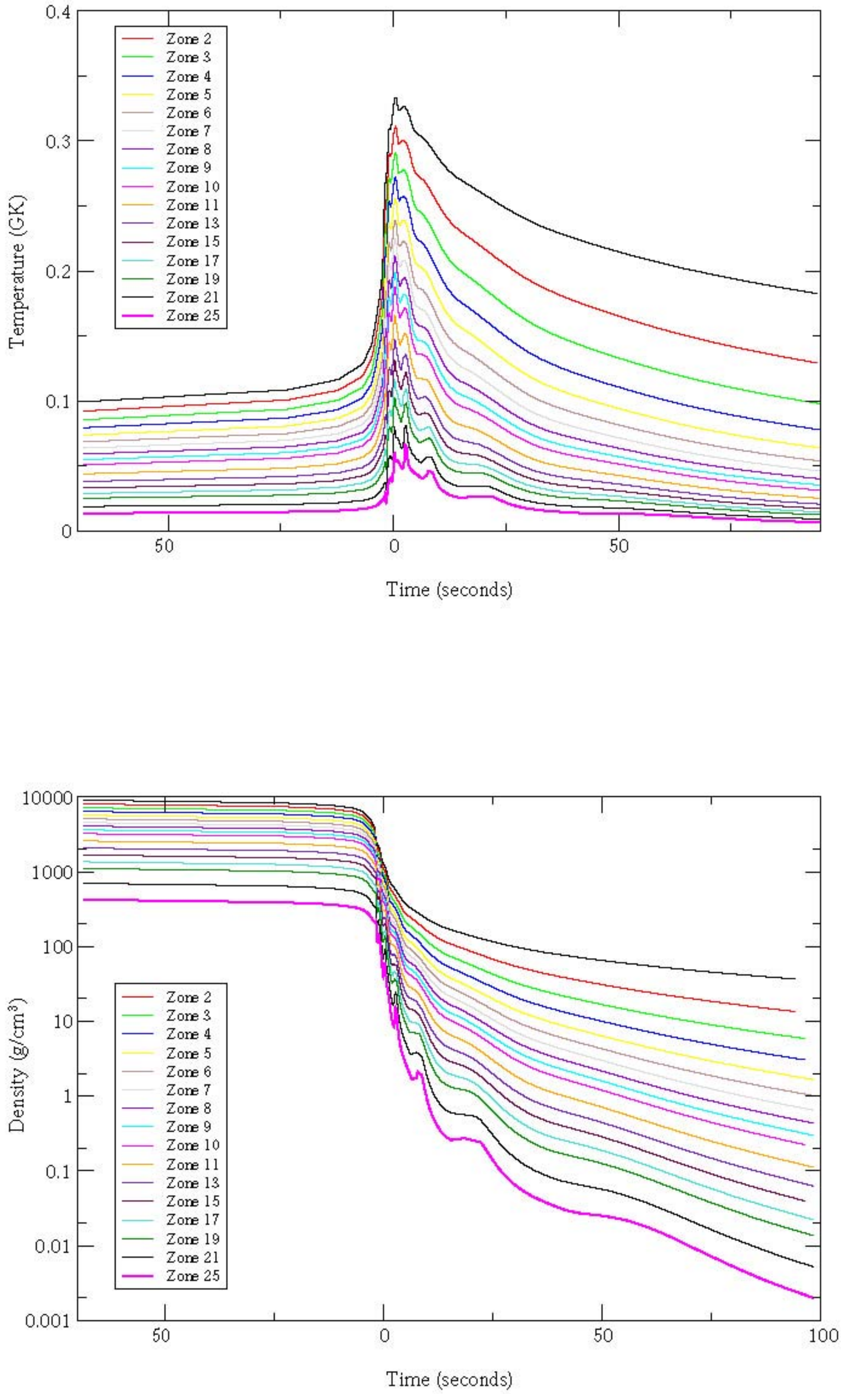

Figure 4.2 Hydrodynamic Trajectory for 1.25 $M_{\odot}$ WD nova.

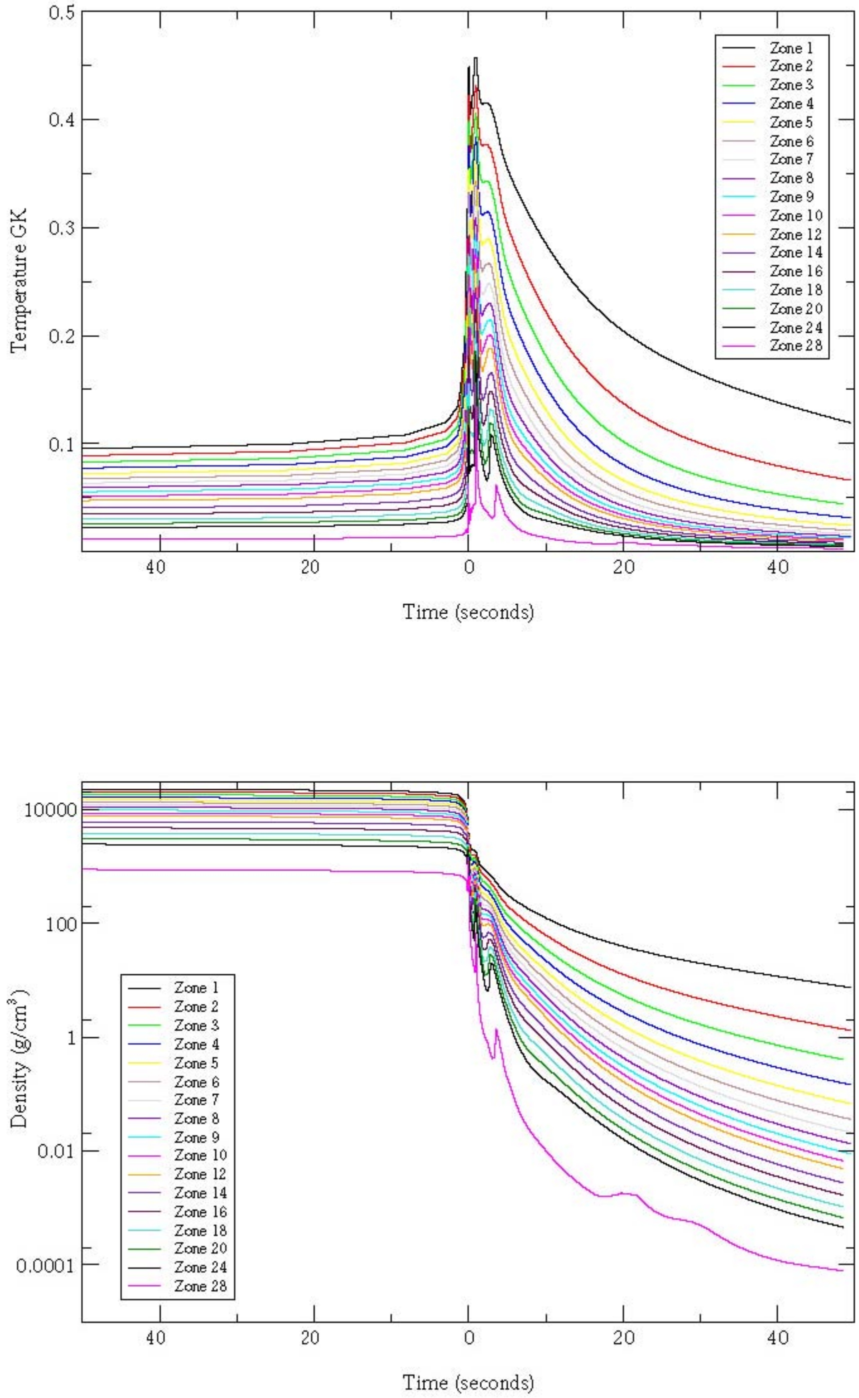

Figure 4.3 Hydrodynamic Trajectory for 1.35 $M_\odot$ WD nova.

4.4 Heavy Anomalies

I began by running the network for the hottest zone to get an abundance pattern for 87 isotopes, from hydrogen to sulfur, for each of the four rates. A program called diff.f had been written that gave the ratio of each isotope in one abundance pattern to another for one zone only. I used this to take the ratio of ORNL case abundance pattern to the Wiescher, Sherr and Garcia case abundance patterns.

I found that that the ORNL case produced up to 1000 times more of several isotopes than the Wiesher rate and up to 5% less than the Sherr or Garcia rates for these same isotopes. Perplexingly, several of the isotopes displaying anomalies were heavy isotopes like ^{39}Ar, ^{33}P, ^{35}S and ^{40}K. See figures 4.4-4.6 shown on pages 38-40. We did not expect the rate of $^{17}F(p,\gamma)^{18}Ne$ to have much effect in nova nucleosynthesis for isotopes this heavy. Before any further work was done, we decided to determine what was causing this.

The heavy isotopes in question occur near the end of the chain of reactions used by the network. Some of the reactions that produce them are coupled to reactions that are beyond the extent of the reactions in the network library. To make sure that there were not errors in their abundance caused by the lack of these later reactions, we extended the network to include169 isotopes, from hydrogen to chromium 54.

To ensure that the changes had been made correctly I compared the first 87 isotopes of the new longer abundance pattern for the ORNL case to the 87 isotopes of the old ORNL abundance pattern. They were consistent. When I took the ratio of the new larger abundance pattern for the ORNL case to each of the other cases' abundance patterns, I found that the same heavy isotopes were still present in approximately the same quantity.

The innermost zone of the 1.35 WD nova reaches a temperature of 0.44 GK at the peak intensity of the outburst. At temperatures above 0.4 GK the ORNL rate for $^{17}F(p,\gamma)^{18}Ne$ is 100 times slower than the Wiesher rate and just slightly faster than the Sherr and Garcia rates. Refer to figure 2.1 on page 23. The ratios for the heavy isotopes were much greater than one for the ORNL/Wiesher comparison and just slightly less than one for the ORNL/Sherr and ORNL/Garcia compressions. This suggested that there really was a correspondence between the rate of $^{17}F(p,\gamma)^{18}Ne$ and the abundance of these heavy isotopes.

We noticed isotopes, such as ^{13}C and ^{17}O, which were involved in free neutron producing reactions were affected in the same manner as the heavy anomalies were affected by the four rates. The heavily outliers could be produced by free neutrons capturing on the heavy stable isotopes which were present in the solar abundances that are part of the initial abundance profile. These heavy outliers have very low abundances. It would only take a small change in neutron abundance to greatly change the ratio between the abundances produced by two different rates.

To see if an increase or deficit in the number of free neutrons could be responsible for the heavy outlying isotopes, we looked at the integrated flux for each reaction. The integrated flux for a reaction shows the total amount of flow through that reaction during the entire network calculation. We found that the largest integrated flux involving free neutrons was for the reaction $^{17}O(\alpha, n)^{20}Ne$. We compared the ratio of the ORNL case to the Wiescher case for the four largest reaction fluxes involving free neutrons and found

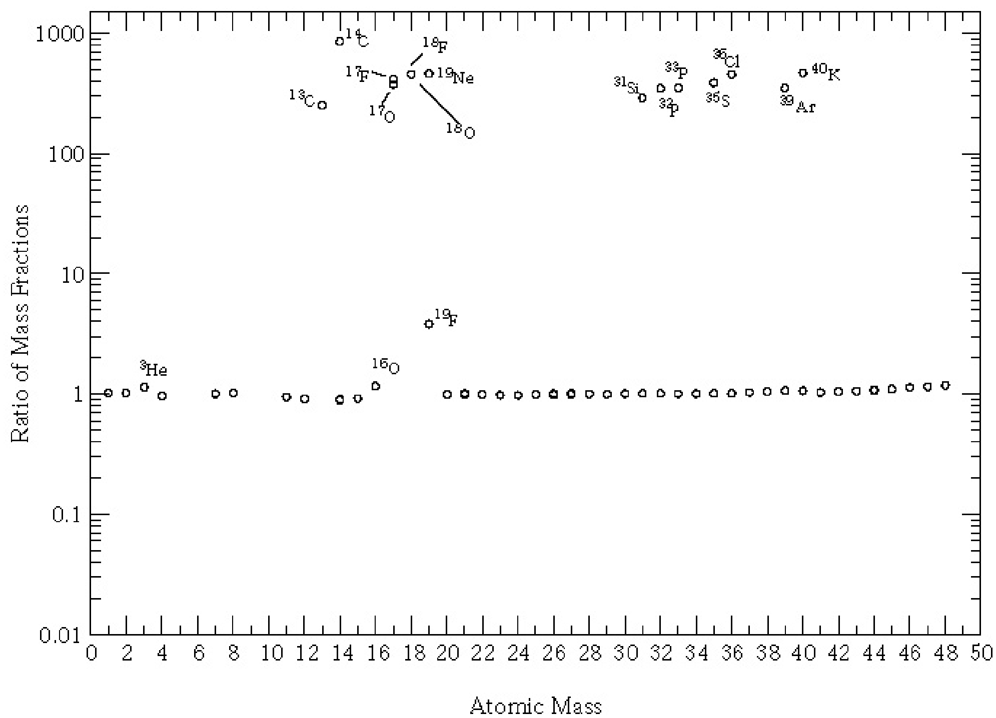

Figure 4.4 The abundance ratios for the ORNL case to the Wiescher case show that the ORNL case produces almost 1000 times more ^{31}Si, ^{32}P, ^{33}P, ^{36}Cl, ^{39}Ar, and ^{40}K.

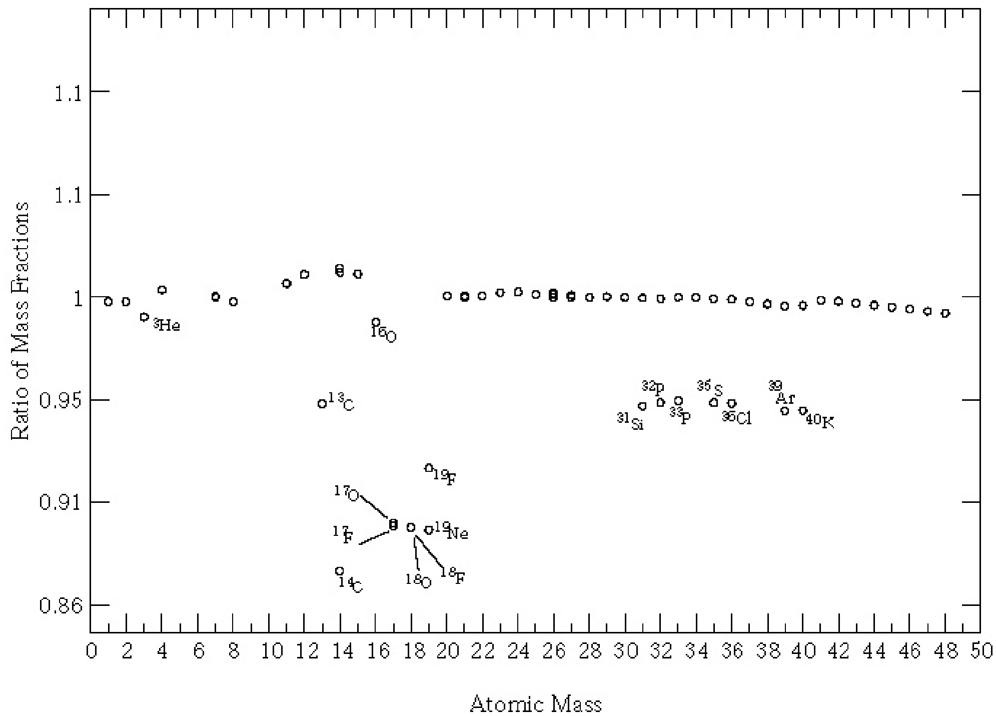

Figure 4.5 The abundance ratios for the ORNL case to the Sherr case show that the ORNL case produces 5% less ^{31}Si, ^{32}P, ^{33}P, ^{36}Cl, ^{39}Ar, and ^{40}K than the Sherr case.

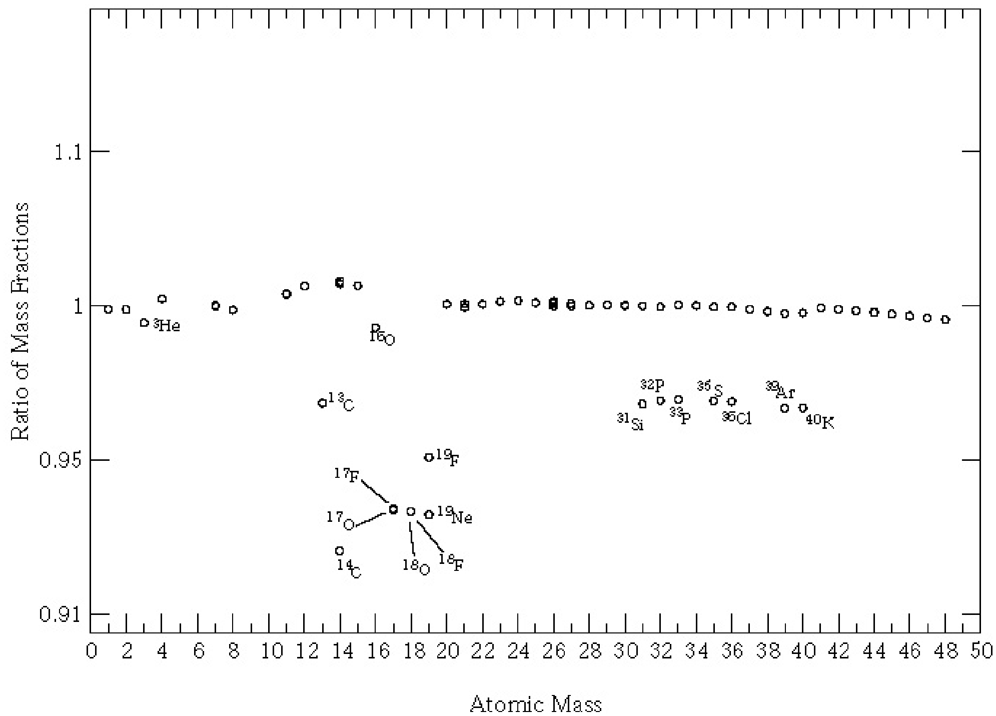

Figure 4.6 The abundance ratios for the ORNL case to the Garcia case show that the ORNL case produces 3% less ^{31}Si, ^{32}P, ^{33}P, ^{36}Cl, ^{39}Ar, and ^{40}K than the Garcia case.

that the flux $^{17}O(a,n)^{20}Ne$ was 6 times greater for ORNL than for Wiescher. Other free neutron reaction fluxes were increased for the ORNL case as well, but this was by far the largest. A similar comparison of the flux ratios for ORNL/Sherr and ORNL/Garcia showed that the flux of $^{17}O(\alpha,n)^{20}Ne$ was slightly less for the ORNL case than for the Sherr or Garcia cases.

To verify that a difference in the rate of the $^{17}O(\alpha,n)^{20}Ne$ reaction could cause the heavy outlying isotopes. I artificially increased the rate of $^{17}O(\alpha, n)^{20}Ne$ by a factor of 6 in the rate library that contained the ORNL rate and then ran the network to get an abundance pattern. The abundance ratio plot of the 6x $^{17}O(\alpha, n)^{20}Ne$ case to the ORNL case displayed in figure 4.7 shows the same pattern of heavy outlying abundances as the ORNL case to Wiescher case ratio plot in figure 4.4 on page 38, however the ratios were not as large. This was to be expected because $^{17}O(\alpha, n)^{20}Ne$ was not the only reaction flux that differed between the two rates as a source of free neutrons. Similar test were run that show that by decreasing the flux of 6x $^{17}O(\alpha, n)^{20}Ne$ to an abundance pattern similar to those of the ratio plots of ORNL/Sherr and ORNL/Garcia could be produced.

In the case of the ORNL and Wiescher rates, the ORNL rate's slower destruction of ^{17}F by the $^{17}F(p,\gamma)^{18}Ne$ reaction shifts the balance of reaction rates so that ^{17}F can more frequently beta-decay to ^{17}O. The increased amount of ^{17}O results in more free neutrons produced by the $^{17}O(\alpha, n)^{20}Ne$ reaction and therefore more of the heavy outlying isotopes. The destruction of ^{17}F by the Sherr and Garcia $^{17}F(p,\gamma)^{18}Ne$ reaction rates is slower than the ORNL rates. So for the Sherr and Garcia cases nucleosynthesis

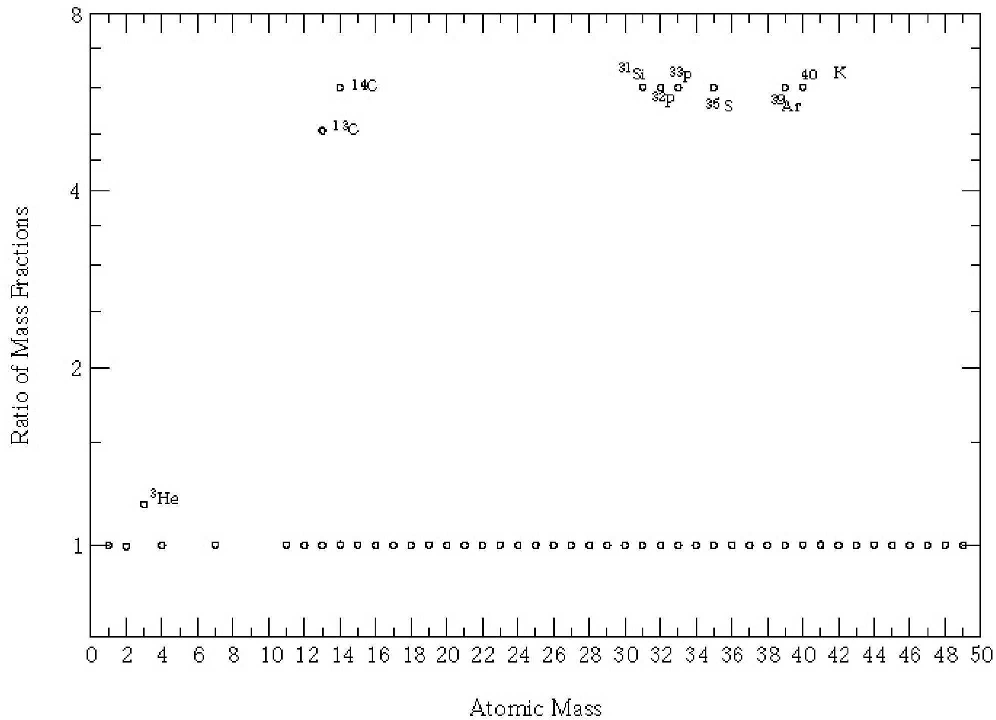

Figure 4.7 The rate of $^{17}O(\alpha, n)^{20}Ne$ was artificially increased by a factor of 6 in the rate library that contained ORNL rate and the network was run to generate an abundance pattern. The abundance ratio plot of the $6x^{17}O(\alpha, n)^{20}Ne$ case to the ORNL case shows the same pattern of heavy outlying abundances as the ORNL case to Wiesher case ratio plot in figure 4.4, however the ratios are not as large.

calculations produce more free neutrons than the ORNL case, and therefore a larger amount of the heavy outlying isotopes than the ORNL case.

These tests convinced us that the heavy outlying isotopes were caused by a change in the flow of free neutrons. However, later we noticed that there was almost no flux into ^{13}C. This circumstance produced a very low final abundance of ^{13}C. We found that the reaction rate for $^{13}N(p,g)^{14}O$ had been poorly fit for nova temperatures, so that the reaction rate was a factor of 10^{11} times too fast at nova temperatures. This prevented the primary reaction that creates ^{13}C, $^{13}N(\beta^{+}\nu)^{13}C$, from occurring because ^{13}N was depleted before it could decay to ^{13}C. A new more correct fit for the $^{13}N(p,\gamma)^{14}O$ reaction was obtained and used to generate the needed reaction rate parameters for this reaction in the rate library. The old $^{13}N(p,\gamma)^{14}O$ rate parameters were replaced by the new parameters in each of the four reaction rate libraries. The nucleosynthesis calculations were redone. The new calculations showed a significant increase in reaction fluxes involving ^{13}C and that a reasonable abundance of ^{13}C was produced. In contrast to the previous calculations, the new calculations showed that in a comparison between the ORNL case, and the Wiescher, Sherr or Garcia cases, the case with the faster $^{17}F(p,\gamma)^{18}Ne$ rate produced more ^{13}C.

The new calculations also showed that the abundance ratios for the heavy anomalies were diminished such that the Wiescher case produced only 2% more than ORNL case, while the ORNL case produced about 5% more than the Sherr case and 2% more than the Garcia case. In contrast to the previous calculations, the calculations done with the faster $^{17}F(p,\gamma)^{18}Ne$ rate produced less of the heavily anomaly isotopes that those done with the slower rate.

This can again be explained by the reaction fluxes involving free neutrons. The flux from $^{17}O(\alpha, n)^{20}Ne$, which was the largest source of free neutron in the old calculations, was still about 5 times greater for the ORNL case than for the Wiescher case. However, the increased reaction fluxes through ^{13}C in the new calculations allowed the reaction $^{13}C(\alpha,n)^{16}O$ to become a larger source of free neutrons than the $^{17}O(\alpha, n)^{20}Ne$ reaction. The Wiescher case has a slightly larger flux for the $^{13}C(\alpha,n)^{16}O$ reaction than the ORNL case because the Wiescher case produces more ^{13}C that the ORNL case. In the previous calculations, which used the incorrect $^{13}N(p,\gamma)^{14}O$ rate, there was no flux though $^{13}C(\alpha,n)^{16}O$ for the ORNL case, the Wiescher case, the Sherr case, and the Garcia case.

Also in the new calculations, the ORNL case had approximately 4 times more flux though the two largest neutron sink reactions, $^{17}F(n,\alpha)^{14}N$ and $^{17}F(n,p)^{17}O$. The ORNL case has a slower $^{17}F(p,\gamma)^{18}Ne$ reaction than the Wiescher case which allows more ^{17}F to survive to capture free neutrons. The previous calculation showed that the ORNL case flux was only 2.5 times greater for $^{17}F(n,\alpha)^{14}N$ and 3 times greater for $^{17}F(n,p)^{17}O$. Table 4.1 summarizes these results.

In summary, correcting the $^{13}N(p,\gamma)^{14}O$ reaction rate allowed more flux through ^{13}C which shifted the balance of reactions so that the production of free neutrons was similar for the ORNL, Wiescher, Sherr and Garcia cases. This also increased the differences in amount of free neutron captures on ^{17}F between the four cases. These two factors reduced the difference in the abundances of the heavy anomalies produced by the four cases and, in a comparison of the abundances produced by the ORNL case any of the other 3 cases, allowed the case the with faster $^{17}F(p,\gamma)^{18}Ne$ rate to produce more of the heavy anomaly isotopes.

4.5 Weighted Addition

There is little difference between the four $^{17}F(p,\gamma)^{18}Ne$ rates at the lower temperatures which are characteristic of the outer zones because the ^{18}Ne $J^{\pi}=3^{+}$ resonance has less effect on the rate at the lower temperatures. Refer to figure 2.1 on page 23. We were not sure if the changes in the $^{17}F(p,\gamma)^{18}Ne$ rate would have as profound an effect on the abundance pattern when all of the ejected zones on each nova were considered in the calculation as opposed to just the hottest zone.

To achieve a composite abundance pattern for all the ejected zones of the nova, I ran the network for each zone separately and then did a weighted addition of the abundances produced by each zone for each isotope. Starrfield *et al* [27] had determined the amount of mass enclosed in each zone. I determined a weighting factor for each zone by dividing its mass by the total mass of all the ejected zones,

$$Wi = \frac{m_i}{\sum_i^n m_i}$$

where m_i is the weight the *i*th zone and n represents the number of zones. I wrote a FORTRAN program to implement this weighed addition, which also converted the abundances to mass fractions by multiplying each isotopic abundance by its atomic mass.

Table 4.1 Largest Free Neutron Fluxes for the ORNL and Wiescher Cases.

Reaction	Flux Old ORNL case	Flux Old Wiescher case	ORNL / Wies. ratio	Flux New ORNL case	Flux New Wiescher case	ORNL / Wies. ratio
$^{13}C(\alpha,n)^{16}O$	0	0	0	3.73E-12	3.77E-12	0.989
$^{17}O(\alpha,n)^{20}Ne$	6.88E-13	1.37E-13	5.02	6.73E-13	1.34E-13	5.02
$^{17}F(n, \alpha)^{14}N$	2.99E-13	1.00E-13	2.99	3.77E-13	1.03E-13	3.66
$^{17}F(n,p)^{17}O$	1.18E-14	3.11E-15	3.79	1.43E-14	3.19E-15	4.48

The label 'Old' denotes fluxes which were calculated using the old incorrect fit for the $^{13}N(p,\gamma)^{14}O$ reaction rate, while 'New' denotes flux calculations done with the new correct fit for the $^{13}N(p,\gamma)^{14}O$ reaction rate. The largest source of free neutrons in the new calculation, $^{13}C(\alpha,n)^{16}O$, was nonexistent in the old calculation. The presence of this reaction diminished the differences in the abundances of the heavy anomaly isotopes produced by the ORNL, Wiescher, Sherr and Garcia cases.

4.6 Stop Time Determination

Before nucleosynthesis calculations could be run, a stop time needed to be picked for the calculation that worked well for all the zones. The earliest point that the calculation can be stopped is when the probability for all reactions other than decay in all zones of the nova is negligible. We actually want to stop at a time when the results could be compared to observations of real nova outbursts. The earliest observation this is feasible is about one hour after the outburst.

The probability for charged particle reactions to occur increases with temperature and density. The inner zones start out hotter and denser than the outer zones. They also cool and expand more slowly than the outer zones. As a result, capture reactions can occur for a longer period of time in the inner zones than in the outer zones. Since we are interested in the total abundance of each isotope produced at a given time after the peak intensity of the outburst, it is essential to stop abundance calculations for all zones at the same time. The capture reactions do not have much probability of occurring within the time scale of the nova after the temperature of the envelope has cooled below 0.01 GK. Also the fit for reaction rates in our reaction rate library was not reliable below this temperature [30].

The outer zone temperatures dropped below 0.01 GK long before the inner zone temperatures did. For temperatures lower than 0.006 GK, the Jacobian matrix used to evolve the abundances can become numerically singular due to the low or nonexistent rates of several capture reactions at this temperature. As a result, the network crashed in the outer zones long before the hottest zone could cool below 0.01 GK.

The last possible time that the coldest outer most zone would run before it crashed the calculation was just 120s after the peak intensity of the 1.25 $M_\odot$ WD nova and only 24s after the peak intensity of the 1.35 $M_\odot$ WD nova. At these stop times, the temperature in the hotter zones of the two novae was still as high as 0.02 GK and, therefore, the probability of reactions other than decays occurring was not negligible. While these stop times are too early to compare to observations, they do allow us to determine if changing the rate of $^{17}F(p,\gamma)^{18}Ne$ still had an effect on the abundance patterns when all zones of each nova were considered. We ran each nova with these stop times. Ratio plots showed that the difference caused by the $^{17}F(p,\gamma)^{18}Ne$ rate between composite abundance patterns was diminished when the cooler zones were included, but it was certainly still present in the 1.35 $M_\odot$ WD nova and 1.25 $M_\odot$ WD simulations. I did not run the 1.00 $M_\odot$ WD nova at this stage.

4.7 Network Modifications

To achieve a later stop time the network had to be modified so that the each zone ran calculations only for decay reactions after the temperature dropped below 0.01 GK. In this manner the inner zones would be allowed to run to suitable stop times while the outer zones ran only decays.

The network program calculates the reaction rates for the reactions at every step in the nova simulation. It then calculates the abundance produced for each isotope. For every step in the calculation these rates are recalculated to reflect the current thermodynamic conditions in the nova as described in chapter 3. An outer shell program controls the network calculation and reads in the initial abundances and the thermodynamic trajectory for the calculations for each zone. This shell also reads in control flags, which among other things, are used to set what kinds of reactions the network runs.

I modified the network to first integrate the abundances including the effects of strong, weak and electromagnetic reactions until the temperature dropped below 0.01GK, then perform a second integration utilizing only the weak reactions (radioactive decays) to reach the desired stop time. This required modifying the reaction rate calculations to ignore strong and electromagnetic reactions when required.

These modifications allowed the calculation for the entire nova to be run to the desired stop time of 1 hour after peak intensity. I chose the second hottest inner zone, zone 3, in the 1.25 $M_\odot$ WD nova to test the network modifications because it could be run out to 3000s after peak without crashing the original version of the network. For the first test I ran this zone with both the original and new versions of the network using the ORNL rate and a stop time that was 3000s after peak intensity. This test showed that there was no difference for most isotopes. However there was a difference of to up to 2% for ^{13}N,^{14}O,^{15}O,^{17}F and ^{30}P. See the uppermost plot in figure 4.8.

I wanted to isolate the cause for this difference so I tested to see if just running the calculations in two steps was responsible for the difference. This was done by running a version of the network that also performed the integration in two parts but did not turn off any reactions. I will call this version the two-step version from now on to distinguish it from the new and original versions of the network. I ran the two-step version for zone 3 and then compared its abundance pattern to the patterns produced by the new and original versions of the network. See Figure 4.8.

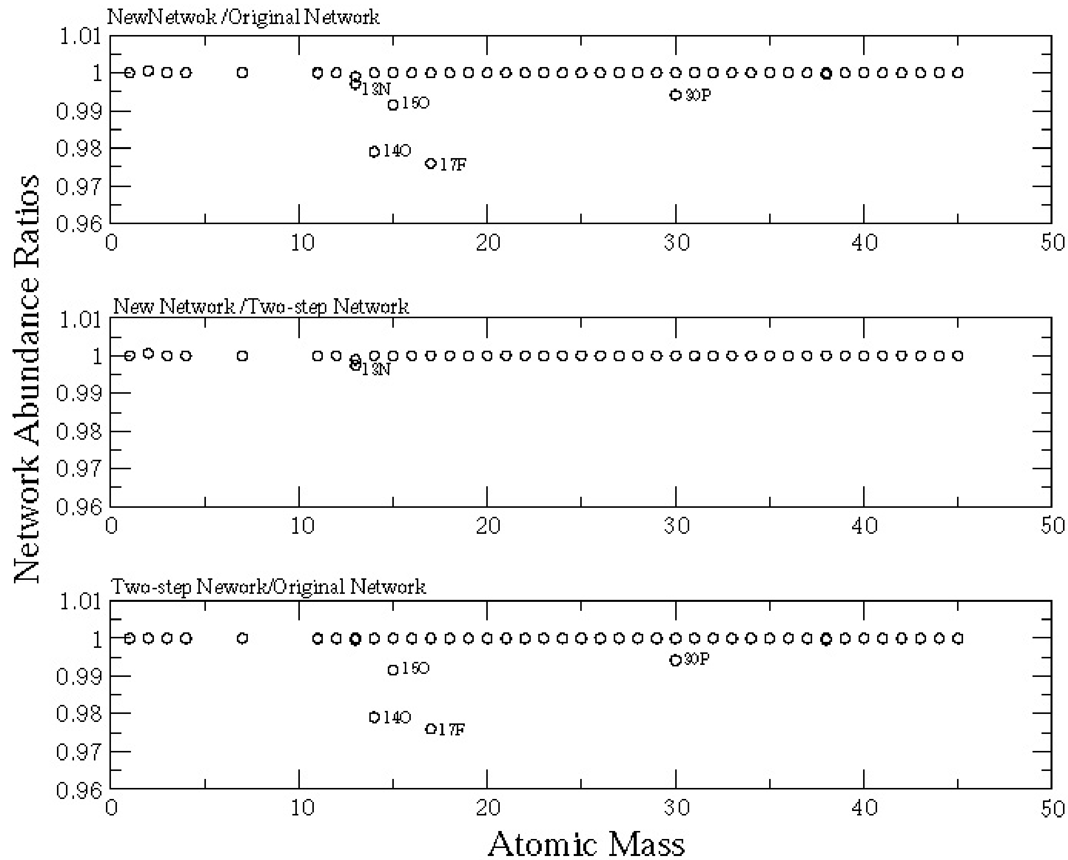

Figure 4.8 These ratio plots compare the abundances produced by one version of the network to another as labeled at the top of each plot. The uppermost plot shows up to 2% difference in abundances produced by the new and original version of the network. The small difference between abundances in the middle plot and lower plot's similarity to the uppermost plot show that the difference results mainly from running the calculation in two steps rather than from turning the strong interaction off. The time-step abundance cut off was set at 10E-7 g/mol for these plots.

For all isotopes other than ^{13}N the difference resulted only from running the calculation in two steps. Further tests showed that the differences in abundances produced by the one part and two-part integration increased the longer the second part of the calculation ran.

When the network starts the second integration of the calculation, it resets the time increment between steps. The time increment between steps must build back up over several steps to the value it had at the end of the first part of the calculations. These are extra steps compared to the number of steps the network runs to get to the same point if the calculation is done in one continuous integration. The nucleosynthesis done during these extra steps could be responsible for the small variations. To see if this caused the difference, comparisons between ratios taken of the two-step network to the original network were made at a stop time that was only a few seconds after the beginning of the send part of the caution and a stop time that was 3000 seconds after the beginning of the second part of the calculation.

If the extra steps at the beginning of the second integration were responsible for the difference, that the ratio produced by the earlier stop time would be almost identical to the ratio of the abundances at the later stop time. This was not the case. The later stop time ratio showed more difference than the earlier stop time ratio. This indicated that the difference was building up over the second part of the calculation rather than occurring at the beginning.

The network program was written so that it did not consider the reaction rates of isotopes with abundances below a certain value for calculation of the size of the time increment between steps. Previously, we had this minimum value set to $1E^{-7}$. The accuracy of the network is less for abundances below this threshold, since these abundances maybe evolved over a time step longer than their characteristic time. The network was not sensitive enough to the lower abundances of the decaying isotopes at the later stop time and this was causing random errors. We set the network so that it would consider abundances of a lower minimum value, $1E^{-10}$, for the calculation of the time increment between steps. A ratio comparison of the original network's abundance pattern at later stop time to the two-step version's abundance pattern was made that showed a considerably reduced difference between the abundance patterns. Figure 4.9 shows that the greatest difference was 0.5%. This was well beyond the level of precision of the results given the uncertainties in the calculation.

In the following sections, we will present the results of simulations run with the $1E^{-10}$ abundance threshold. The successful modified version of the new network was implemented for the 1.35, 1.25 and 1.00 $M_{\odot}$ WD novae. All the zones were run for each nova model. The data were processed and mass fraction ratio plots were made for ORNL/(other rate) for all rates in each model.

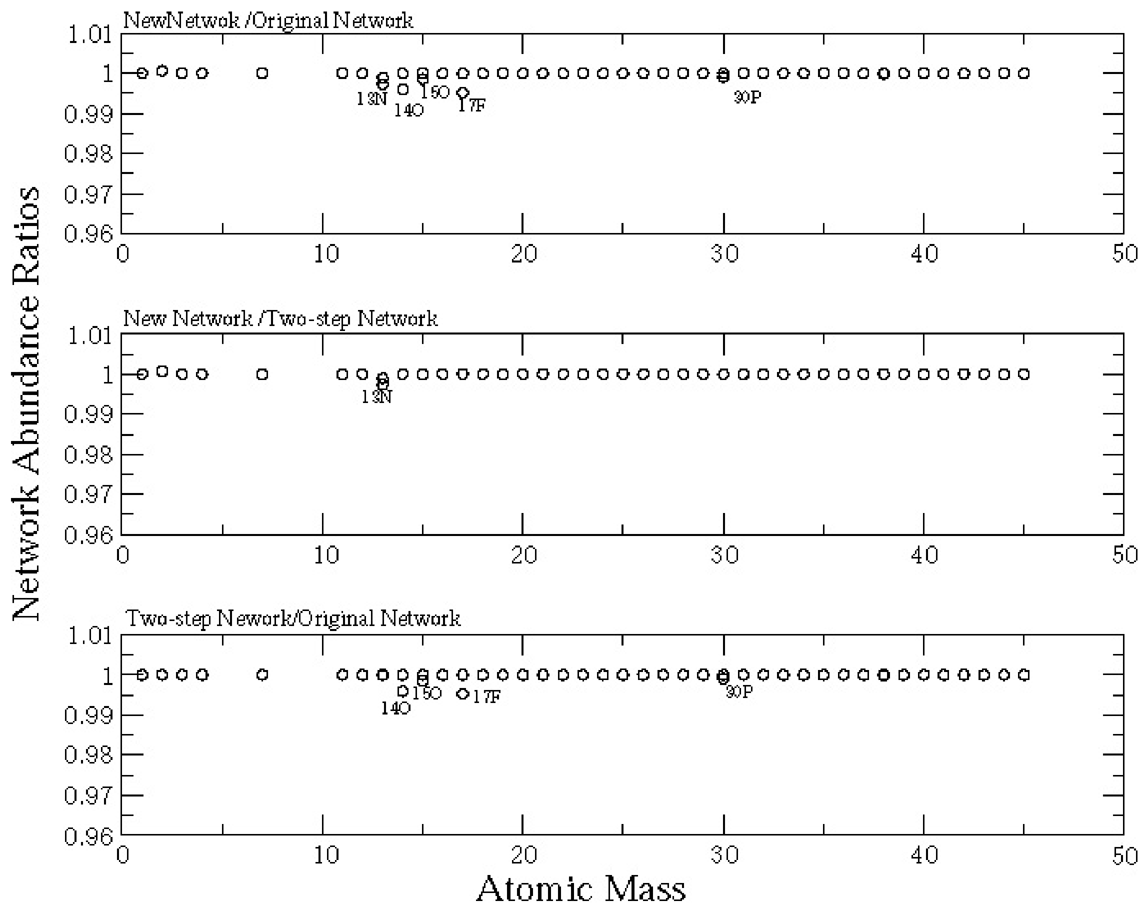

Figure 4.9 The time-step abundance cut off was set at 10E-10 g/mol for the abundances shown in these plots. Compared to figure 4.8, these plots show a greatly reduced difference in the abundances produced by different versions of the network.

CHAPTER 5

Results

Our nucleosynthesis calculations based on improved nuclear physics input will be an improvement over those based on older nuclear physics input. Additionally, we find quantitative differences when using the new input, which we detail in this chapter.

The two likely fates for ^{17}F in novae are shown in figure 5.1. It can capture a proton to become ^{18}Ne or it can beta decay to ^{17}O with a half-life of 64.49s. Most often ^{18}Ne beta decays to ^{18}F with a half-life of 1.672s [21]. ^{18}F can capture a proton to form a compound state that either emits a ^{4}He nucleus (also called an alpha particle) to become ^{15}O, which beta decays with a half-life of 122.24s to ^{15}N, or emits a gamma ray to become ^{19}Ne, which decays with a half-life of 17.22s to ^{19}F [21]. ^{18}F can also beta decay to ^{18}O by with a half-life of 109.77 minutes [21]. For the ^{17}F($\beta^{+}\nu$)^{17}O path, ^{17}O is stable but it can capture a proton to become ^{18}F and then follow through the reactions described above or it can capture a proton and emit an alpha particle to become ^{14}N, which can capture a proton to become ^{15}O which then decays to ^{15}N.

The Wiescher rate for ^{17}F(p,γ)^{18}Ne is as much as 30 times faster than the ORNL rate at nova temperatures. This leads to the hypothesis that the ORNL rate will produce a greater mass fraction of ^{17}F and ^{17}O by the end of the nova simulations, while the Wiescher rate will produce a larger mass fraction of ^{18}F than the ORNL rate, since ^{18}F is the direct decay product of ^{18}Ne. The ORNL rate is slightly faster than the Sherr or Garcia rates at nova temperatures, so one would expect to see reversed and diminished

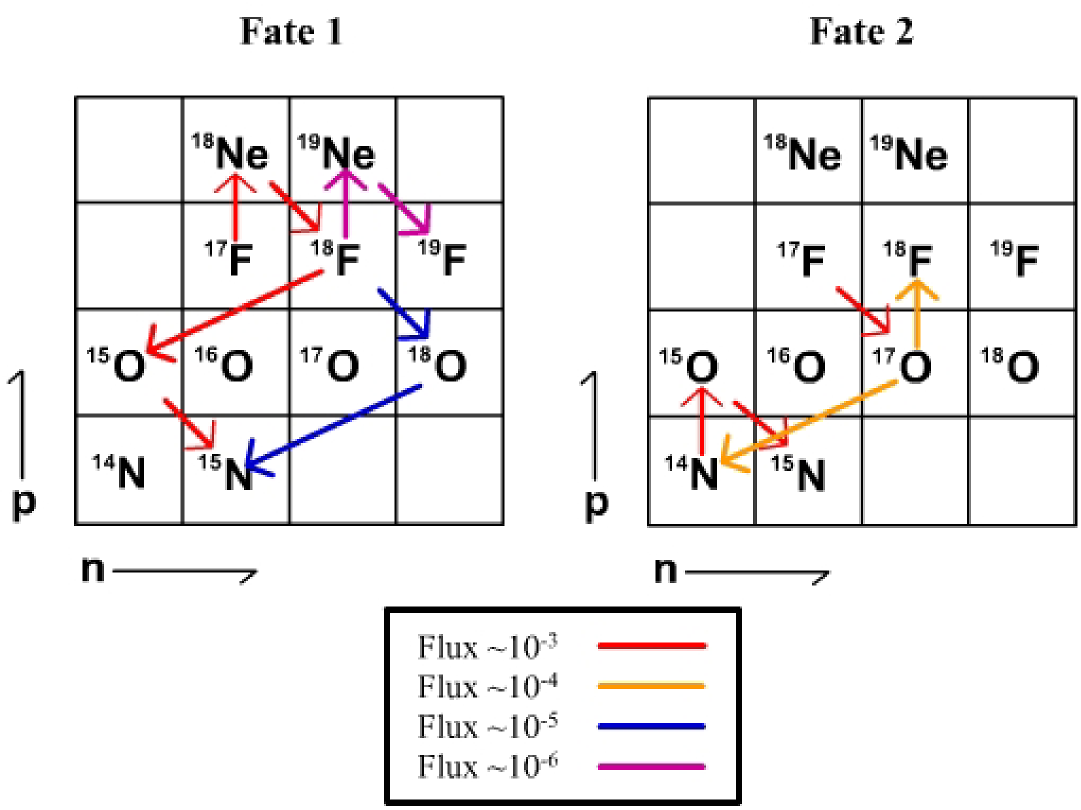

Figure 5.1 Two fates of ^{17}F in novae.

versions of what was said above for the mass fractions of ^{17}F, ^{17}O and ^{18}F produced by those rates when compared to their production by the ORNL rate.

5.1 Novae Simulations on a 1.25 $M_\odot$ ONeMg WD

I begin with the 1.25 $M_\odot$ WD nova. Figures 5.2 and 5.3 are plots of the ratio of mass fractions produced by the network with the ORNL $^{17}F(p,\gamma)^{18}Ne$ rate to the mass fractions produced by the network with the Wiescher $^{17}F(p,\gamma)^{18}Ne$ rate. The ratio of the mass fractions for each isotope is plotted against atomic mass. Figure 5.2 is a composite weighted average of all the zone contributions to the mass fraction of each isotope. Figure 5.3 is just the mass fractions generated by the inner (hottest) zone. The hottest zone plot is shown because this zone is the largest zone by mass and our simulation shows that it does the most nucleosynthesis. It is also believed that the inner hotter zones may play a bigger role in the overall mass fraction pattern of the nova when zone mixing is taken into consideration.

In the weighted average plot, figure 5.2, the mass fractions of ^{14}N, ^{15}N, ^{17}F, ^{17}O, ^{18}F, ^{18}O and ^{19}F are changed by up to a factor of 2. For the hottest inner zone the mass fractions of ^{17}F, ^{17}O, ^{18}F and ^{18}O differ by as much as a factor of 600. In both cases the ORNL rate results in more ^{17}F and ^{17}O than the Wiescher rate, as expected. But the ORNL rate also produces more ^{18}F and its decay product, ^{18}O, than the Wiescher rate. This contradicted our expectations and prompted weeks of verifying the programs written to do the analysis and the modifications made to the nuclear reaction network. No significant errors were found in these programs.

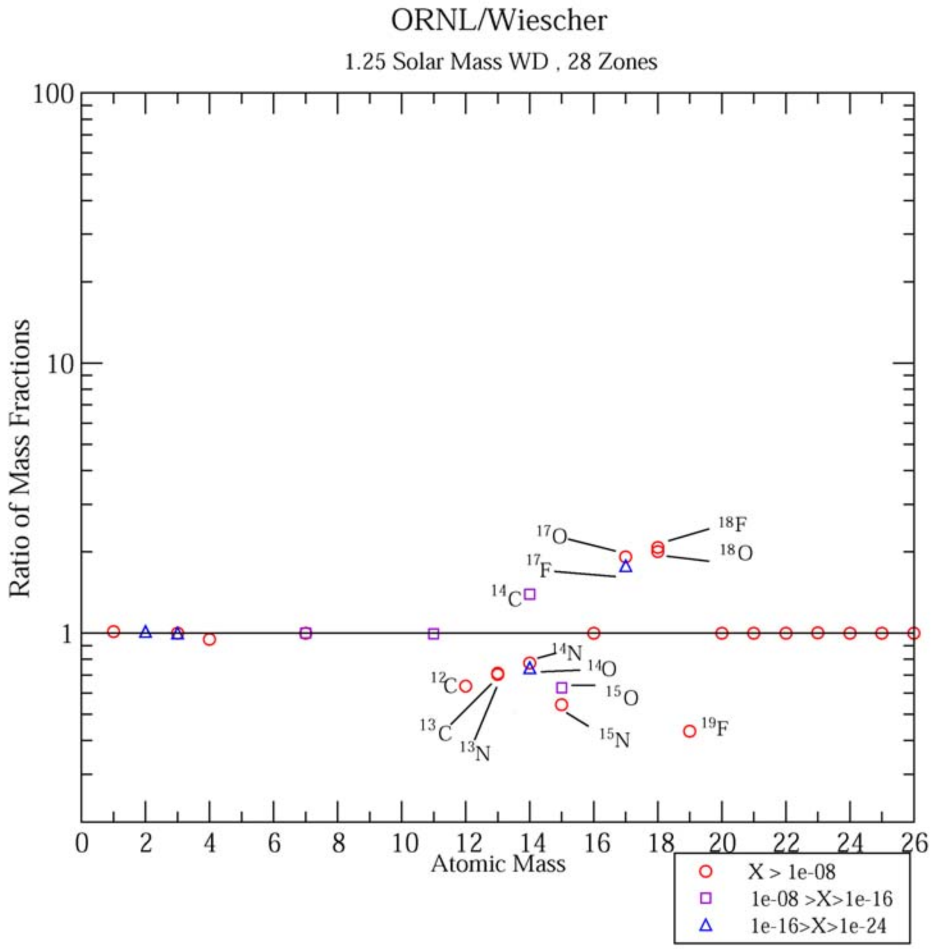

Figure 5.2 The ratio of the ORNL case to the Wiescher case of the mass fractions from the composite weighted average of all the zones ejected by the 1.25 $M_{\odot}$ WD nova.

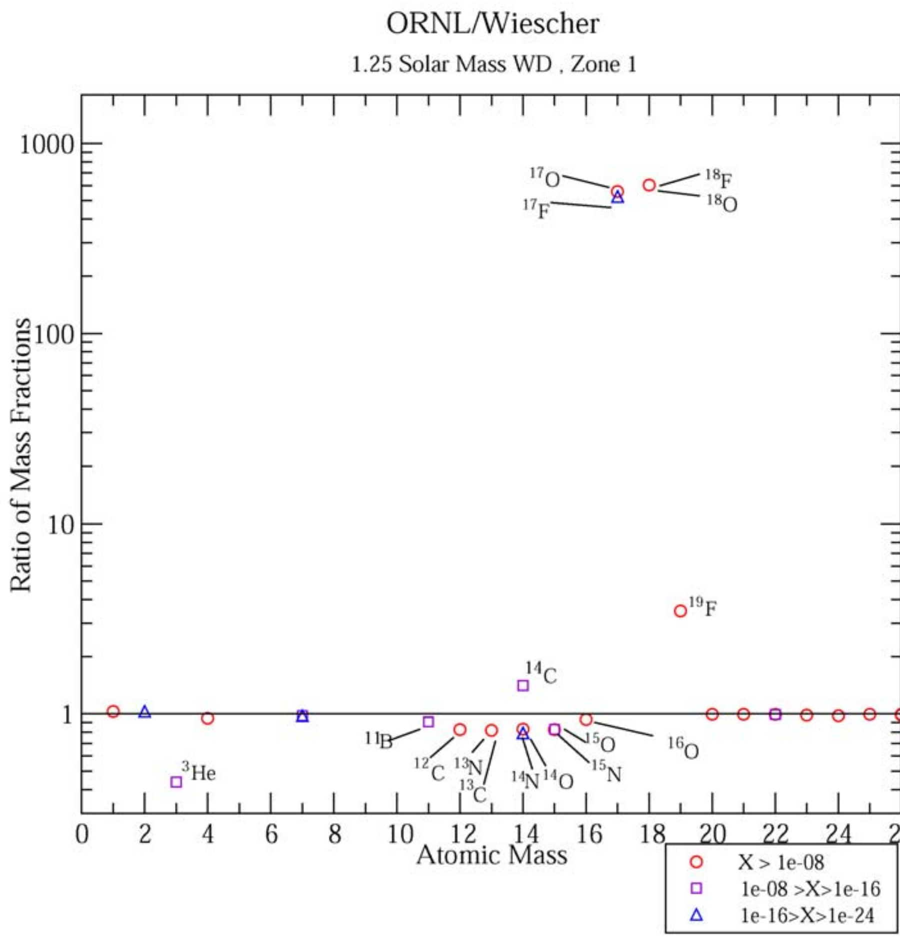

Figure 5.3 The ratio of the ORNL case to the Wiescher case of the mass fractions from the hottest zone ejected by the 1.25 $M_{\odot}$ WD nova.

Figure 5.4 shows a zone by zone analysis of the ^{18}F production in the 1.25 $M_\odot$WD nova. From this we see that the ORNL rate produces much more ^{18}F than the Wiescher rate for the 3 innermost zones of the nova. For the rest of the zones the Wiescher rate produces slightly more ^{18}F than the ORNL rate. To explore this, the abundance as a function of time is plotted for ^{15}O, ^{17}O, ^{17}F, ^{18}F, ^{18}Ne and ^{19}F for zone 2, figure 5.5, and zone 5, figure 5.6. In these plots, the solid lines represent the abundance produced by the ORNL case and the dashed lines represent the abundance produced by the Wiescher case.

Zone 2 (figure 5.5) is an example of the case for overproduction of ^{18}F by the ORNL case. A careful study of this plot reveals that the production of ^{18}F happens in two phases. In the first phase, which shall be called the peak phase because it occurs during the peak temperatures of the nova, the production of ^{18}F is dominated by $^{17}F(p,\gamma)^{18}Ne(\beta^+\nu)\ ^{18}F$. In the second phase, which shall be called the expansion phase, production of ^{18}F is dominated by $^{17}F(\beta^+\nu)^{17}O(p,\gamma)^{18}F$.

The peak phase occurs around the peak temperature of the nova and lasts for about 20 seconds after the peak. The end of this phase comes when the abundance of ^{17}O becomes greater than the abundance of ^{18}Ne. Figure 5.5 shows that the peak phase lasts a bit longer with the Wiescher rate than with the ORNL rate. At peak temperatures for this zone in the 1.25 $M_\odot$ case, the Wiescher rate of $^{17}F(p,\gamma)\ ^{18}Ne$ is 30 times faster than the ORNL rate. Immediately following the outburst, the Wiescher rate produces much more ^{18}Ne and therefore more ^{18}F than the ORNL rate. In so doing, the Wiescher case depletes the supply of ^{17}F more completely than the ORNL case. About 7 seconds after the peak temperature, the Wiescher rate results in 300 times less ^{17}F than the ORNL rate. Due to

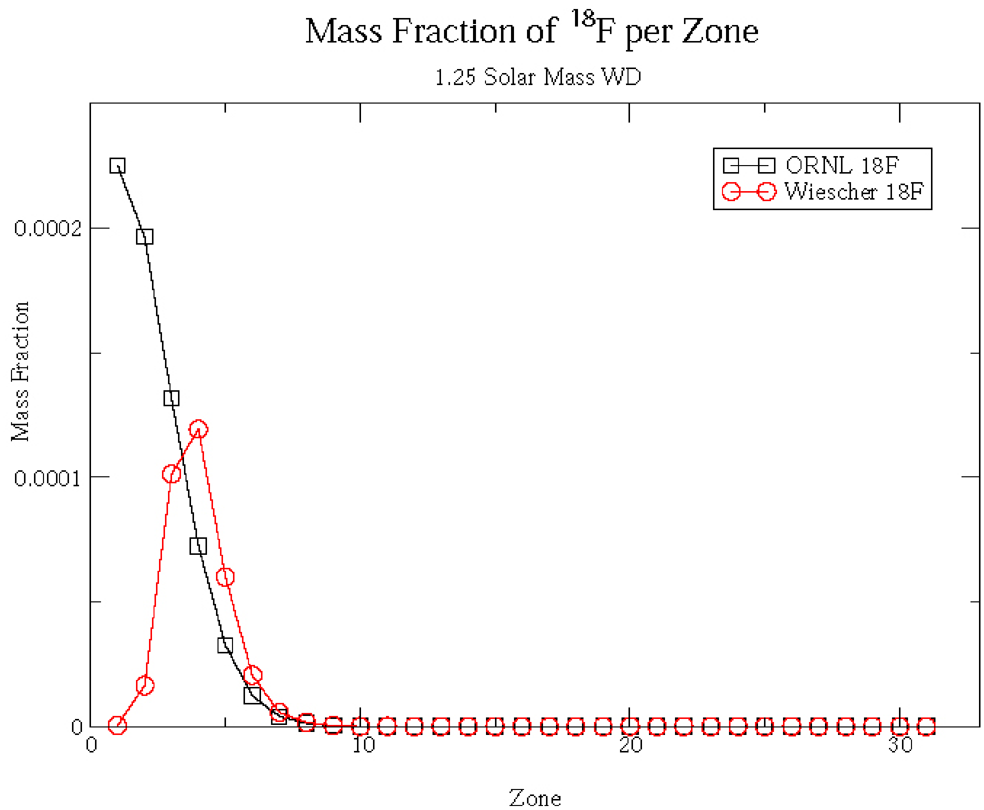

Figure 5.4 A zone by zone analysis of the ^{18}F production in the 1.25 $M_{\odot}$WD nova.

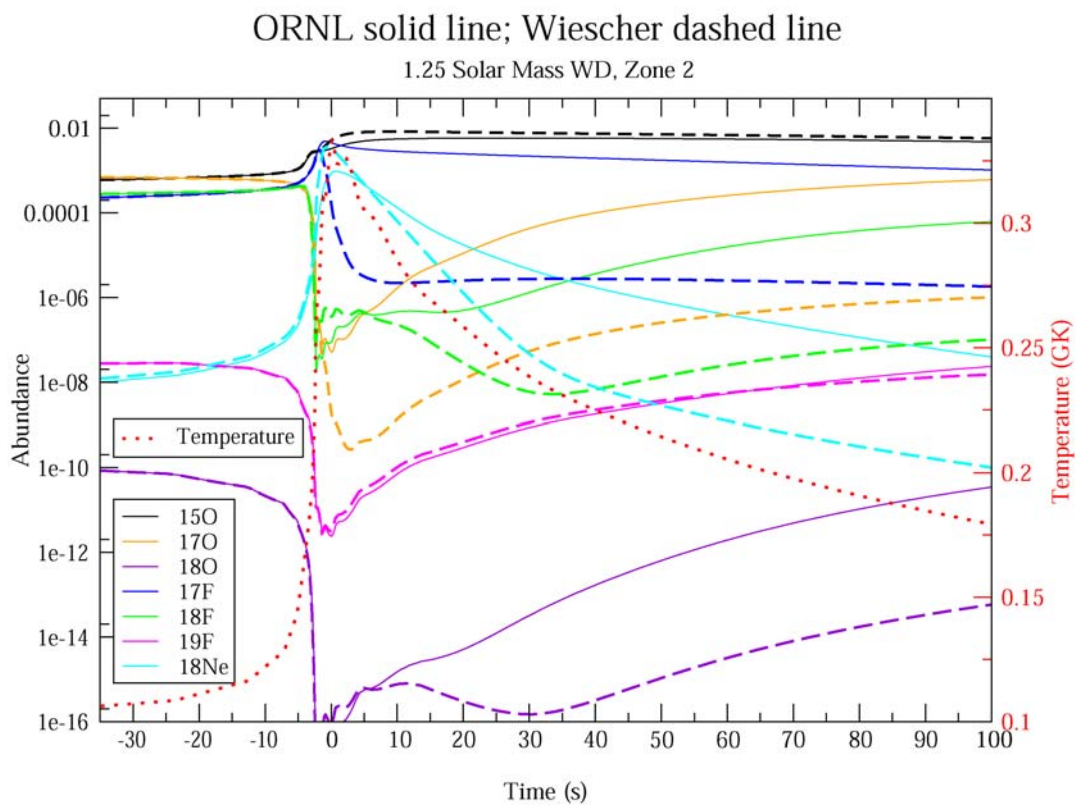

Figure 5.5 Abundance plotted as a function of time for Zone 2 of the 1.25 $M_\odot$ WD nova.

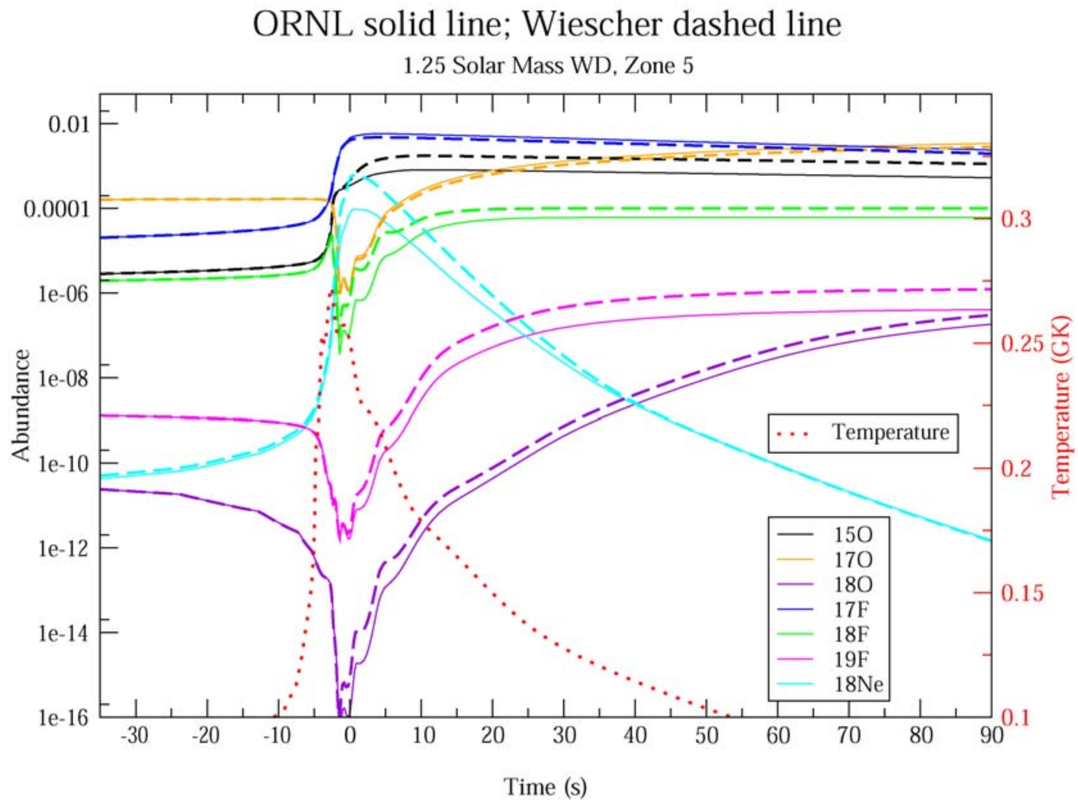

Figure 5.6 Abundance plotted as a function of time for Zone 5 of the 1.25 $M_\odot$ WD nova.

this depletion, the ORNL rate's production of ^{18}Ne (Cyan line) overtakes the Wiescher rate's production at a later time. After this time, the production of ^{18}F which results from the ORNL rate also overtakes the ^{18}F production that results from the Wiescher rate.

Also in this phase we see that the mass fraction of ^{17}O drops for both the ORNL and Wiescher cases, but much more for the Wiescher case than for ORNL case. The drop in ^{17}O for both is due to $^{17}O(p,\gamma)^{18}F$. The Wiescher case's over-depletion can be explained by the fact that even though the half-life of $^{17}F\ (\beta^{+}\nu)^{17}O$, 64.49s, is long compared to the 20 second duration of the peak phase, the ORNL case's large over-abundance of ^{17}F accelerates the effective rate of ^{17}O production by the decay.

The temperature in the peak phase for this zone drops from 0.33 GK, at peak, to 0.14 GK. These high temperatures allow a large portion of the ^{18}F created to capture a proton and emit ^{4}He, producing ^{15}O (black line). In figure 5.5 on page 61, starting at peak temperature the Wiescher case produces more ^{15}O than the ORNL case. As the peak phase draws to an end, production of ^{15}O in the ORNL case almost catches up to the Wiescher case's production but does not overtake it, despite the substantial excess of ^{18}F over the Wiescher case. This can be explained by the declining temperature.

The expansion phase begins about 20 seconds after peak and occurs over a temperature range of 0.14 GK to 0.01 GK. In this phase ^{18}F production is dominated by $^{17}F\ (\beta^{+}\nu)^{17}O(p,\gamma)^{18}F$. Graphically this can be seen in figure 5.5 on page 61 when the cyan line that represents the ^{18}Ne abundance drops below the gold line that represents the ^{17}O abundance. The ORNL case starts this phase with 300 times more ^{17}F than the Wiescher case and 300 times more ^{17}O. Thus the ORNL case has a big head start in ^{18}F production over the Wiescher case during the hottest temperatures of the expansion phase. During this phase we see that the ^{18}F build up follows the build up of ^{17}O by noting that the shape of the green lines that represent ^{18}F parallels the gold lines that represent ^{17}O. Also in this phase there is little change in the abundance of ^{15}O. This is because the temperature is lower in this phase, allowing more ^{18}F to survive as ^{18}F and its decay product ^{18}O instead of capturing a proton.

Zone 5, figure 5.6 on page 62, is an example of overproduction of ^{18}F by the Wiescher case. The peak temperature of this zone is only 0.257GK, making it a much cooler than zone 2. The temperature also drops more rapidly in this zone than in zone 2. The depletion of ^{17}F is much less for both the ORNL and Wiescher cases and there is little difference between the amount of ^{17}F depleted by the two rates. The Wiescher rate produces more ^{18}Ne than the ORNL rate throughout the peak phase because it never depletes its ^{17}F source. By the end of the peak phase, the temperature is so low that the ^{17}F which has decayed to ^{17}O mostly survives as ^{17}O, with few proton captures to ^{18}F. In this zone and the rest of the outer cooler zones, the early overproduction of ^{18}Ne and ^{18}F by the Wiescher case dominates throughout the nova.

Figures 5.7 and 5.8 are mass fraction ratio plots of ORNL/Sherr for the 1.25 $M_{\odot}$WD Nova. Figure 5.7 is the composite mass fraction plot for all the zones and figure 5.9 is the hottest innermost zone only. Figures 5.9 and 5.10 are mass fraction ratio plots of ORNL/Garcia for the 1.25 $M_{\odot}$WD Nova. Figure 5.9 is the composite mass fraction plot for all the zones and figure 5.10 is the hottest innermost zone only. The nucleosynthesis for these rates is discussed at the same time because both the Garcia and

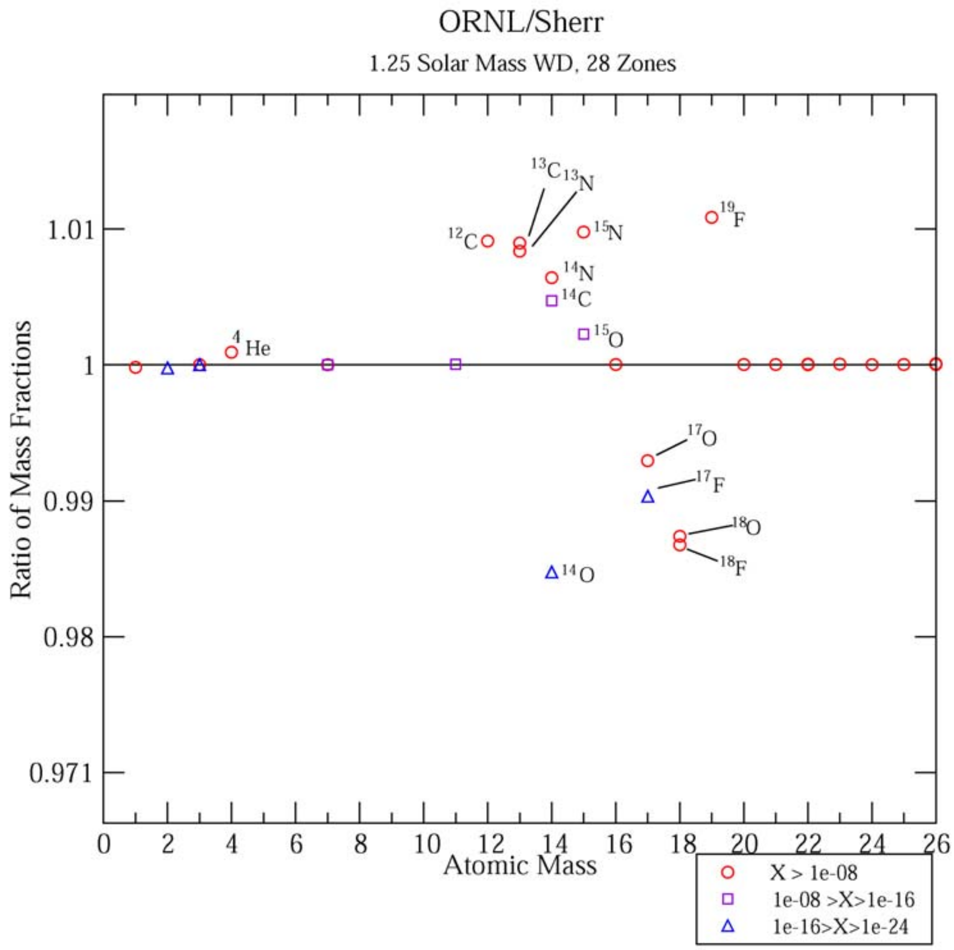

Figure 5.7 For the composite of all the zones ejected by the nova, the comparison of the ORNL case mass fractions to the Sherr case mass fractions shows differences of up to 1.6%.

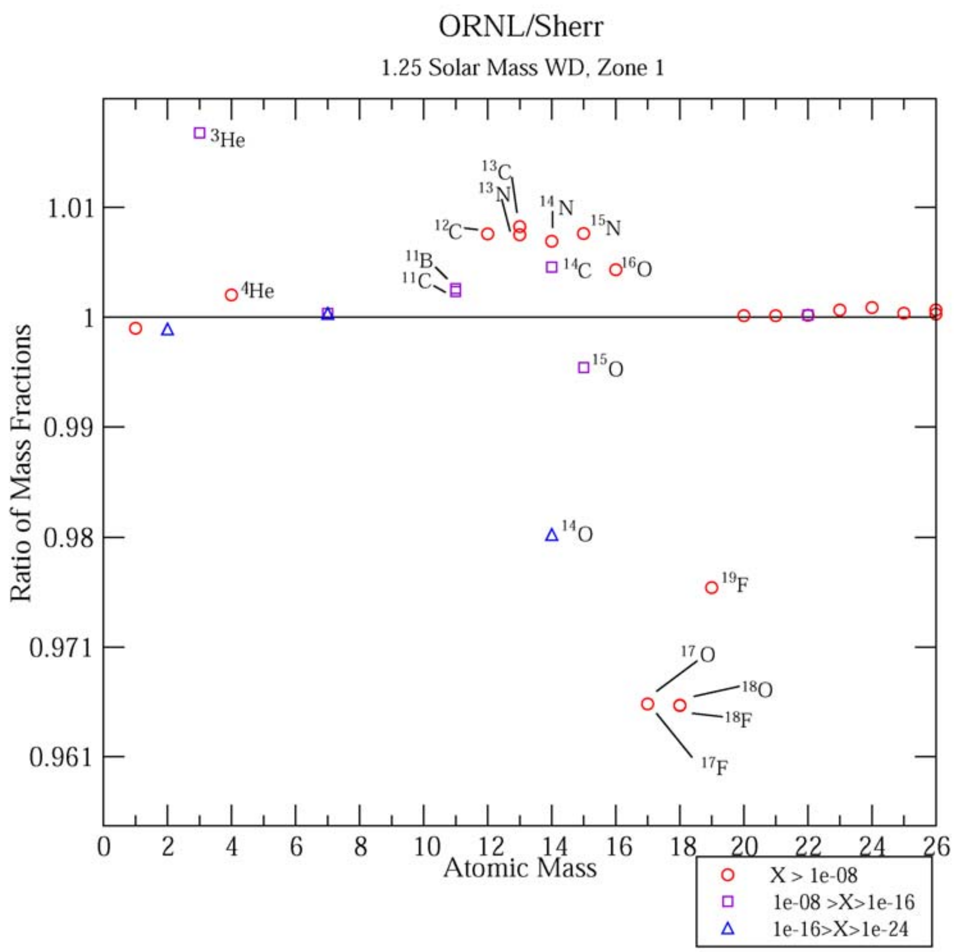

Figure 5.8 The comparison of the ORNL case mass fractions to the Sherr case mass Fractions show differences of up to 6% for the hottest zone.

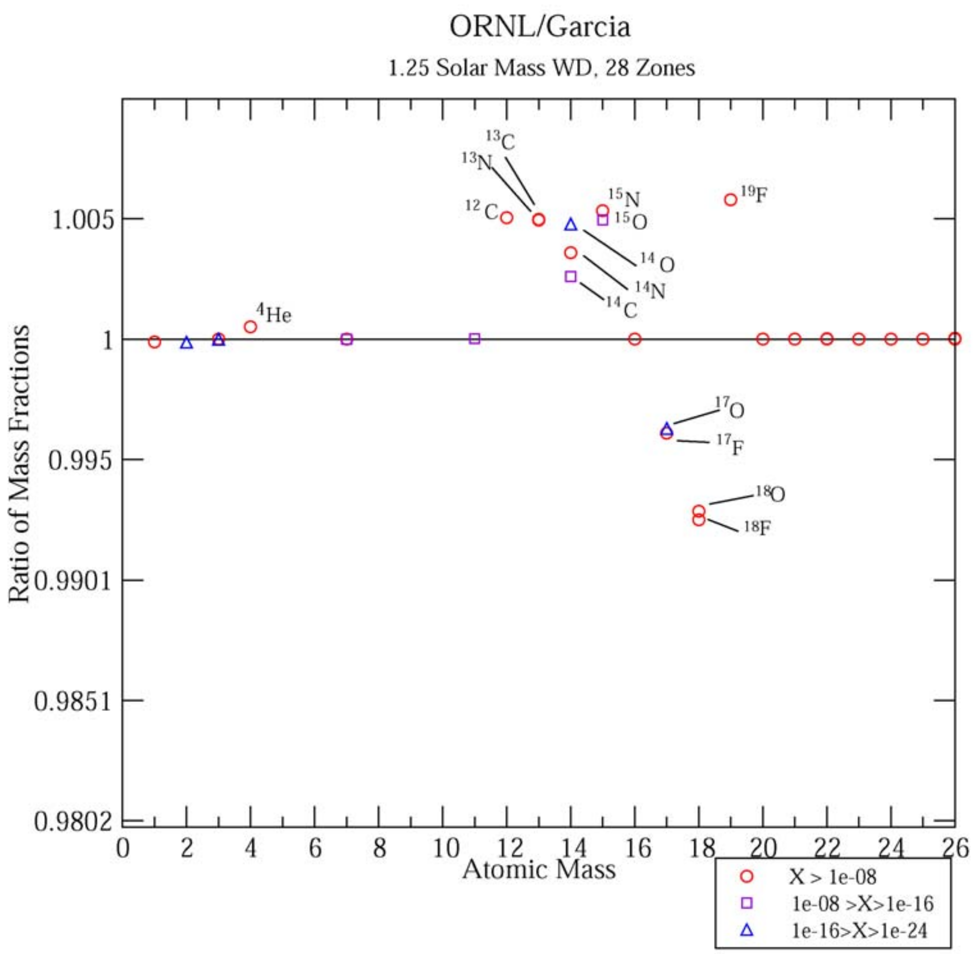

Figure 5.9 The comparison of the ORNL case mass fractions to the Garcia case mass fractions for a composite of all zones ejected by the nova shows differences of only fractions of percent.

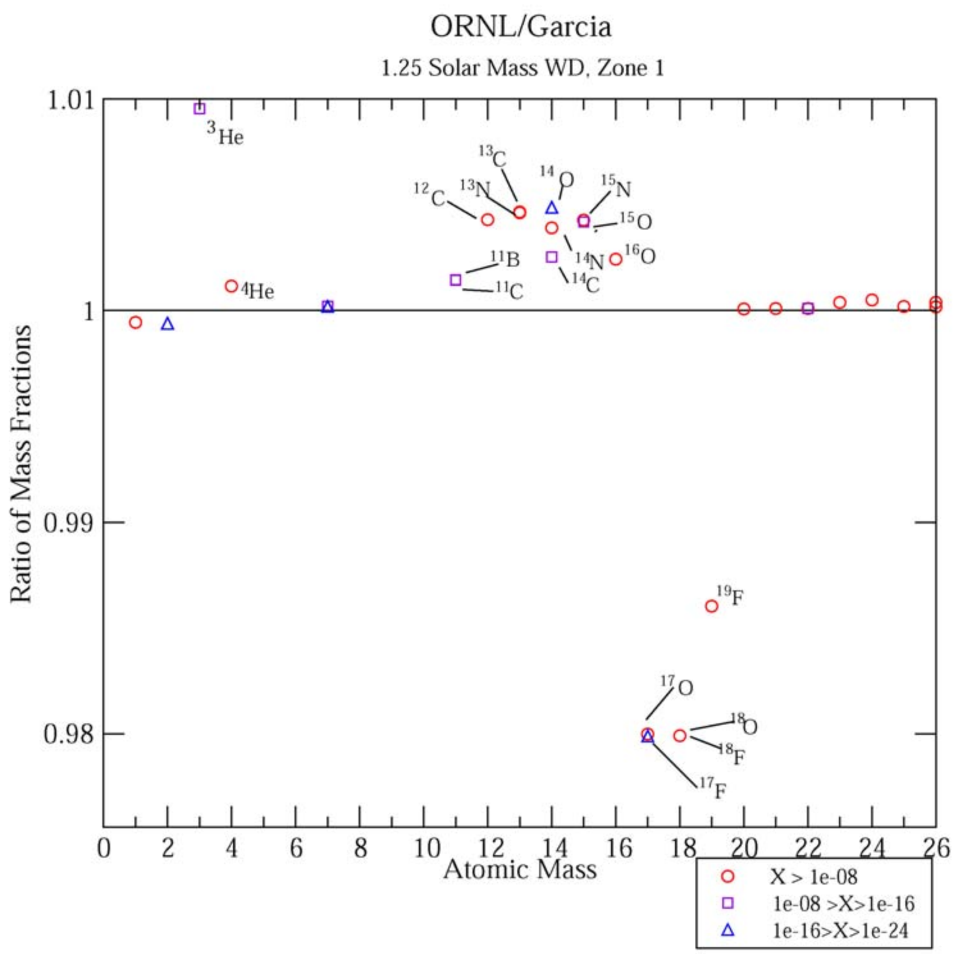

Figure 5.10 The comparison of the ORNL case mass fractions to the Garcia case mass fractions shows difference of up to 2% for the hottest zone.

Sherr rates are slightly slower than the ORNL rate. At peak temperature the ORNL rate is about 12% faster than the Sherr rate and 8% faster than the Garcia rate.

First note that the difference in mass fractions of isotopes produced by the ORNL case and the Sherr case or Garcia case are smaller compared to the difference between the ORNL and Wiescher cases. The Garcia rate is more similar to the ORNL rate than the Sherr rate, so its production of all isotopes is more similar to the ORNL case's production.

The zone by zone analysis reveals that the Sherr case produces more ^{18}F than the ORNL case for the first three zones, and the Garcia case produces more ^{18}F than ORNL for only the first two zones. In these cases the ORNL rate is faster so it plays the role that the Wiescher rate did previously. The Sherr and Garcia rates play the role the ORNL rate did previously. Figure 5.11 shows plots of abundance as a function of time for the Sherr and ORNL cases in zone 2. The abundance as a function of time plot for the Garcia case is not shown because it is very similar to the Sherr case shown in figure 5.11 The scale for this plot had to be greatly expanded in order to show the difference produced by the rates. Depletion does not play as large a role as it did in the ORNL/Wiescher case. There is only a small difference in the depletion of ^{17}F by the ORNL case and the Sherr case. The main reason for the overproduction of ^{18}F by the Sherr case is that the Sherr case produces the majority of ^{18}F later, and therefore, at lower temperatures than the ORNL case does. Consequently, more of the ORNL case’s early overproduction of ^{18}F is destroyed by (p,α) and (p,γ) reactions, while more of the Sherr case's later overproduction of ^{18}F survives as ^{18}F and its decay product ^{18}O.

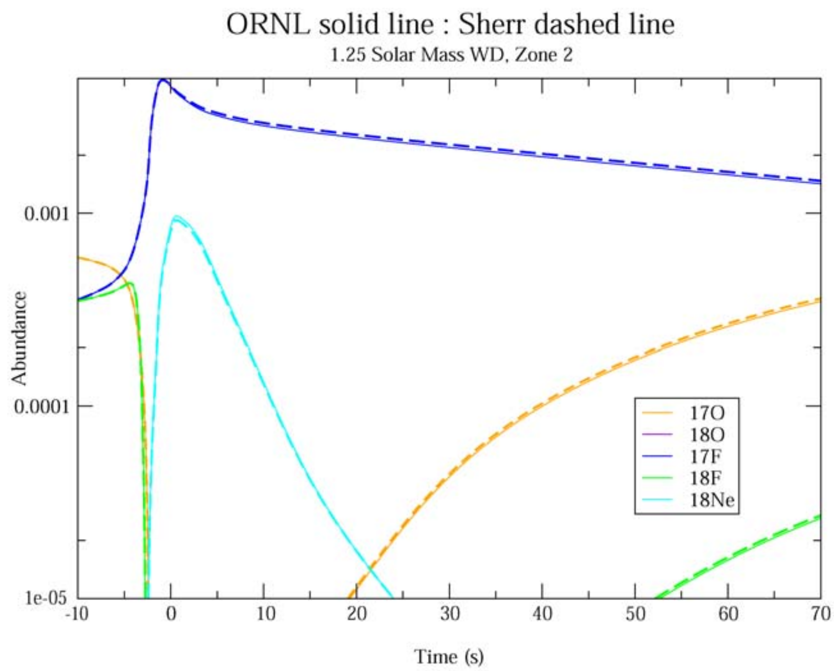

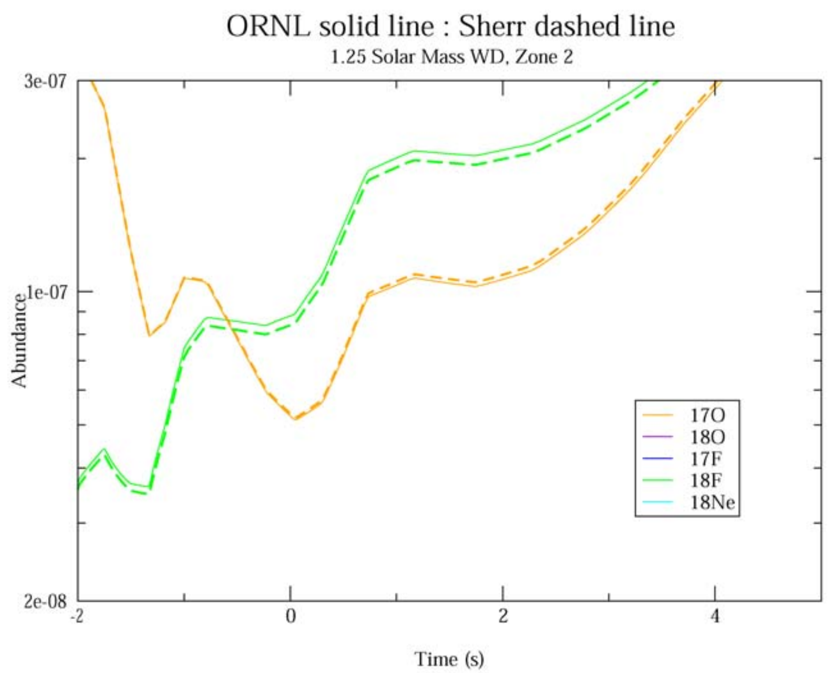

Figure 5.11 The top plot shows the ORNL case's early overproduction of ^{18}Ne the lower plot is an expanded view of the ORNL case's early overproduction of ^{18}F.

In summary, the dominant production of ^{18}F by the slower $^{17}F(p,\gamma)^{18}Ne$ rate in the inner zones of the 1.25 $M_\odot$ WD nova can be explained by the fact that the faster rate creates ^{18}F by $^{17}F\ (p,\gamma)^{18}Ne(\beta^+\nu)^{18}F$ at a higher temperature when it is more likely to be destroyed by (p,α) or (p,γ) reactions. The slower rate produces most of its ^{18}F by $^{17}F\ (\beta^+\nu)^{17}O(p,\gamma)^{18}F$ at a lower temperatures when it is more likely to remain in mass 18 isotopes. While significant depletion of ^{17}F and ^{17}O by the faster rate is not necessary to produce this effect, it greatly accentuates the difference between the two rates for the production of ^{18}F. The outer zones do not produce more ^{18}F for the slower rate because their overall lower temperatures do not allow much $^{17}F\ (\beta^+\nu)^{17}O(p,\gamma)^{18}F$ to occur by the time the $^{17}F\ (p,\gamma)^{18}Ne(\beta^+\nu)^{18}F$ process is no longer dominant.

5.2 Nova Simulations on a 1.35 $M_\odot$ ONeMg WD

As discussed in the introduction, more massive white dwarfs in nova systems result in more violent explosions. Thus the 1.35 $M_\odot$ WD nova model represents a much faster and hotter explosion than the 1.25 $M_\odot$WD nova model. The 1.35 $M_\odot$ WD nova's peak temperature is over 0.1GK hotter than the peak temperature of the 1.25 $M_\odot$ WD nova model. The envelope expands faster because of the greater force of the explosion and therefore cools faster than the 1.25 $M_\odot$ WD nova model.

Figures 5.12, 5.13 and 5.14 shown on pages 73-75 are the mass fraction ratio plots for the ORNL/ Wiescher rates in the 1.35 $M_\odot$ WD nova. Figure 5.12 on page 73 is the composite contribution from all the zones. In this plot the ORNL case produces 4 times more ^{17}O than the Wiescher case and just over a third as much ^{18}F and ^{18}O. This follows more closely to our original expectations for the nucleosynthesis of ^{18}F. Figure 5.13 is a plot of the hottest zone, zone 1. In this zone the ORNL case produces 20% more ^{18}F than the Wiescher case. We see that the ORNL case produces 80 times more ^{17}O and ^{17}F than the Wiescher case. In zone 3, figure 5.14, the ORNL case produces almost 15,000 time more ^{17}O than the Wiescher case. The production of ^{18}F is almost the same for both the ORNL and Wiescher cases. However, the Wiescher case produces more ^{19}F, ^{15}O and its decay product ^{15}N than the ORNL case.

A zone by zone analysis of the 1.35 $M_\odot$ WD nova shows that zone 1 is the only zone where the ORNL case produces more ^{18}F than the Wiescher case. To explore this, the abundance as a function of time has been plotted for ^{15}O, ^{17}O, ^{17}F, ^{18}F, ^{18}Ne and ^{19}F for zones 1, 3 and 6.

Zone 1, in figure 5.15, represents the case for overproduction of ^{18}F by ORNL. The nucleosynthesis of ^{18}F in this zone can be described in two phases as in zone 2 of the 1.25 $M_\odot$ WD Nova. ^{18}F production in the peak phase is again dominated by $^{17}F(p,\gamma)^{18}Ne(\beta^+,\nu)$ ^{18}F. In this case, the peak phase begins just before the peak temperature and lasts for roughly 25 seconds. The temperature in the peak phase ranges from 0.45 GK down to 0.20 GK. At the beginning, as in the 1.25 case, the Wiescher rate depletes ^{17}F much more rapidly than the ORNL rate. However, because the temperature is higher than in the 1.25 case, the ORNL rate also significantly depletes ^{17}F. Despite this depletion, the ORNL case still produces 300 times more ^{17}F than the Wiescher case.

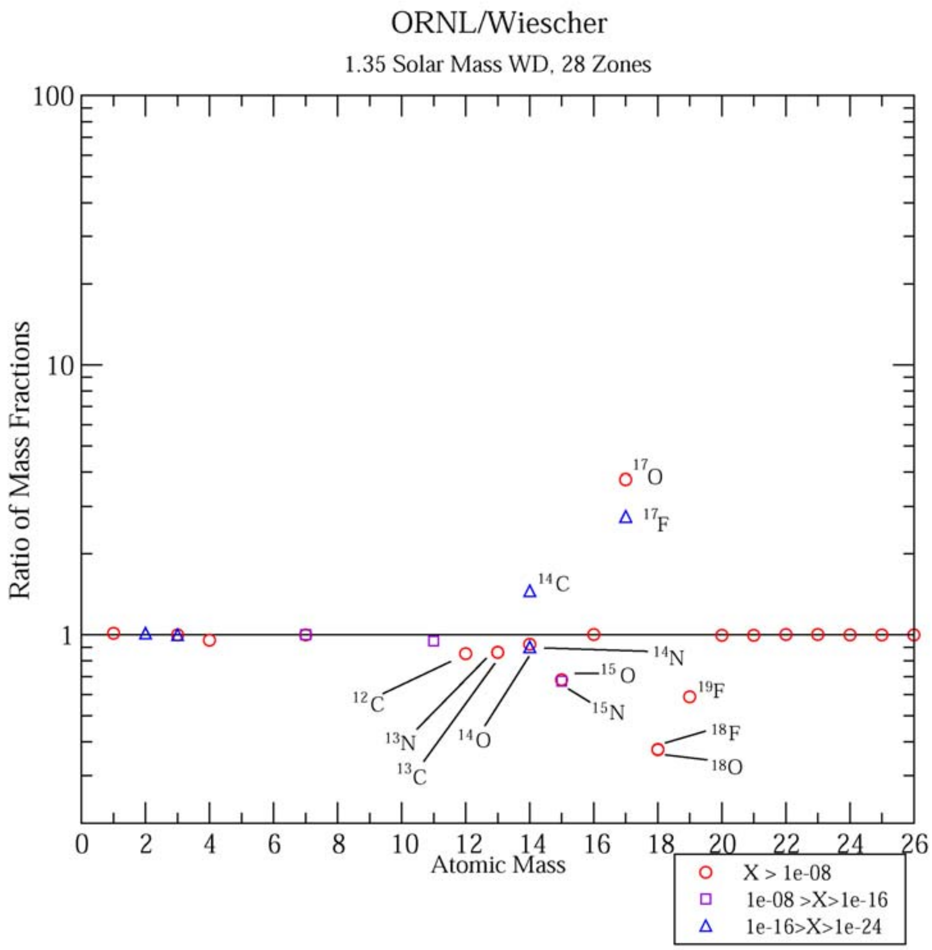

Figure 5.12 The comparison of the ORNL case mass fractions to the Wiescher case mass fractions for a composite of all zones ejected by the nova shows differences of up to a factor of 4.

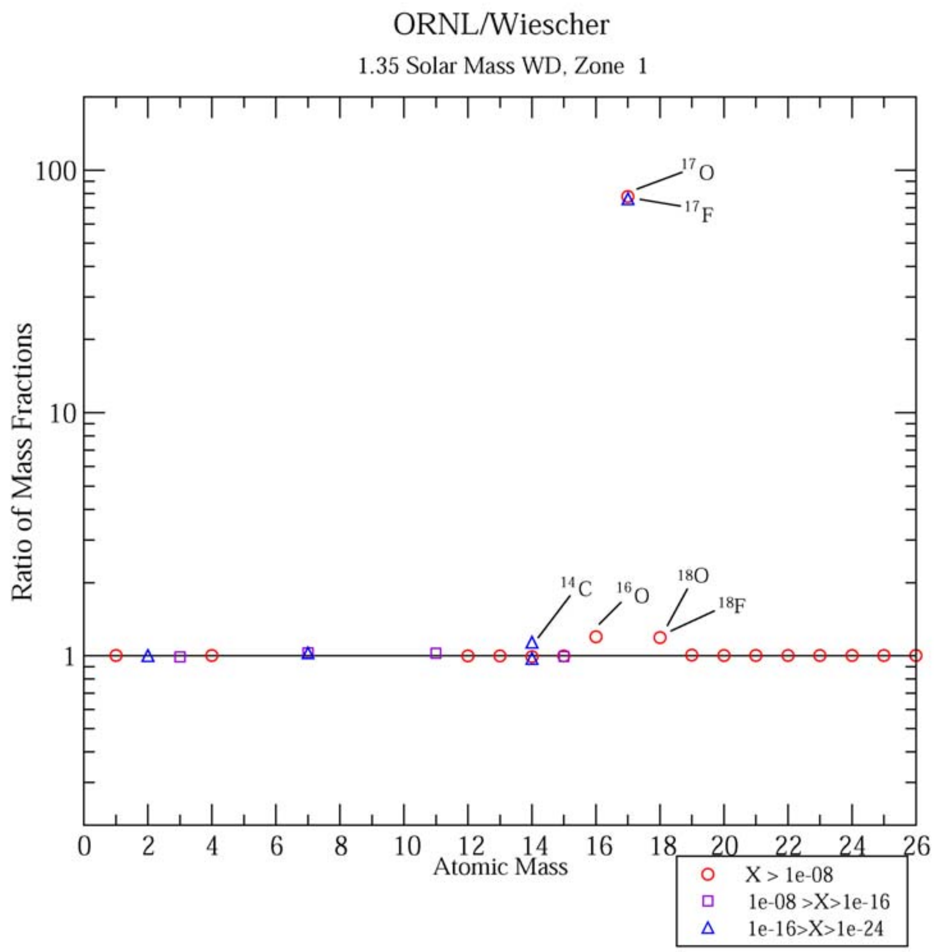

Figure 5.13 The comparison of the ORNL case mass fractions to the Wiescher case mass fractions for the hottest zone ejected by the nova shows differences of up to a factor of 80.

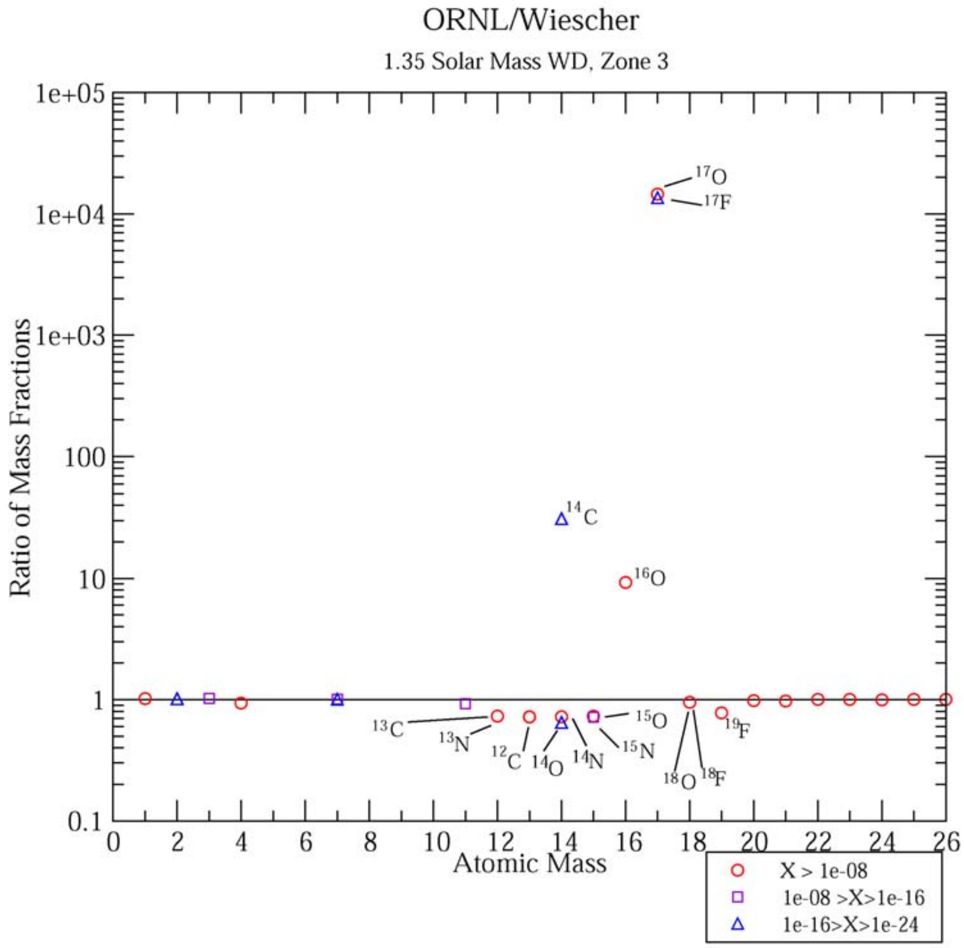

Figure 5.14 The ORNL case produces 15,000 times more ^{17}O and ^{17}F than the Wiescher case in Zone 3.

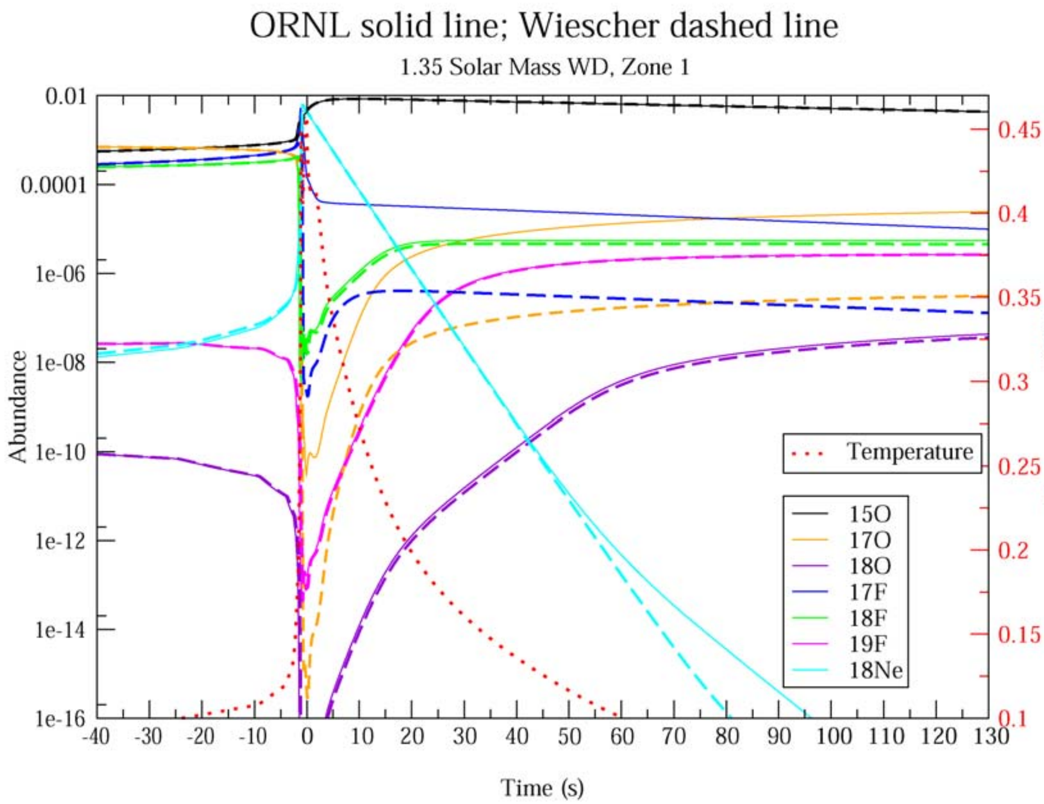

Figure 5.15 The abundances of several species are plotted as a function of time for the hottest zone of the 1.35 $M_\odot$ WD nova.

Within 2 seconds after peak temperature, the ORNL rate's production of ^{18}Ne overtakes the Wiescher rate's by a very slim margin. The Wiescher case produces more ^{15}O than the ORNL case, but the Wiescher case's overproduction is diminished by nearly even production of ^{18}F by the two rates. The overall production of ^{18}Ne and ^{18}F by the two rates in the 1.35 case is similar because both rates significantly deplete ^{17}F.

When the expansion phase begins, the temperature has already dropped to 0.2 GK. The production of ^{18}F in this phase is dominated by $^{17}F(\beta^+,\nu)^{17}O(p,\gamma)^{18}F$. Both the Wiescher and ORNL cases start this phase with depleted amounts of ^{17}F and ^{17}O, but the ORNL case has 300 times more ^{17}F and ^{17}O than the Wiescher case. This allows the ORNL case to create more ^{18}F than the Wiescher case at the very beginning. However, within 40 seconds the temperature drops below 0.10 GK. Few proton captures occur at temperatures below 0.10 GK. Thus, this rapid decrease in temperature reduces the possibility of proton capture on ^{17}O. The production of ^{18}F levels out for both the ORNL and Wiescher cases early in the expansion phase.

In summary, in this zone like in zone 2 of the 1.25 $M_\odot$ WD nova, the ORNL case produced more ^{18}F than the Wiescher case because the Wiescher case produced more ^{18}F during the hottest period of the nova where ^{18}F is likely to be destroyed by (p,α) or (p,γ) reactions. However, unlike the 1.25 $M_\odot$ WD nova, the high peak temperatures rapidly deplete ^{17}F for both the Wiescher and ORNL cases. After this depletion, the further production of isotopes which are the progeny of ^{17}F is done nearly equally by the two rates. In addition to depletion of ^{17}F and ^{17}O, the rapid decrease in temperature during the expansion phase further limits production of ^{18}F in either case.

For zone 3, figure 5.16, the peak phase lasts about 9 seconds. The temperature range is lower than in zone 1, ranging from 0.406 GK to 0.19 GK. Again both the ORNL and Wiescher cases significantly deplete ^{17}F, but less so than in zone 1. The Wiescher rate's early overproduction of ^{18}Ne and ^{18}F dominates throughout the expansion phase. However, over-depletion of ^{17}F by the Wiescher rate and the cooler temperatures in the later part of the peak phase allow the ORNL rate's ^{18}Ne and ^{18}F production to catch up and run almost even with that from the Wiescher rate's by the end of the peak phase. Since the ORNL case's production of ^{18}Ne is never greater than the Wiescher case's production of ^{18}Ne, the ORNL case never produces more ^{18}F or ^{15}O than the Wiescher case during the peak phase. In the Wiesher case a larger fraction of the ^{18}F overproduction is converted to ^{15}O, so at the end of the peak phase the Wiescher case has more ^{15}O than the ORNL case.

When the expansion phase begins, the ORNL case has significantly larger amounts of ^{17}F and ^{17}O than the Wiescher case, but the temperature is low enough that there is insufficient proton capture on ^{17}O to make a significant difference in the amount of ^{18}F produced. For the ORNL case the larger amount ^{17}F that is left just decays to ^{17}O. For the Wiescher case, there is little ^{17}F left to decay to ^{17}O and little ^{17}O produced in the peak phase.

In summary, nearly equal amounts of ^{18}F are produced by both the ORNL and Wiescher cases, because the excess ^{18}F produced by the Wiescher case early in the peak phase captures protons to become ^{15}O and ^{19}Ne, while the slower and later production of ^{18}F by the ORNL case allows more ^{18}F to survive as ^{18}F due to the cooler temperatures which occur later in the peak phase. The slower ORNL $^{17}F(p,\gamma)^{18}Ne$ rate also leaves the

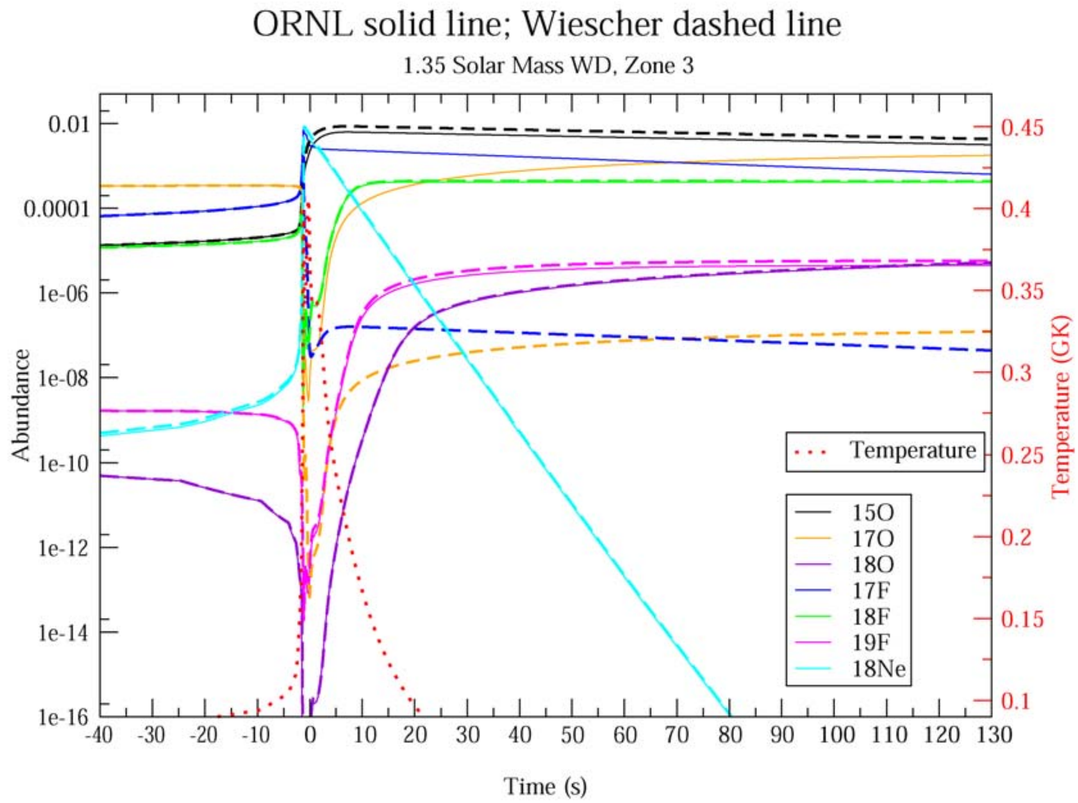

Figure 5.16 The abundances of several species are plotted as a function of time for zone 3 of the 1.35 $M_\odot$ WD nova.

ORNL case with an excess of ^{17}F and ^{17}O at the end of peak phase. The rapid drop in temperature prevents significant production of ^{18}F by the $^{17}F(\beta^+,\nu)^{17}O(p,\gamma)^{18}F$ sequence during the expansion phase for either case. The excess ^{17}O in the ORNL case survives as ^{17}O.

Zone 6, in figure 5.17, is representative of the remaining zones where the Wiescher case produces more ^{18}F than the ORNL case. The explanation for zone 6 is very similar to the explanation for zone 5 from the 1.25 $M_\odot$ WD nova. Neither the ORNL case nor the Wiescher case significantly depletes ^{17}F. The Wiescher case never overdepletes ^{17}F so the Wiescher case's ^{18}Ne production dominates throughout the nova simulation. As a result the Wiescher case dominates in the production of ^{18}F and ^{15}O and ^{19}F. Within 20 seconds of peak temperature in zone 6, the temperature drops below 0.10 GK and further proton captures are unlikely. The ORNL case produces more ^{17}O than the Wiescher case, but by the time $^{17}F(p,\gamma)^{18}Ne(\beta^+,\nu)^{18}F$ is no longer the dominate source of ^{18}F, the temperature has dropped enough that most of the ^{17}O survives as ^{17}O rather than capturing a proton.

Figures 5.18-5.23 on pages 82-87 show the mass fraction ratio plots for ORNL/Sherr and ORNL/Garcia. Differences in the mass fraction produced by the two rates run up to 5% for Sherr's composite plot and only up to 3% for Garcia's composite plot. In zone 1 the ORNL case produces about half as much ^{17}F and ^{17}O as the Garcia or Sherr cases. See figures 5.19 and 5.21. Also in zone 1, the Sherr and Garcia cases produce more ^{18}O and ^{18}F than the ORNL case. Again, as in the 1.25 $M_\odot$ WD nova, this is a diminished and reversed version of the ORNL/Wiescher case. The Sherr and Garcia

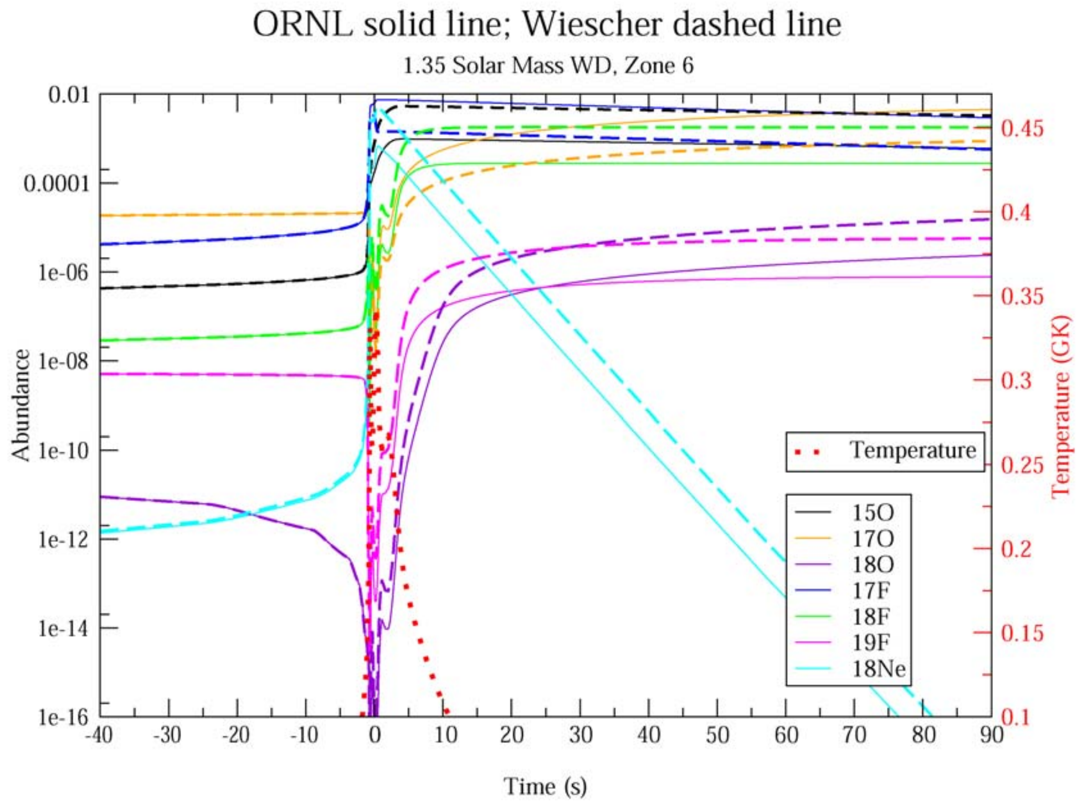

Figure 5.17 The abundances of several species are plotted as a function of time for zone 6 of the 1.35 M$_\odot$ WD nova.

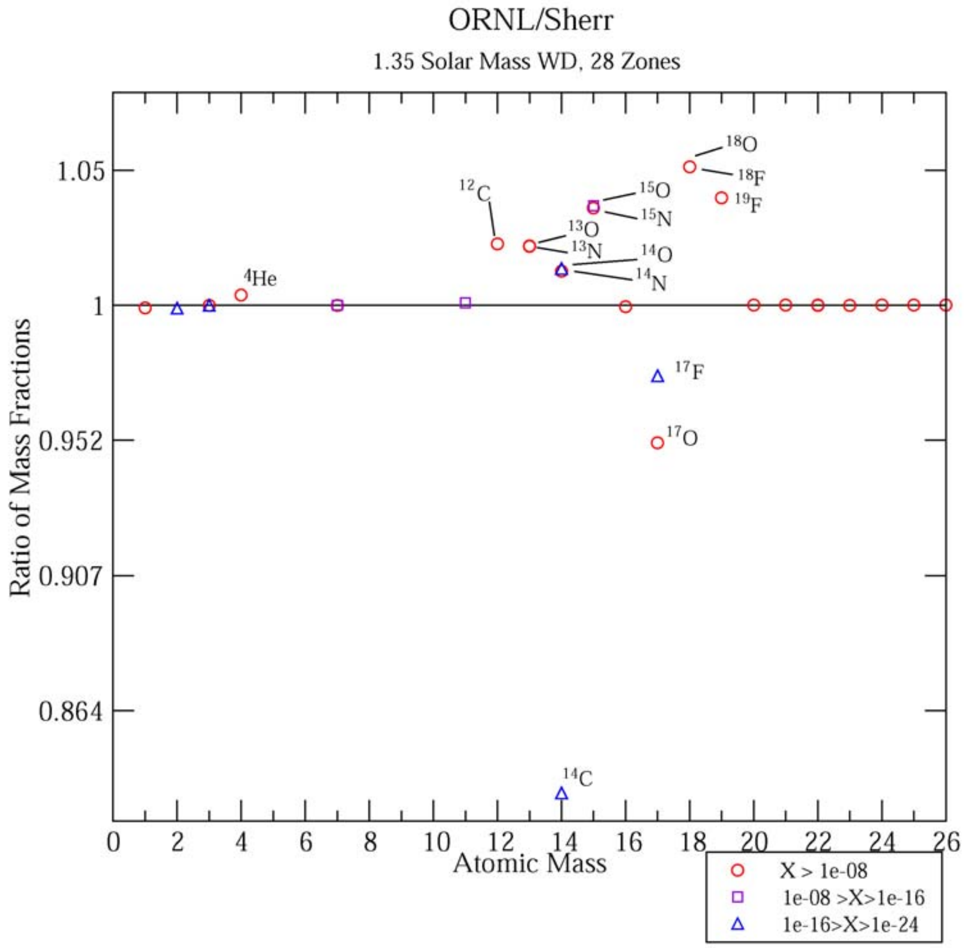

Figure 5.18 The comparison of the ORNL case mass fractions to the Sherr case mass fractions for a composite of all zones ejected by the nova shows differences of up to 5%.

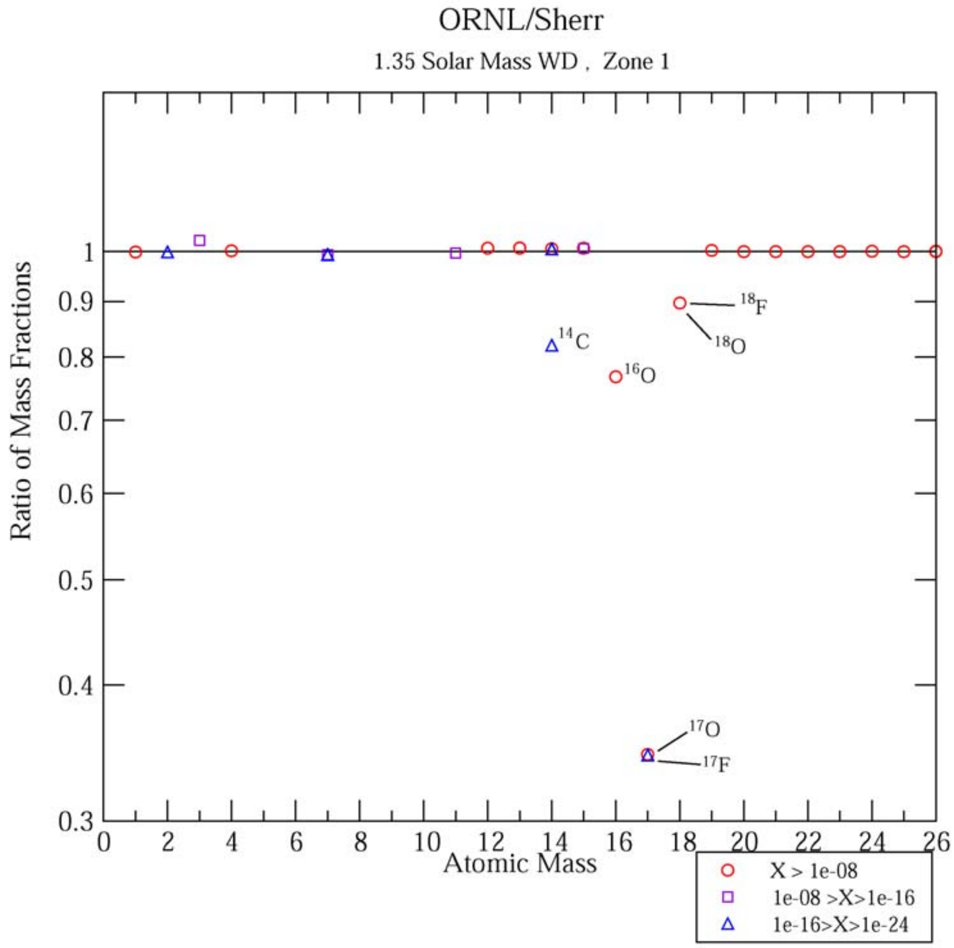

Figure 5.19 The comparison of the ORNL case mass fractions to the Sherr case mass fractions for the hottest zone ejected by the nova shows differences of up to a factor of 3.

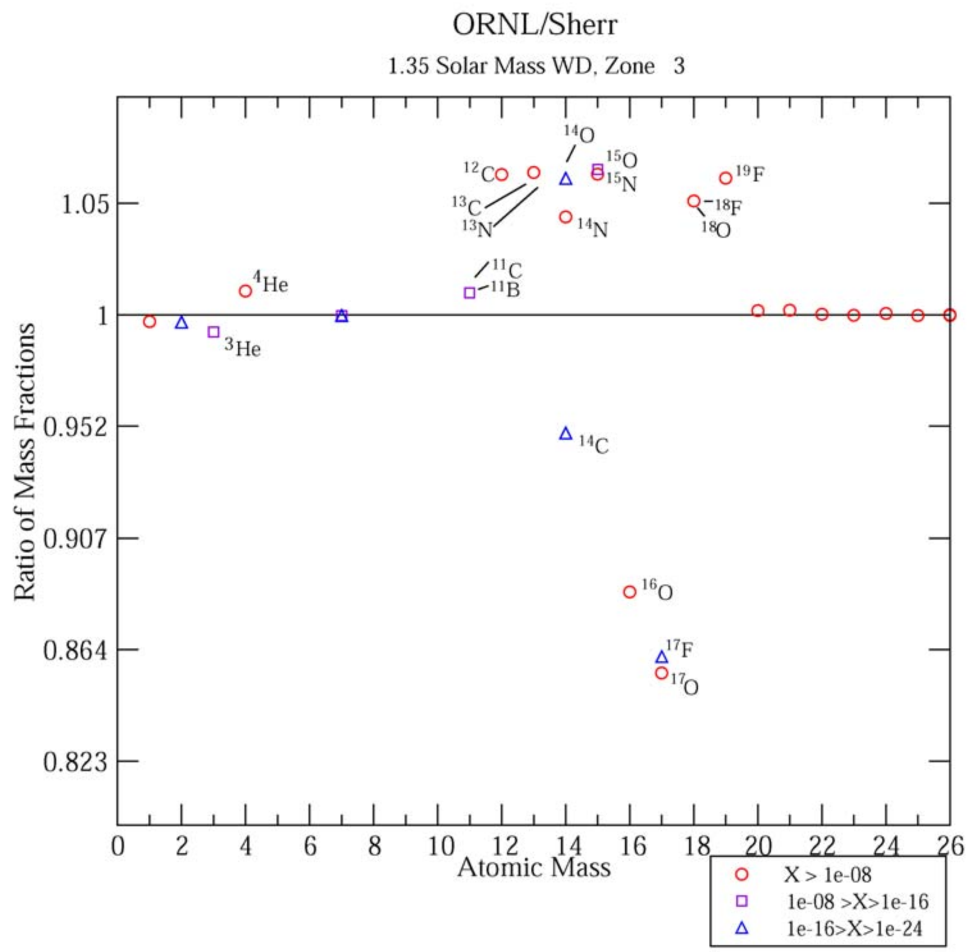

Figure 5.20 The comparison of the ORNL case mass fractions to the Sherr case mass fractions for zone 3 shows differences of up to 17%.

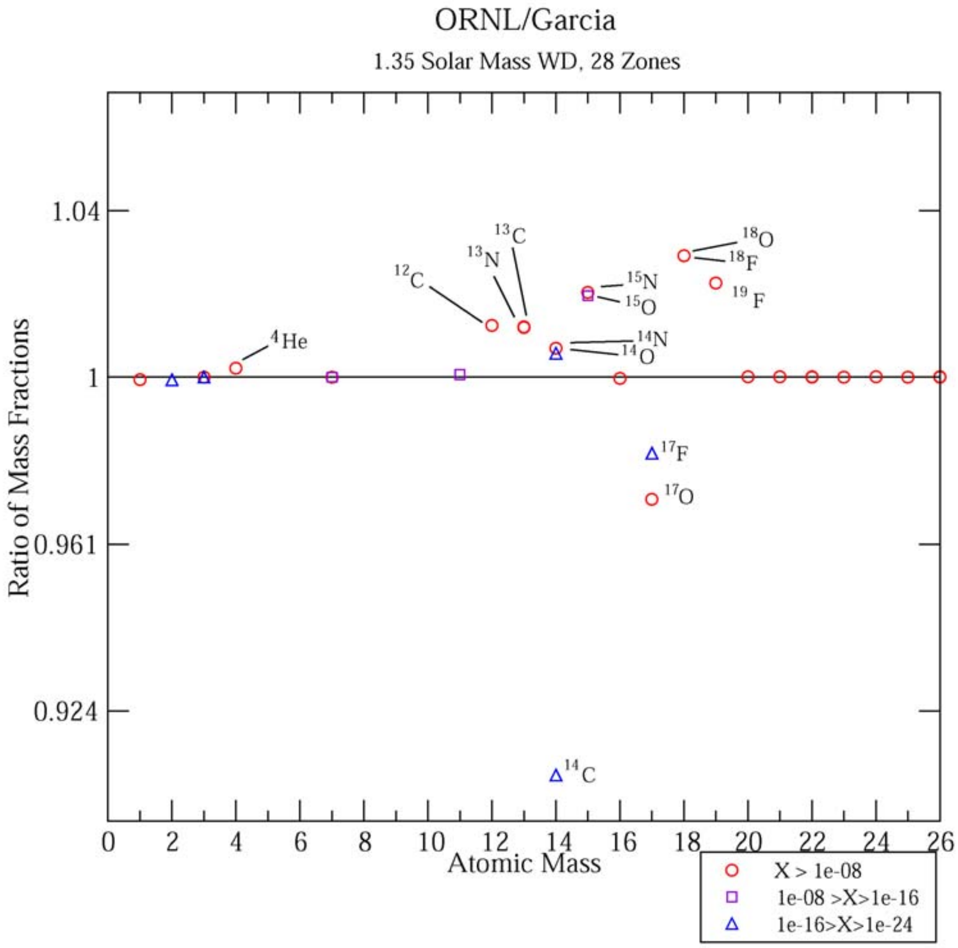

Figure 5.21 The comparison of the ORNL case mass fractions to the Garcia case mass fractions for a composite of all zones ejected by the nova shows differences of up to 3% for isotopes with abundances over 10^8 g/mol.

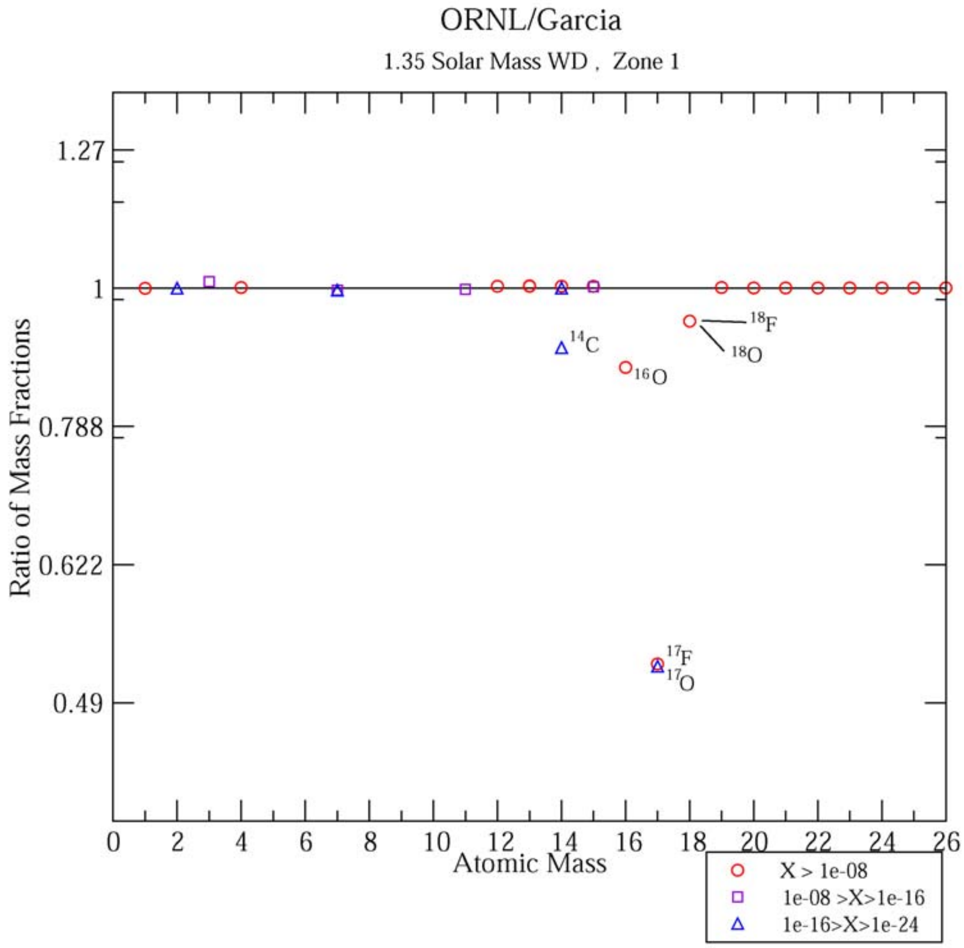

Figure 5.22 The comparison of the ORNL case mass fractions to the Garcia case mass fractions for the hottest zone ejected by the nova shows differences of up to 50%.

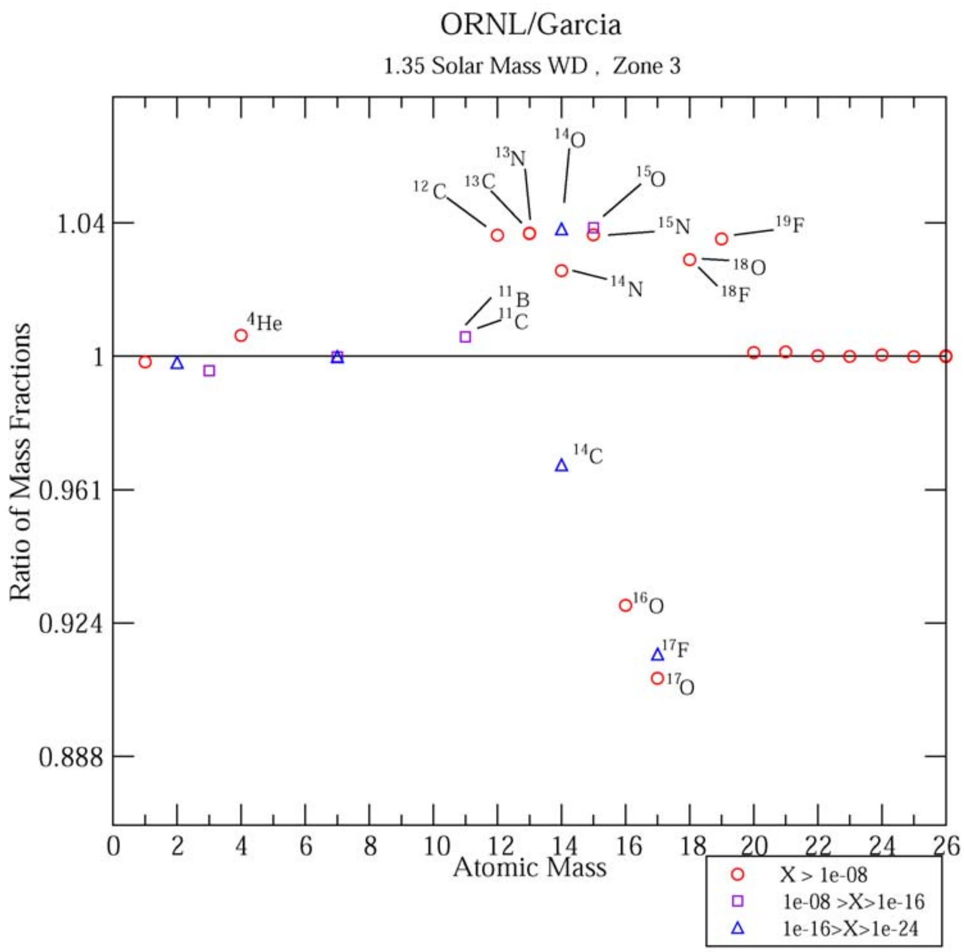

Figure 5.23 The comparison of the ORNL case mass fractions to the Garcia case mass fractions for zone 3 shows differences of up to 10%.

cases play the role that the ORNL case did in the ORNL /Wiescher case while the ORNL case plays the role that the Wiescher case did.

Again, for zone 1, depletion does not play as large a role as it did in the ORNL/Wiescher case. The main reason for the overproduction of ^{18}F by the Sherr and Garcia cases is that they produce the majority of ^{18}F later and, therefore, at lower temperatures than the ORNL case does. Consequently, more of the ORNL case's early overproduction of ^{18}F is destroyed by (p,α) and (p,γ) reactions, while more of the Sherr and Garcia case's later overproduction of ^{18}F survives as ^{18}F and its decay product ^{18}O.

The reason that we do not see ratios which are greater than one for ^{15}O or its decay product ^{15}N in figures 5.19 and 5.22 is because ^{15}N has an abundance on the order of 10^3 while ^{18}F and ^{18}O have abundances on the order of 10^6. The small change in ^{15}O caused by the ^{18}F(p,α)^{15}O reaction does not show up on the ratio plot's scale, however; the ORNL case does produce slightly more ^{15}O and ^{15} N than the Sherr case or the Garcia case.

For the remaining zones the ORNL case's ^{18}Ne and ^{18}F overproduction dominates throughout the nova because of nearly equal depletion of ^{17}F by both the faster and slower ^{17}F(p,γ)^{18}Ne rates, and because the temperature drops so rapidly that by the time ^{17}F(p,γ)^{18}Ne($\beta^+\nu$)^{18}F reaction is no longer the dominant, ^{17}O survives as ^{17}O rather than capturing a proton to become ^{18}F.

5.3 Novae Simulations on a 1.00 M⊙ CO WD

The 1.00 M⊙ WD Nova is the slowest and least violent explosion explored in this study. The peak temperature of this nova never reaches above 0.17 GK. At this temperature the four $^{17}F(p,\gamma)^{18}Ne$ rates we are considering differ only slightly from each other so we don't expect to see much difference in the nucleosynthesis. Figures 5.24-5.35 show the mass fraction ratio plots for the 1.00 M⊙WD nova.

Figure 5.24 is the composite plot for ORNL/Wiescher and shows that there is little difference in the nucleosynthesis for the two rates, except that the Wiescher rate produces about 14% more ^{18}Ne. A magnified view of this plot in figure 5.25 reveals that the Wiescher case produces a mere fraction of a percent more ^{15}N, ^{15}O, ^{18}F, ^{18}O, ^{19}F and ^{19}Ne than the ORNL case, while the ORNL case produces fractions of a percent more ^{17}F and ^{17}O as we expect. These differences are well below the expected precision of the network (which will be discussed in section 5.5).

Figure 5.26 is the ORNL case to Wiescher case ratio plot for the hottest zone and figure 5.27 is an expanded scale version of this plot. These plots are very similar to the zone composite plots demonstrating that the majority of the nucleosynthesis involving charged particle interactions probably occurs in the hottest zone, which reaches a peak temperate of only 0.17 GK. Only the first fourteen zones of this nova achieve temperatures above 0.01 GK.

Figures 5.28 and 5.29 show mass fraction ratio plots for the ORNL/Sherr case for the zone composite and hottest zone. Both plots reveal that the ORNL case produces 2%

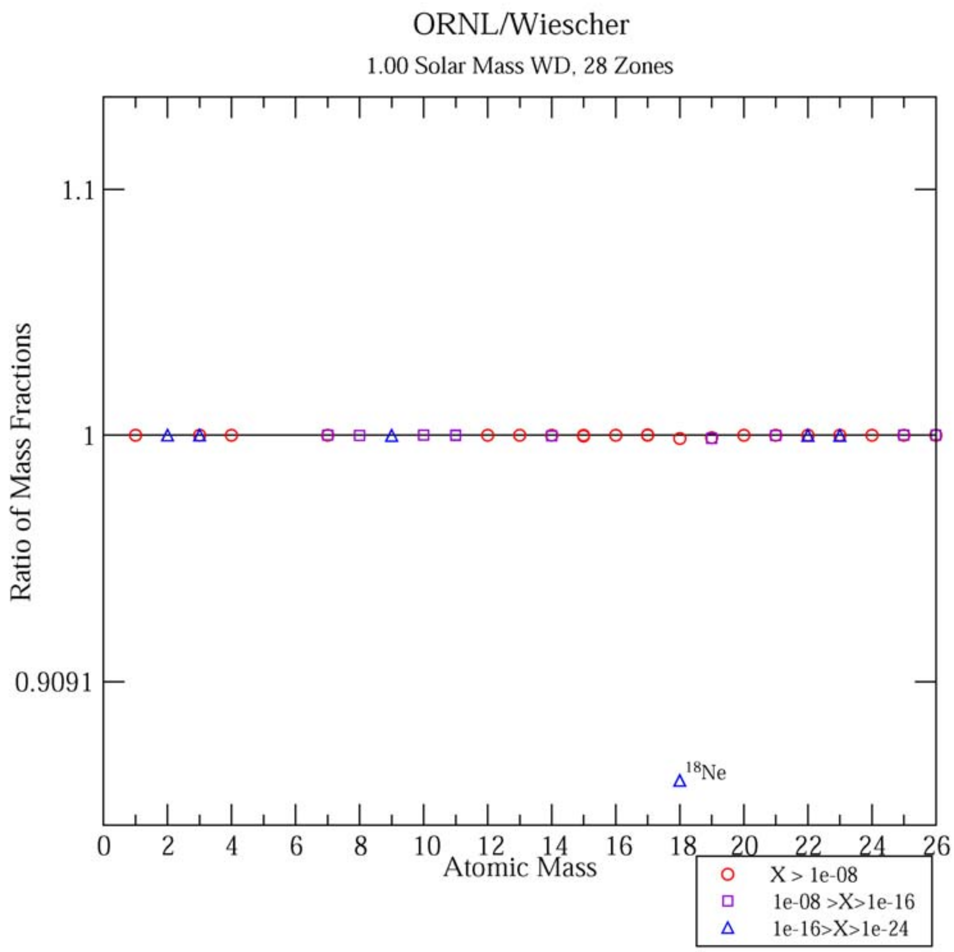

Figure 5.24 The zone composite plot for the ORNL/Wiescher mass fraction comparison shows that there is little difference in the nucleosynthesis for the two rates, except that the Wiescher rate produces about 14% more ^{18}Ne.

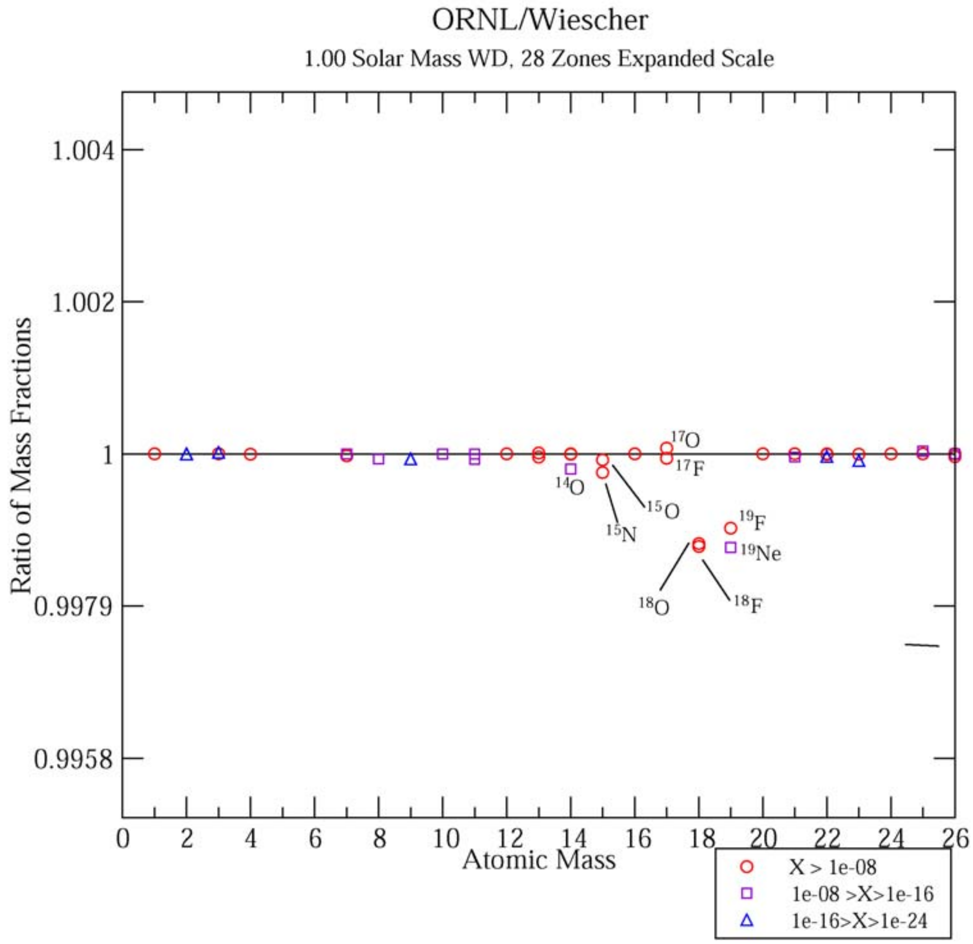

Figure 5.25 A magnified view reveals that the Wiescher case produces a mere fraction of a percent more ^{15}N, ^{15}O, ^{18}F, ^{18}O, ^{19}F and ^{19}Ne than the ORNL case, while the ORNL case produces a minute fraction of a percent more ^{17}O.

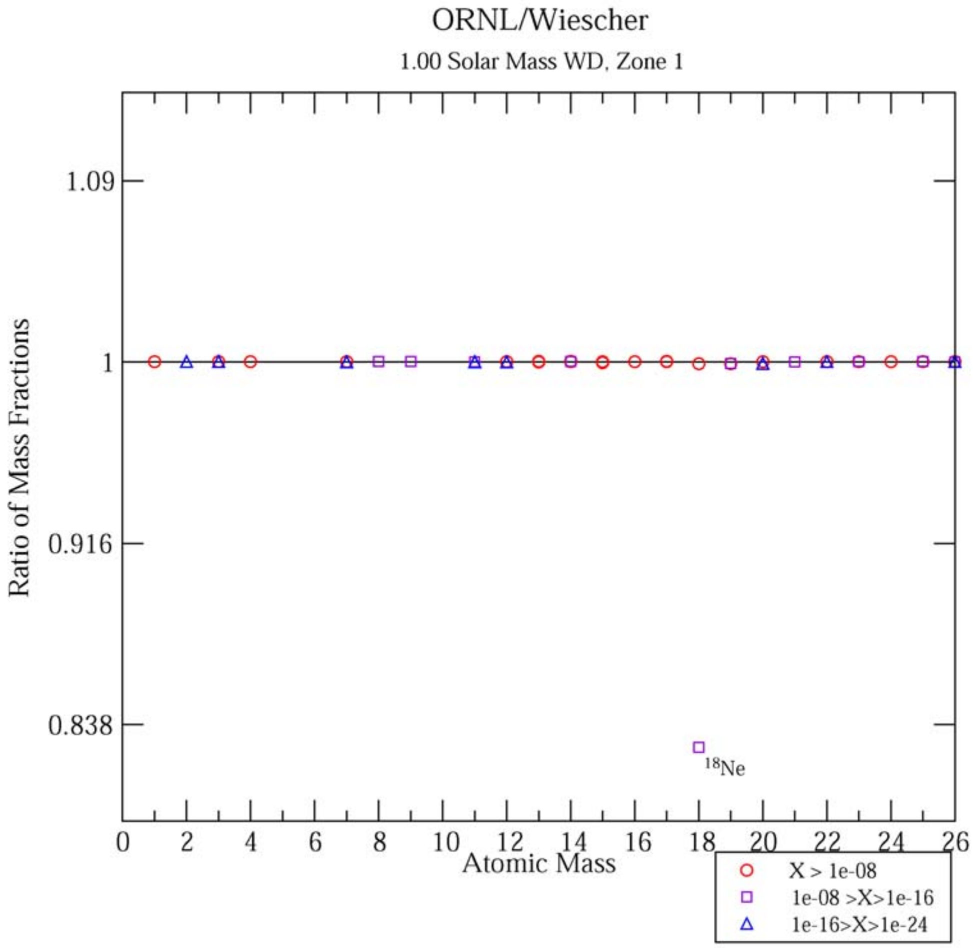

Figure 5.26 There is little difference in the nucleosynthesis produced by the ORNL and Wiescher rates even in the hottest zone, except that the Wiescher rate produces about 20% more ^{18}Ne.

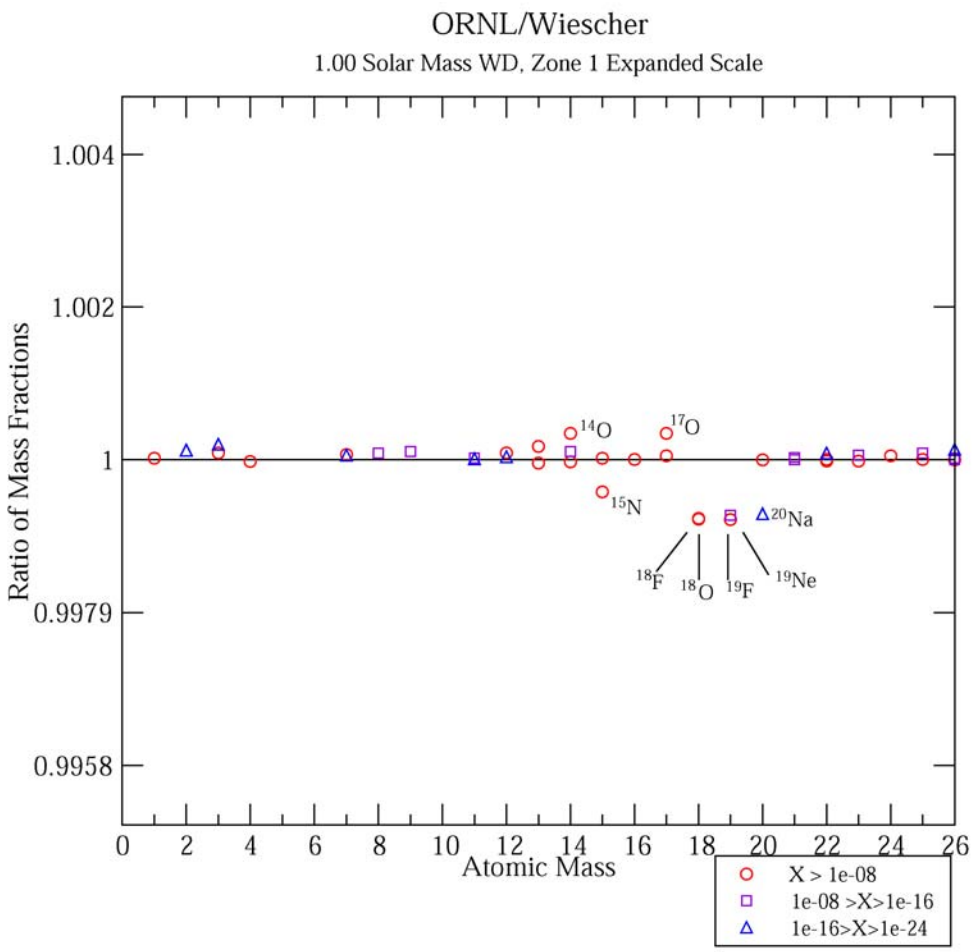

Figure 5.27 The expanded scale plot of the ORNL/ Wiescher mass fraction comparison for the hottest zone is very similar to the zone composite expanded scale plot of the ORNL/ Wiescher mass fractions.

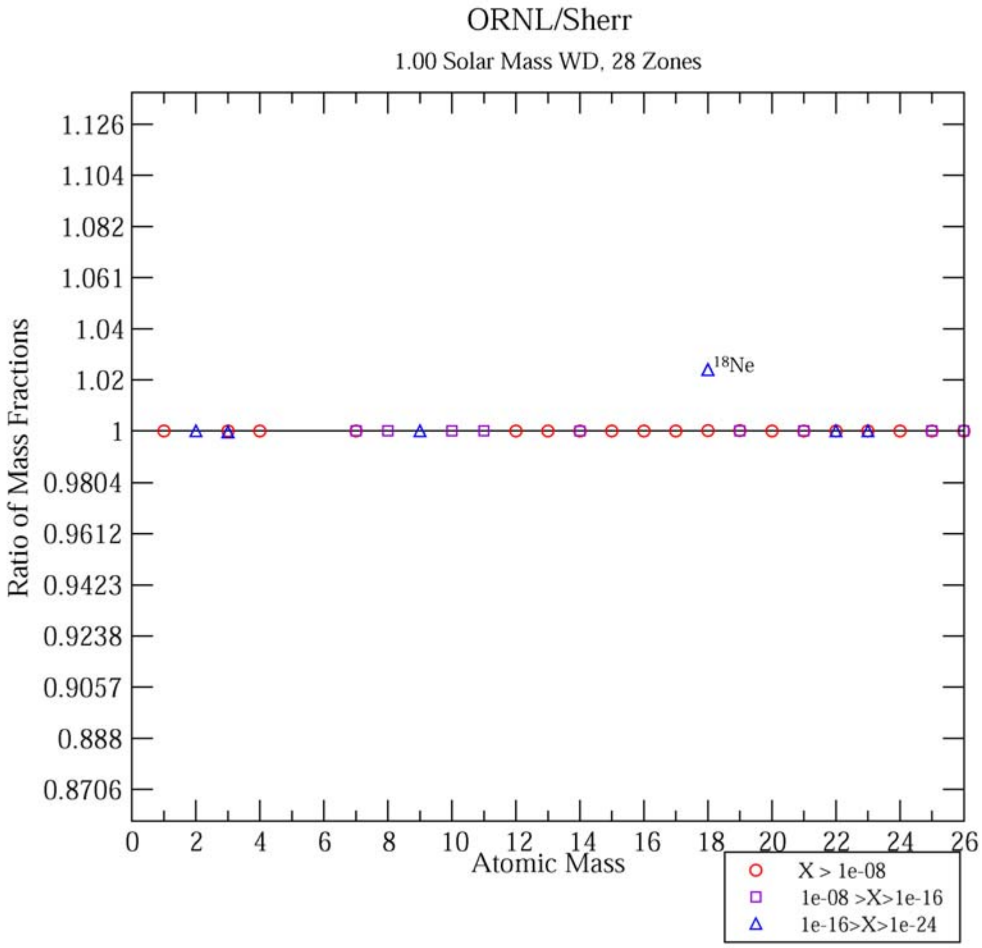

Figure 5.28 There is little difference in the nucleosynthesis produced by the ORNL and Sherr rates. The ORNL rate produces about 2% more ^{18}Ne than Sherr the Sherr rate.

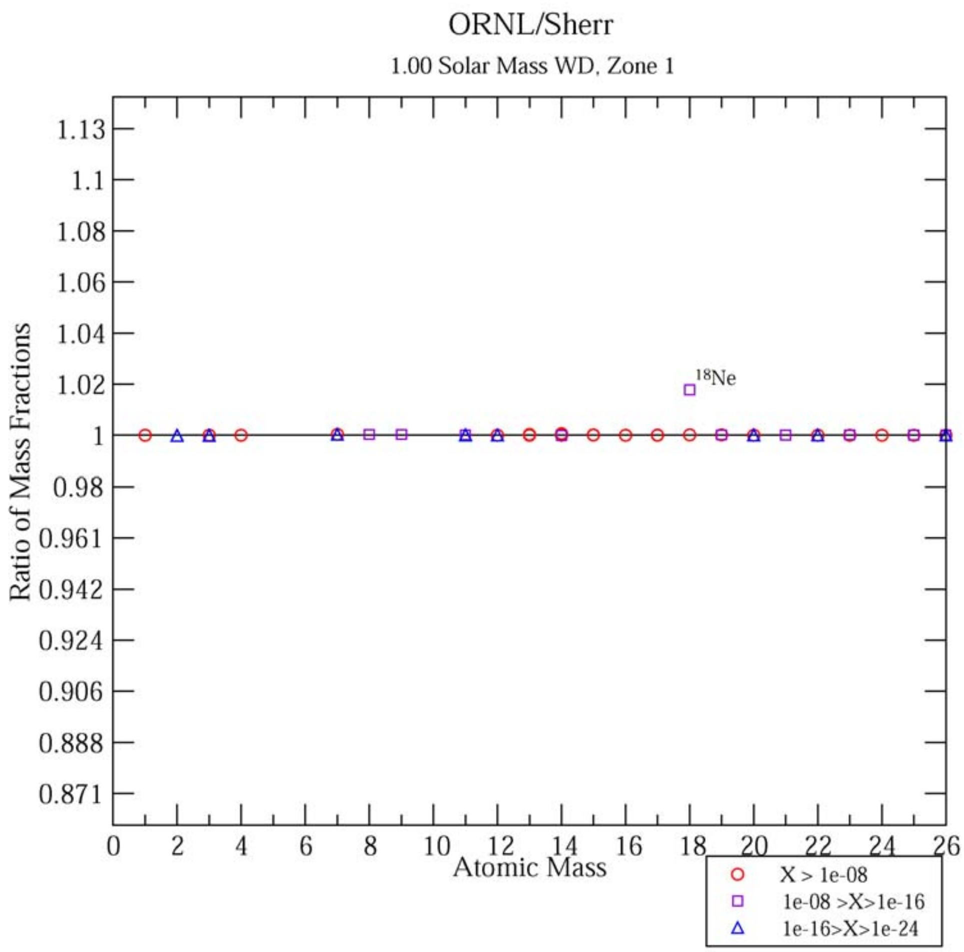

Figure 5.29 There is little difference in the nucleosynthesis produced by the ORNL and Sherr rates even in the hottest zone.

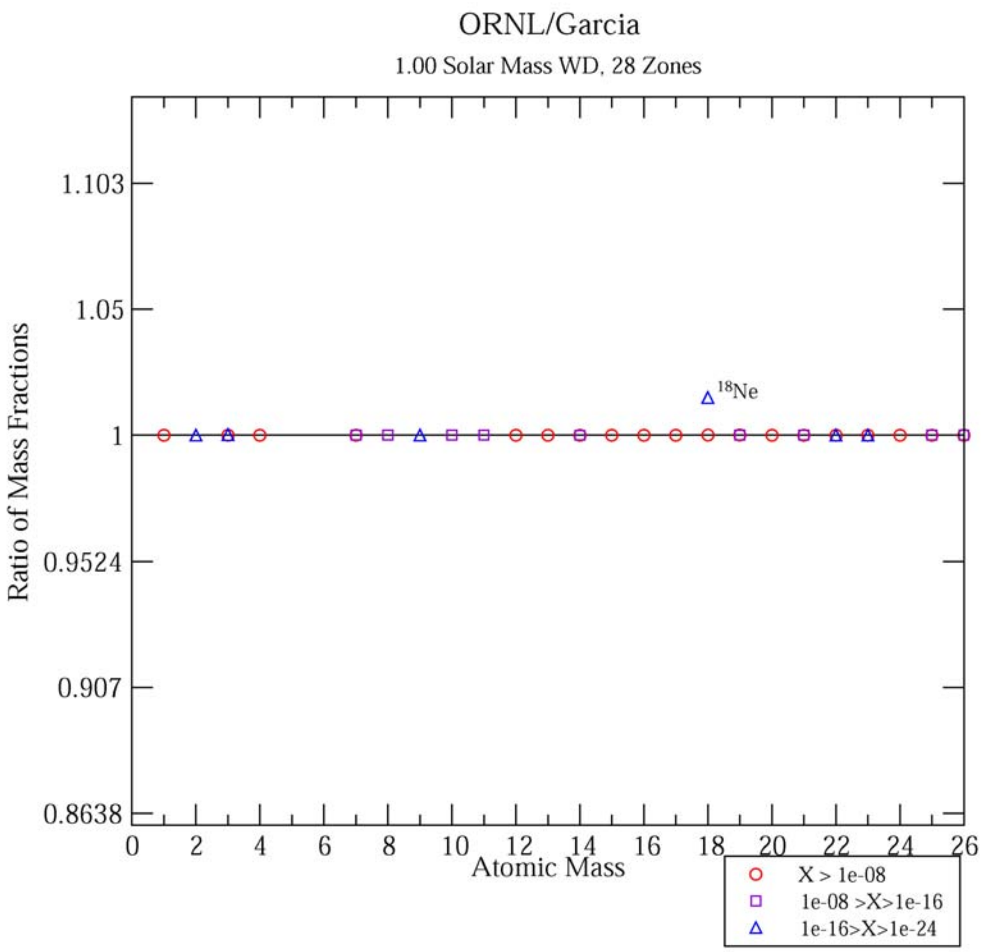

Figure 5.30 There is little difference in the nucleosynthesis produced by the ORNL and Sherr rates. The ORNL rate produces about 2% more ^{18}Ne than the Sherr rate.

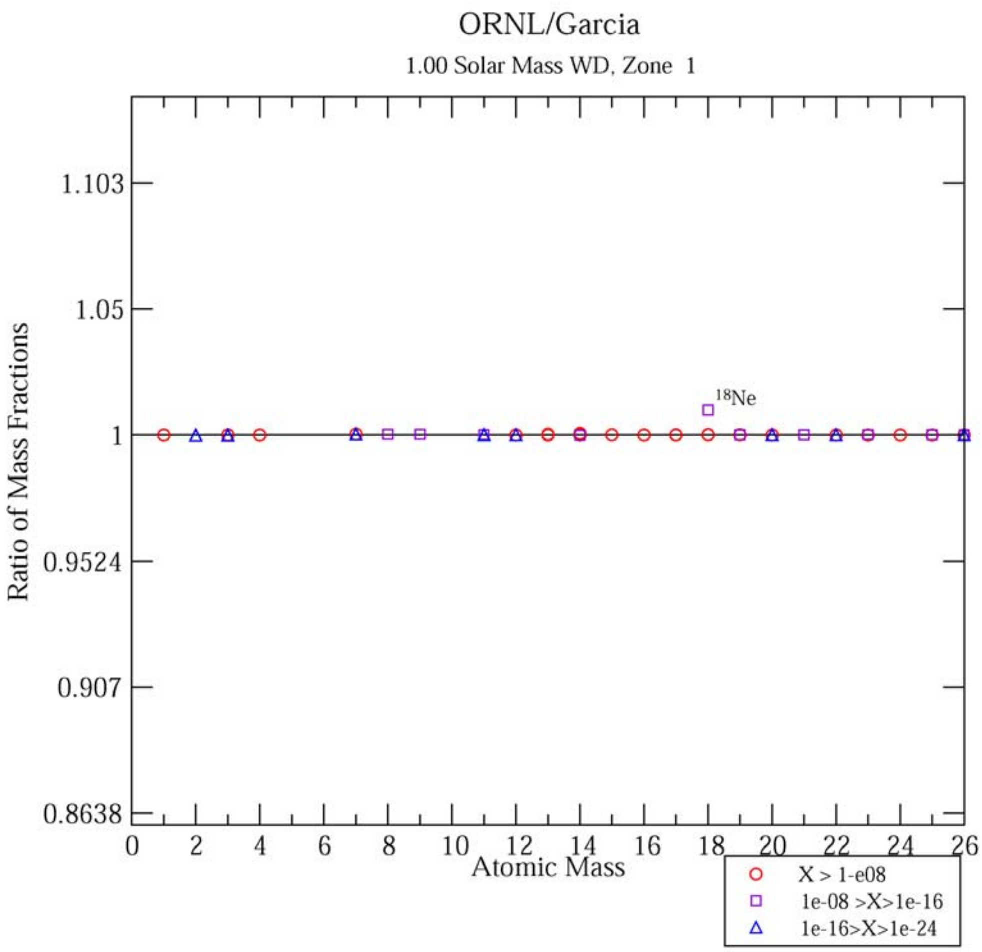

Figure 5.31 There is little difference in the nucleosynthesis produced by the ORNL and Garcia rates even in the hottest zone.

more ^{18}Ne than the Sherr case. I have not shown the expanded scale plots in this case because the difference for all other isotopes are much less than 1%.

The mass fraction ratio plots for the composite and hottest zones of the Garcia case are shown in plots 5.30 and 5.31 on pages 96 and 97. For both the hottest zone and the zone composite the ORNL case produces about 1% more ^{18}Ne than the Garcia case. The differences for all other isotopes are much less than 1%.

5.4 Conclusion and Summary

Variation of the $^{17}F(p,\gamma)^{18}Ne$ reaction rate produces large differences in the amount of ^{17}O, ^{17}F, ^{15}O, ^{15}N, ^{18}F, and ^{18}O produced by the 1.35 and 1.25 $M_\odot$ ONeMg WD nova nucleosynthesis calculations. The 1.00 $M_\odot$ CO WD nova nucleosynthesis calculations, where the temperatures are too low to allow proton captures to compete efficiently with beta decays, showed that variation of the $^{17}F(p,\gamma)^{18}Ne$ rate made little difference in the nucleosynthesis.

The hotter 1.35 $M_\odot$ white dwarf nova simulation showed the greatest variation in the abundance patterns produced by the four rates. The new ORNL $^{17}F(p,\gamma)^{18}Ne$ rate changed the abundances of some nuclei, such as ^{17}O, that are synthesized in the hottest zones of the nova by up to 15,000 times when compared to the network results with the Wiescher rate, and up to 4 times when compared to the network results with the Wiescher rate when all zones of the nova were considered. Also in the 1.35 $M_\odot$ WD nova simulation, the ORNL rate produced 3 times less ^{17}O than the Sherr rate in the hottest zones and 5% less ^{17}O when all zone were considered. The ORNL rate produced about

50% less ^{17}O in the hottest zone than the Garcia rate and 3% less when all zones were taken into consideration.

The ORNL to Wiescher rate comparisons for the l.25 $M_\odot$ WD nova nucleosynthesis calculations showed differences of up to 600 times for nuclei like ^{17}O in the hottest zones and up to 2 times when all zones of the nova were considered. The ORNL to Sherr rate comparisons for this nova showed differences of up to 6% for nuclei, such as ^{17}O, in the hottest zones and up to 1.6% difference when all zones were considered. The ORNL to Garcia rate comparisons showed less variation with differences of up to 2% for nuclei in the hottest zones and differences of only a fraction of a percent when all zones were considered.

These models demonstrate that a faster $^{17}F(p,\gamma)^{18}Ne$ rate allows for the synthesis of less ^{17}O in all zones of the 1.25 and 1.35 $M_\odot$WD novae. The faster rate is more likely to allow the reaction sequence $^{17}F(p,\gamma)^{18}Ne(\beta^+\nu)^{18}F$ to process ^{17}F to ^{18}F during the hottest temperatures of the nova where ^{18}F is likely to undergo further proton capture. Therefore, in the hotter zones of the 1.25 and 1.35 $M_\odot$WD novae the faster $^{17}F(p,\gamma)^{18}Ne$ rate leads to the synthesis of more ^{15}O by $^{18}F(p,\alpha)$ or ^{19}Ne by $^{18}F(p,\gamma)$. This result is relevant because observation suggests that novae may be important sources of ^{15}N and ^{17}O.

One such observation is that of the isotopic composition of dust grain inclusions in meteorites. Novae produce large quantities of gas and dust. It is believed that this material can become included in meteors. Five recently discovered meteorites have dust grain inclusions with isotopic signatures that match the isotopic composition predicted for ONeMg nova ejecta by nucleosynthesis calculations like those done in this study [31]. The five meteoritic dust grains are characterized by low $^{12}C/^{13}C$ and $^{14}N/^{15}N$ abundance ratios compared to solar composition, high abundance ratios of $^{26}Al/^{27}Al$ compared to solar composition and large excesses of ^{30}Si [31]. Theoretical nucleosynthesis calculations show that novae ejecta are the only stellar sources that match this isotopic composition [31]. Table 5.1 show isotopic ratios measured for five meteoritic dust grains that are believed to have originated from ONeMg novae, a the isotopic ratios predicted by the ORNL case for the 1.25 and 1.35 $M_\odot$ WD novae, and predictions made by other nova nucleosynthesis calculations. In the table we see that the isotopic ratios determined from our 1.25 and 1.35 $M_\odot$ WD novae nucleosynthesis calculations qualitatively match the isotopic ratio measurements from the meteoritic dust grains. They also compare well with the ratios predicted by nucleosynthesis calculations from other studies.

Theoretical nova nucleosynthesis calculations like those in this study predict that meteoritic oxide dust grains of nova origin would display a large excess of ^{17}O and smaller excess of ^{18}O compared to solar composition [31]. No oxide grains of this nature have been identified yet. The new ORNL rate for $^{17}F(p,\gamma)^{18}Ne$, which is the most accurate determination so far, differs most from all previous $^{17}F(p,\gamma)^{18}Ne$ rate predictions in its production of ^{17}O in ONeMg nova nucleosynthesis calculations. Our study shows that nucleosynthesis calculations done with the ORNL $^{17}F(p,\gamma)^{18}Ne$ rate predict greater excesses of ^{17}O and ^{18}O than those done with the Wiescher $^{17}F(p,\gamma)^{18}Ne$ rate, which is currently the most widely used rate in nucleosynthesis calculations of this type.

Table 5.1 Isotopic ratios for Candidates of Meteoric Dust Grains with Nova Origin

Grain	$^{13}C/^{12}C$	$^{14}N/^{15}N$	$^{26}Al/^{27}Al$
AF15bB-429-3[1]	9.4		
AF15bC-126-3[1]	6.8	5.22	
KJGM4C-100-3[1]	5.1	19.7	0.0114
KJGM4C-311-6[1]	8.4	13.7	>0.08
KJC112[1]	4.0	6.7	
KFC1a-551[1]	8.5	273	
Solar Composition[2]	89.9	270	~0
1.25 $M_\odot$ ONeMg WD Nova Calculations.[3]	3.2	0.51	0.15
1.35 $M_\odot$ ONeMg WD Nova Calculations.[3]	5.6	0.068	0.03
Other ONeMg nova Calculations.[1]	0.3~3	0.1~10	0.07~0.7

Sources : 1. S, Amari et al, ApJ., **551**, 1065-1072. (2001)
2. E. Anders & N. Grevesse, Geochim. Cosmochim. Acta, **53**,197 (1989).
3. Ratios based on nucleosynthesis calculations from this study.

It is crucial to use the best nuclear physics inputs to get the best predictions from nucleosynthesis calculations. Studies like this one are important because they determine the impact of the new nuclear physics inputs such as rate determinations.

5.5 Future Directions

The Sherr and Garcia rate $^{17}F(p,\gamma)^{18}Ne$ rates differ more from the ORNL rate at temperatures typical of x-ray bursts. We plan to follow this work with an analysis of the effect of the $^{17}F(p,\gamma)^{18}Ne$ rate on x-ray nucleosynthesis using a nuclear reaction network with the hydrodynamic profile and initial abundances of an x-ray burst. In addition to this, the techniques and programs used for this research can be easily modified to test other reaction rates as new measurements are made.

For nova nucleosynthesis simulation an important source of uncertainty is the nuclear reaction data input for the reaction rates in the calculation [32]. Since many of the reactions occur on unstable (radioactive) nuclei, few experimental measurements of their rates have been made. Many of the reactions rates used in the reaction rate library are therefore determined by theoretical calculations rather than by experimental measurements. Even reaction rate determinations based on experimental measurements suffer from large uncertainties, often due to the effect of missing or unknown resonances that can dramatically change the reaction rate at nova temperatures. For the hydrodynamic conditions of typical novae, many reaction rates are dominated by individual resonances. These factors lead to a wide variation in the rate determinations. The ORNL and Wiescher determinations for rate of $^{17}F(p,\gamma)^{18}Ne$ are an example of this variation and not an isolated one.

Hix *et al.* [32] estimated these uncertainties by performing Monte Carlo studies of nova nucleosynthesis. For these simulations each reaction rate is randomly assigned an enhancement factor and the network calculation is run to produce an abundance for each isotope. This is repeated thousands of times with different enhancement factors for each reaction. The variance in the abundance for each isotope from all of these trials is then determined.

It is estimated that there is an error of up to 25%-45% for many abundances of metals and up to a factor of 2 for abundances of long-lived radioactive isotopes [32]. A preliminary study of ^{17}O for the hottest zone in the 1.25 $M_{\odot}$ WD nova shows that there may be an uncertainty of up to a factor of 3 for the abundance of ^{17}O [32]. Recall that the difference in the abundance of ^{17}O produced when the ORNL case is compared to the Wiescher case for this zone was about a factor of 600, so a factor of 3 error does not wash out this result. However the difference for ^{17}O when averaged over all the zones is only a factor of 4. We plan to follow up the work described here with more complete studies in which Monte Carlo simulations will be run for all the zones to determine more precisely the errors associated with the zone composite abundances.

REFERENCES

REFERENCES

[1] M.S. Smith, Probing Stellar Explosions with Radioactive Beams at ORNL, (Oak Ridge:ORNL), in preparation (2001)

[2] D.W. Bardayan, *et al.*, Phys. Rev. Lett. **83**, 45 (1999)

[3] M. Wiesher, J. Gorres, and F.-K. Thielemann, Astrophys. J. **326**, 384 (1988)

[4] R. Sherr and H.T. Fortune, Phys. Rev. **C58**, 3292 (1998)

[5] A. Garcia, *et al.*, Phys Rev. **C43**, 2012 (1991)

[6] M. Wiescher, J. Gorres and H. Schatz , J. Phys. G: Nucl. Part. Phys., **25**, R133, (1999)

[7] R.D. Gehrz, *et al.,* Astronomical Society of the Pacific **110**,3 (1998)

[8] J.W. Truran & M. Livio, Astrophys. J. **308**,721(1986)

[9] W.M. Sparks, S. Starrfield, J.W. Truran, Astrophys. J. **220**, 1063 (1978)

[10] M.F. Bode and A. Evans, *Classical Nova*, John Wiley & Sons LTD, Chichester, (1989)

[11] R.Kippenhan & H.-C.Thomas, Astr.Ap., **63**, 256 (1978)

[12] D. Prialnik and A. Kovetz, Astrophys. J.**281**,367 (1984)

[13] M.Guidry, Private Communication, unpublished Astrophysics note.

[14] D.Clayton, *Principles of Stellar Evolution and Nucleosynthesis*, University of Chicago Press, Chicago, (1983)

[15] S. Starrfield, *et al.*, ApJ. Supplement, **127**, 485, (2000)

[16] K. Nomoto, Astophys. J., **253**, 798 (1982)

[17] J. MacDonald, Astrophys. J. **267**, 732 (1983)

[18] M. Politano, *et al.*, Astrophys. J. **448**, 807 (1995)

[19] R. Kippenhann & A. Weigert, *Stellar Structure and Evolution*, Springer-Verlag, Berlin, (1990)

[20] A.C. Phillips, *Physics of Stars*, John Wiley & Sons LTD, Chichester, (1994)

[21] http://www2.bnl.gov/CoN/ (December, 2001)

[22] D. Bardayan, Phys. Rev., **C62**, 055804 (2000)

[23] C. Rolfs & W.S. Rodney, *Cauldrons in the Cosmos,* University of Chicago Press, Chicago, (1988)

[24] W.R. Hix & F.K. Thielemann, Journal of Computational and Applied Mathematics, **109,** 321-351, (1999)

[25] M.S. Smith *et al.*, A New $^{17}F(p,\gamma)^{18}Ne$ Reaction Rate and Its Implications for Nova Nucleosynthesis, in Proceedings of Nuclear Science with Radioactive Ion Beams at ISOL Facilities, ed. C. J. Gross & M.S. Smith (Oak Ridge:ORNL), in press

[26] D. Arnett, *Supernovae and Nucleosynthesis*, Princeton University Press, Princeton N.J.(1996)

[27] S. Starrfield private communication

[28] F.K. Tielemann, *et al.*, http://ie.lbl.gov/astro/friedel.html (August, 2001)

[29] Anders, E. & Grevesse, N., *Geochim. Cosmochim. Acta*, **53**, 197 (1989)

[30] F.K. Thielemann 1995 private communication

[31] S, Amari *et al.*, Astrophys. J., **551**, 1065-1072. (2001)

[32] W. R. Hix *et al.*, Nuclear Reaction Rate Uncertainties and Their Effects on Nova Nucleosynthesis Modeling, in Proceedings of the 2nd Chicago Conference on Astrophysical Explosions, ed. E. Brown, J. Niemeyer, R. Rosner & J. Truran, in press

[33] http://www.onlineastronomy.com/ (December, 2001)

VITA

Suzanne Parete-Koon was born in 1974, in Oswego, New York. She received a Bachelor of Arts degree in 1997 from Bluffton College in Bluffton, Ohio where she double majored in Physics and Chemistry. She received a Masters degree in Physics from the University of Tennessee in Knoxville in December of 2001.